NKS-382
ISBN 978-87-7893-468-0

Sparger Tests in PPOOLEX on the Behaviour of Thermocline

Markku Puustinen
Lauri Pyy
Jani Laine
Antti Räsänen

Lappeenranta University of Technology
School of Energy Systems
Nuclear Engineering
Finland

March 2017

Abstract

This report summarizes the results of the two sparger pipe tests (SPA-T8R and SPA-T9) carried out in the PPOOLEX facility at LUT in 2016. Steam was blown through the vertical DN65 sparger type blowdown pipe to the condensation pool filled with sub-cooled water. Two different flow conditions were tested. Flow was either through all the 32 injection holes at the sparger head or just through eight holes in the bottom row.

The main objective of the tests was to obtain data for the development of the EMS and EHS models to be implemented in GOTHIC code by KTH. KTH plans to extend the models to cover also situations where steam injection into the pool is via a sparger pipe. The test parameters were selected by KTH on the basis of pre-test simulations and analysis of the results of the earlier sparger tests in PPOOLEX. Particularly the behaviour of the thermocline between the cold and warm water volumes was of interest. For this purpose also PIV measurements were tried during the tests.

In SPA-T8R, where flow was via 32 injection holes, the thermocline seemed to be around the elevation of 670 mm at the end of the stratification phase just as predicted by the pre-test simulations. The thermocline moved downwards as the erosion process progressed. The prevailing mixing mechanism during the final mixing phase was also erosion rather than internal circulation.

In SPA-T9, where flow was via eight injection holes, the thermocline was at first at a higher elevation than in SPA-T8R. It then started to shift downwards as the flow rate was increased in small steps. Complete mixing of the pool was achieved with the steam mass flow rate of 85 g/s. Erosion was again the prevailing mechanism in the mixing process.

The few sequences with recognized flow patterns from the PIV measurements indicate that some kind of swirls could exist at the elevation of the thermocline. The flow direction just under the thermocline can also be opposite to that just above the thermocline. The somewhat chaotic nature of the investigated phenomenon creates problems when measuring with a slow-speed PIV system and therefore definitive conclusions on the detailed behaviour of the thermocline can’t be made.

These tests in PPOOLEX verified that mixing of a thermally stratified water pool can happen through an erosion process instead of internal circulation if suitable flow conditions prevail.

Key words

condensation pool, sparger, thermocline, mixing

NKS-382
ISBN 978-87-7893-468-0
Electronic report, March 2017
NKS Secretariat
P.O. Box 49
DK - 4000 Roskilde, Denmark
Phone +45 4677 4041
www.nks.org
e-mail nks@nks.org

Research Report
Lappeenranta University of Technology
Nuclear Engineering

INSTAB 1/2016

SPARGER TESTS IN PPOOLEX ON THE BEHAVIOUR OF THERMOCLINE

Markku Puustinen, Lauri Pyy, Jani Laine, Antti Räsänen

Lappeenranta University of Technology
School of Energy Systems
Nuclear Engineering
P.O. Box 20, FIN-53851 LAPPEENRANTA, FINLAND
Phone +358 5 621 11

Lappeenranta, 31.1.2017

Open your mind. LUT.
Lappeenranta University of Technology

Research organization and address	Customer
Lappeenranta University of Technology Nuclear Engineering P.O. Box 20 FIN-53851 LAPPEENRANTA, FINLAND	VYR / SAFIR2018 NKS SSM
Project manager Markku Puustinen	**Contact person** Jari Hämäläinen (SAFIR2018) Christian Linde (NKS), Maria Agrell (NORTHNET)
Diary code 125/322/2015	**Order reference** Drno SAFIR 9/2016
Project title and reference code SAFIR2018-INSTAB NKS-COPSAR	**Report identification & Pages** / **Date** INSTAB 1/2016 — 31.1.2017 28 p. + app. 46 p.

Report title and author(s)

SPARGER TESTS IN PPOOLEX ON THE BEHAVIOUR OF THERMOCLINE

Markku Puustinen, Lauri Pyy, Jani Laine, Antti Räsänen

Summary

This report summarizes the results of the two sparger pipe tests (SPA-T8R and SPA-T9) carried out in the PPOOLEX facility at LUT in 2016. Steam was blown through the vertical DN65 sparger type blowdown pipe to the condensation pool filled with sub-cooled water. Two different flow conditions were tested. Flow was either through all the 32 injection holes at the sparger head or just through eight holes in the bottom row.

The main objective of the tests was to obtain data for the development of the EMS and EHS models to be implemented in GOTHIC code by KTH. KTH plans to extend the models to cover also situations where steam injection into the pool is via a sparger pipe. The test parameters were selected by KTH on the basis of pre-test simulations and analysis of the results of the earlier sparger tests in PPOOLEX. Particularly the behaviour of the thermocline between the cold and warm water volumes was of interest. For this purpose also PIV measurements were tried during the tests.

In SPA-T8R, where flow was via 32 injection holes, the thermocline seemed to be around the elevation of 670 mm at the end of the stratification phase just as predicted by the pre-test simulations. However, the thickness of the thermocline was larger than expected. The thermocline moved downwards as the erosion process progressed. The prevailing mixing mechanism during the final mixing phase was also erosion rather than internal circulation.

In SPA-T9, where flow was via eight injection holes, the thermocline was at first at a higher elevation than in SPA-T8R. It then started to shift downwards as the flow rate was increased in small steps. Complete mixing of the pool was achieved with the steam mass flow rate of 85 g/s. Erosion was again the prevailing mechanism in the mixing process.

The few sequences with recognized flow patterns from the PIV measurements indicate that some kind of swirls could exist at the elevation of the thermocline. The flow direction just under the thermocline can also be opposite to that just above the thermocline. The somewhat chaotic nature of the investigated phenomenon creates problems when measuring with a slow-speed PIV system and therefore definitive conclusions on the detailed behaviour of the thermocline can't be made. However, certain flow field information from the obtained short duration measurement sequences may be useful in the development work of simulation tools and models.

These tests in PPOOLEX verified that mixing of a thermally stratified water pool can happen through an erosion process instead of internal circulation if suitable flow conditions prevail.

Distribution

Members of the SAFIR2018 Reference Group 4

C. Linde (SSM), M. Agrell (SSM), P. Kudinov (KTH), I. G. Marcos (KTH), W. Villanueva (KTH), J. Hämäläinen (VTT), V. Suolanen (VTT), T. Pättikangas (VTT), I. Karppinen (VTT), S. Hillberg (VTT)

Principal author or Project manager	Reviewed by
Markku Puustinen, Senior Research Scientist	Vesa Riikonen, Senior Research Scientist
Approved by	**Availability statement**
Heikki Purhonen, Research Director	SAFIR2018 limitations

Open your mind. LUT.
Lappeenranta University of Technology

Acknowledgement

NKS conveys its gratitude to all organizations and persons who by means of financial support or contributions in kind have made the work presented in this report possible.

Disclaimer

CONTENTS

NOMENCLATURE

A	Area
D	Pressure difference measurement
F	Flow rate measurement
P	Pressure measurement
S	Strain measurement
T	Temperature measurement

Abbreviations

BWR	Boiling Water Reactor
CCD	Charge-Coupled Devices
CCTV	Closed Circuit TeleVision
CFD	Computational Fluid Dynamics
CONDEX	CONdensation EXperiments project
DCC	Direct Contact Condensation
ECCS	Emergency Core Cooling System
EHS	Effective Heat Source
EMS	Effective Momentum Source
EXCOP	EXperimental studies on COntainment Phenomena project
INSTAB	couplings and INSTABilities in reactor systems project
KTH	Kungliga Tekniska Högskolan
LRR	Load Reduction Ring
LOCA	Loss-Of-Coolant Accident
LUT	Lappeenranta University of Technology
MSLB	Main Steam Line Break
NKS	Nordic nuclear safety research
NORTHNET	NORdic nuclear reactor Thermal-Hydraulics NETwork
PACTEL	PArallel Channel TEst Loop
PIV	Particle Image Velocimetry
POOLEX	condensation POOL EXperiments project
PSP	Pressure Suppression Pool
RHR	Residual Heat Removal
PPOOLEX	Pressurized condensation POOL EXperiments test facility
SAFIR	SAfety of nuclear power plants - FInnish national Research programme
SPA	SPArger experiment series
SRV	Safety/Relief Valve
SSM	Strålsäkerhetsmyndigheten
TC	ThermoCouple
VTT	Technical Research Centre of Finland
VYR	State nuclear waste management fund

1 INTRODUCTION

A pressure suppression pool (PSP) of a BWR reactor containment serves as a heat sink and steam condenser during a postulated main steam line break (MSLB) or loss of coolant accident (LOCA) inside the containment or during safety relief valve (SRV) opening in normal operations. It thus prevents containment pressure build-up when steam released from the reactor vessel is vented through the blowdown pipes (in case of MSLB and LOCA) or through the spargers (in case of SRV operation) to the pool.

Different phenomena inside the drywell and wetwell compartments of BWR containment during steam discharge has been extensively studied in the PPOOLEX test facility at LUT and simulated with computer codes during recent years in the framework of the national research programmes on nuclear power plant safety (SAFIR, SAFIR2014) as well as via participation to NORTHNET RM3 and NKS research projects in co-operation with VTT and Kungliga Tekniska Högskolan (KTH). Research topics have included, for example, dynamic loads caused to PSP structures by direct contact condensation (DCC), behaviour of parallel blowdown pipes during the chugging flow mode, effect of blowdown pipe outlet design on structural loads, wall condensation in the drywell and development/break-up of thermal stratification in the PSP [1…10].

The current SAFIR2018/INSTAB project as well as the related NKS and SSM funded research efforts aim to broaden the database to cover experiments with SRV spargers, residual heat removal (RHR) system nozzles, strainers and containment spray systems. Calculation models and numerical methods including CFD and system codes are developed and validated on the basis of the PPOOLEX experiment results at VTT and KTH within the SAFIR2018, NKS, and SSM funded projects. Also analytical support is provided for the experimental part by pre- and post-calculations of the experiments.

As a result of steam venting into the suppression pool the coolant temperature in the pool gradually increases. With certain flow modes a thermally stratified condition could develop where the pool's surface temperature is higher than the pool bulk temperature. This leads to a reduction of the pool's pressure suppression capacity because the pool surface temperature determines the steam partial pressure in the wetwell gas space. An increase of the pool's surface temperature due to stratification can therefore lead to a significant increase in containment pressure if mixing of the pool coolant inventory fails [11]. Pool mixing can occur due to steam injection itself if the injection flow mode changes as a result of increasing or decreasing steam flow rate. Mixing can be achieved also with the help of plant systems designed for that purpose or as a result of water suction from the pool by the Emergency Core Cooling System (ECCS) pumps.

KTH has developed the Effective Heat Source (EHS) and Effective Momentum Source (EMS) models for steam injection through a vertical pipe submerged in a pool and proposed them to be used for simulation of thermal stratification and mixing during a steam injection into a large pool of water [12]. These models have been implemented in GOTHIC® software and validated against POOLEX and PPOOLEX tests carried out at LUT. Excellent agreement in averaged pool temperature and water level in the pool between the experiment and simulation has been achieved. The development of thermal stratification and mixing of the pool are also well captured in the simulations. The EMS and EHS models will be available to be implemented also in the APROS containment code for the calculation of phenomena related to pool stratification and mixing.

At the moment KTH is improving the EHS and EMS models for blowdown pipes in order to reduce uncertainties and enhance accuracy in predictions as well as extending the models to SRV spargers. Later the models will be extended further to other elements of the PSP such as nozzles of the residual heat removal system and strainers in order to be able to carry out comprehensive safety analysis of realistic transients in a BWR containment.

Suitable experimental data is limited for validation of the EHS and EMS models. So far, the only available and sufficiently detailed experimental vent pipe data are the POOLEX/PPOOLEX steam discharge experiments with blowdown pipes. The PPOOLEX database was broadened to cover SRV spargers in the test series carried out in 2014 and 2015 [13, 14]. Main motivation for the additional sparger tests reported here was to study the behaviour of a thermocline during steam injection through the sparger head. Chapter two gives a short description of the test facility and its measurements as well as of the PIV and data acquisition systems used. The test parameters, initial conditions and test procedure are introduced in chapter three. The test results are presented and discussed in chapter four. Chapter five summarizes the findings of the test series.

2 PPOOLEX TEST FACILITY

The PPOOLEX test facility was taken into use at LUT in the end of 2006. PPOOLEX models the containment of a BWR plant. During the years the facility has gone through several modifications and enhancements as well as improvements of instrumentation. For the sparger tests described in this report the facility was equipped with a model of a safety relief valve sparger. The PPOOLEX facility is described in more detail in reference [15]. However, the main features of the facility and its instrumentation are introduced below.

2.1 TEST VESSEL

The PPOOLEX facility consists of a wetwell compartment (condensation pool), drywell compartment, inlet plenum and air/steam-line piping. An intermediate floor separates the compartments from each other. Usually a route for gas/steam flow from the drywell to the wetwell is created by a vertical blowdown pipe attached underneath the floor. During the sparger tests the drywell compartment was, however, bypassed i.e. steam was blown directly into the wetwell via the sparger pipe.

The main component of the facility is the ~31 m^3 cylindrical test vessel, 7.45 m in height and 2.4 m in diameter. It is constructed from three plate cylinder segments and two dome segments. The test facility is able to withstand considerable structural loads caused by rapid condensation of steam. The dry and wetwell sections are volumetrically scaled according to the compartment volumes of the Olkiluoto containment (ratio approximately1:320). There are several windows for visual observation in both compartments. A DN100 (∅ 114.3 x 2.5 mm) drain pipe with a manual valve is connected to the vessel bottom. A relief valve connection is mounted on the vessel head. The removable vessel head and a man hole (DN500) in the wetwell compartment wall provide access to the interior of the vessel for maintenance and modifications of internals and instrumentation. The drywell is thermally insulated.

A sketch of the test vessel is shown in Figure 1. Table 1 lists the main dimensions of the test facility compared to the conditions in the Olkiluoto plant.

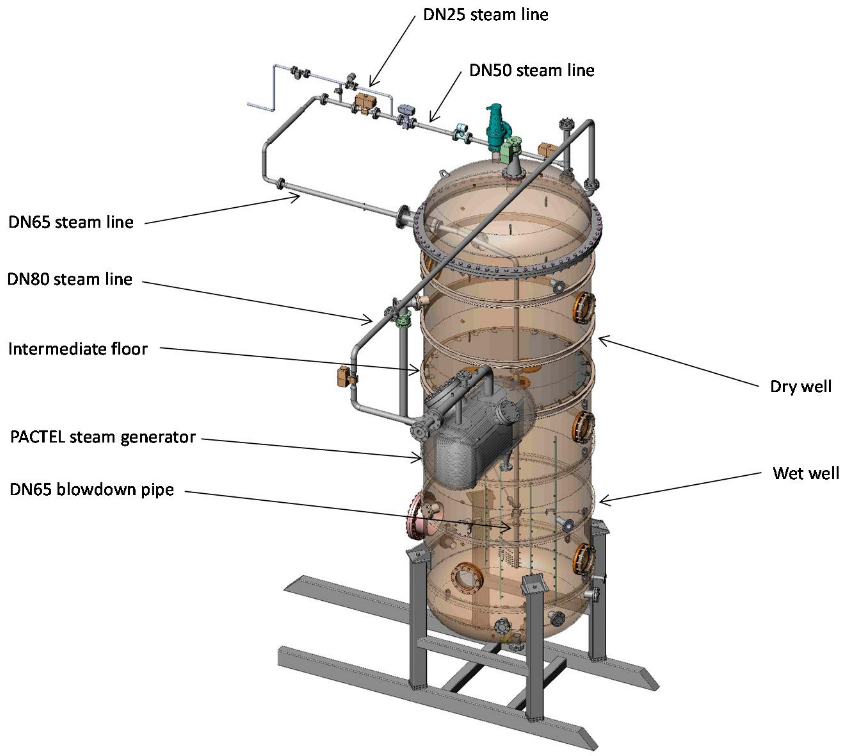

Figure 1. PPOOLEX test vessel.

Table 1. Test facility vs. Olkiluoto 1 and 2 BWRs.

	PPOOLEX test facility	Olkiluoto 1 and 2
Number of blowdown pipes	1-2	16
Inner diameter of the blowdown pipe [mm]	214.1	600
Suppression pool cross-sectional area [m^2]	4.45	287.5
Drywell volume [m^3]	13.3	4350
Wetwell volume [m^3]	17.8	5725
Nominal water volume in the suppression pool [m^3]	8.38*	2700
Nominal water level in the suppression pool [m]	2.14*	9.5
Pipes submerged [m]	1.05	6.5
A_{pipes}/A_{pool}x100%	0.8 / 1.6**	1.6

* Water volume and level can be chosen according to the experiment type in question. The values listed in the table are based on the ratio of nominal water and gas volumes in the plant.
** With one / two blowdown pipes.

2.2 PIPING

Steam needed in the tests is generated with the nearby PACTEL [16] test facility, which has a core section of 1 MW heating power and three horizontal steam generators. Steam is led through a thermally insulated steam line, made of sections of standard DN80 (Ø88.9x3.2), DN50 (Ø60.3x3.0) and DN65 (Ø76.1x3.0) pipes, from the PACTEL steam generators towards the PPOOLEX test vessel. The section of the steam piping inside the drywell (bypass) is made of uninsulated DN65 (Ø76.1x3.0) pipe.

2.3 SPARGER PIPE

The DN65 (Ø76.1x4.0) sparger type blowdown pipe is positioned vertically inside the pool in a non-axisymmetric location, i.e. the pipe is 420 mm away from the centre of the condensation pool.

The total length of the sparger pipe is approx. 5.0 m. The pipe is made from austenitic stainless steel EN 1.4571.

There are 32 Ø8 mm holes drilled radially in the lower part of the pipe (sparger head). These holes are in four rows, eight holes in each row. There is a load reduction ring 700 mm above the pipe outlet with 8 axially drilled Ø8 mm holes.

2.4 AIR REMOVAL SYSTEM

For the sparger tests the PPOOLEX facility was equipped with an air removal system. The system consists of a filter unit and an air removal device. Air is removed in a vacuum chamber by a vacuum pump during the preparation period for the experiments. However, the system was not used in all experiments.

2.5 MEASUREMENT INSTRUMENTATION

The applied instrumentation depends on the experiments in question. Normally, the test facility is equipped with several thermocouples (T) for measuring steam, pool water and structure temperatures and with pressure transducers (P) for observing pressures in the drywell, inside the blowdown pipes, at the condensation pool bottom and in the gas space of the wetwell. Steam flow rate is measured with a vortex flow meter (F) in the steam line. Additional instrumentation includes, for example, strain gauges (S) on the pool outer wall and valve position sensors.

For the sparger tests a 6x7 grid of temperature measurements (thermocouples T4000–T4056) was installed in the pool in front of the injection holes of the sparger head. For measuring vertical temperature distribution inside the sparger pipe nine temperature measurements (thermocouples T4070…T4078) were installed with a varying interval. Four trains of temperature measurements (thermocouples T4100…T4113, T4200…T4219, T4300…T4319 and T4400…T4413) were installed in the pool below the water level for detecting vertical temperature distribution.

Figures in Appendix 2 show the locations of the PPOOLEX measurements during the SPA series and the table in Appendix 2 lists their identification codes and other details.

2.6 CCTV SYSTEM

Standard video cameras with 25 fps connected to a laptop computer were used for visual observation of the test vessel interior during the test series.

2.7 DATA ACQUISITION

National Instruments PXIe PC-driven measurement system was used for data acquisition. The system enables high-speed multi-channel measurements. The maximum number of measurement channels is 64 with additional eight channels for strain gauge measurements. The maximum recording capacity depends on the number of measurements and is in the region of three hundred thousand samples per second. Measurement software was LabView 2015. The data acquisition system is discussed in more detail in reference [17].

Self-made software using the National Instruments FieldPoint measurement system was used for monitoring and recording the essential measurements of the PACTEL facility generating the steam. Both data acquisition systems measure signals as volts. After the tests, the voltage readings are converted to engineering units with conversion software.

The used measurement frequency of LabView was 20 Hz. The rest of the measurements (for example temperature, pressure and flow rate in the steam line) were recorded by the self-made software with the frequency of 0.67 Hz.

2.8 PIV MEASUREMENT SET-UP

PIV measurements were conducted in the SPA-T8, SPA-T8R and SPA-T9 tests in order to produce velocity field data. The PIV system's laser is a Neodym-YAG double-cavity laser. The two pulsed lasers emit the beam in infrared range at 1064 nm and they are polarization combined. A second harmonic generator is used to convert the beam to visible range at 532 nm. The appropriate thickness of the light sheet is achieved with the two spherical lenses. The system's cameras are Imager Pro X 4M CCD cameras having progressive-scan technology with a dual frame-technique for cross correlation. The CCD sensors are cooled with Peltier element to +10°C to reduce background noise. With remote controlled focus rings the focus and aperture of the camera lenses can be controlled with computer software. The system has also a remote controlled Scheimpflug mount which allows all areas of the image plane to be in focus. For collecting PIV recording and other data the equipment has a system computer. The system utilizes DaVis software solution for image acquisition and analysis of flow fields in both 2D and 3D cases.

The general measurement area of PIV was restricted due to the thermocouple structures as well as the elevation of the thermocline. The small size of the viewing windows was also a restrictive factor. The measurement area was chosen so that the cameras would be approximately equidistant. Laser was shot between the windows of the cameras as the structures of the thermocouples were on the way for the use of the normal laser window. Setting up the PIV system inside the PPOOLEX is challenging in many ways but after all the calibration process could be conducted successfully and the laser sheet could be lined up to the measurement plane. The horizontal cross section of the calibration set-up scheme is presented in Figure 2.

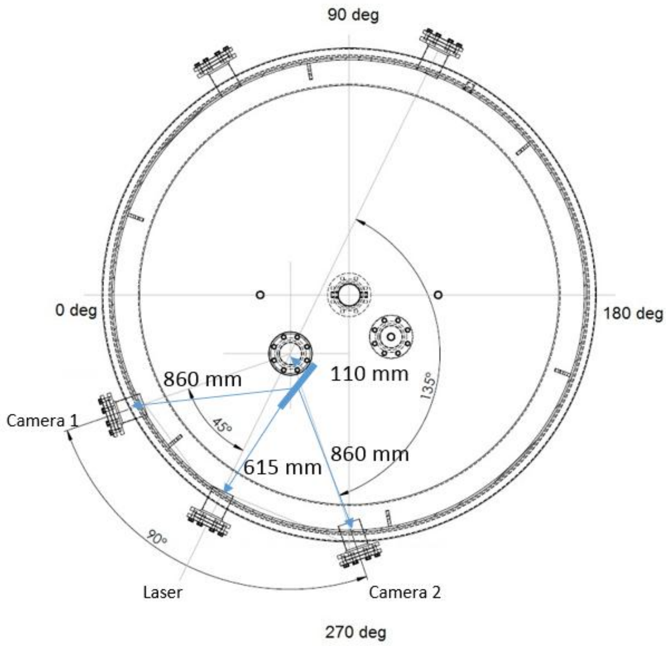

Figure 2. Horizontal cross section of the calibration set-up scheme for PIV measurements in the SPA-T8, SPA-T8R and SPA-T9 tests.

The distance from the camera windows to the centre of the measurement plane was approximately 860 mm and from the laser window to the edge of the calibration plate 615 mm measured with a laser distance meter. The calibration plate was 110 mm from the centre of the sparger pipe measured with a tape ruler. The vertical cross section of the calibration set-up is presented in Figure 3.

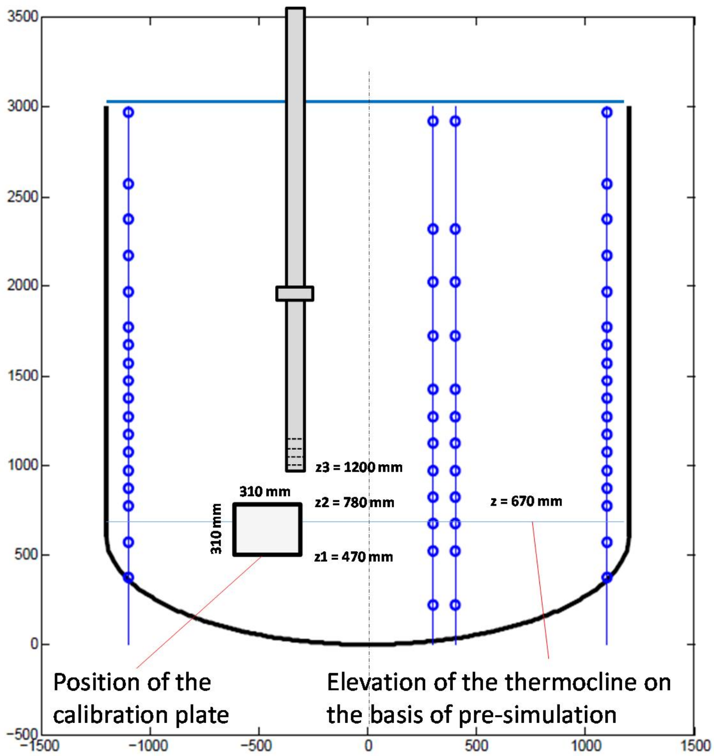

Figure 3. Vertical cross section of the calibration set-up scheme for PIV measurements in the SPA-T8, SPA-T8R and SPA-T9 tests.

On the basis of the pre-test analysis the thermocline was expected to be at z = 670 mm. The top of the calibration plate was positioned 420 mm below the sparger pipe outlet (which is at 1200 mm). This means that about 1/3 of the FOV would be above the thermocline and 2/3 below it.

3 TEST PROGRAM

Three sparger pipe tests labelled as SPA-T8, SPA-T8R and SPA-T9 were carried out in the PPOOLEX facility. The SPA-T8R test was a repetition of the SPA-T8 test and it was done because a broken pressure sensor in the flow meter prevented accurate measurement of steam flow rate during the original SPA-T8 test. The main purpose of the tests was to obtain additional data for the development of the EMS and EHS models to be implemented in GOTHIC code by KTH. Particularly the behaviour of the thermocline between the cold and warm water volumes was of interest. Information on the flow fields below and above of the thermocline would be of great help in validating the EMS and EHS models for spargers. For this purpose PIV measurements were tried in the tests reported here.

In the SPA-T8 and SPA-T8R tests all the 32 injection holes of the sparger head were open but in the SPA-T9 test only the eight holes of the lowest row of injection holes were open. The injection holes of the LRR were blocked in all the tests.

Detailed test specifications put together on the basis of pre-test calculations and analysis of the results of the previous tests were provided by KTH before the tests [18, 19]. The SPA-T8 and SPA-T8R tests had a stratification phase, an erosion phase with slightly increased flow rate and a mixing period with a high flow rate. In SPA-T9, there was first a stratification period and then succeeding phases where the flow rate was increased in steps until the pool was mixed.

Before the tests, the wetwell pool was filled with isothermal water (~14 °C in SPA-T8, ~13 °C in SPA-T8R and ~15 °C in SPA-T9) to the level of 3.0 m i.e. the sparger pipe outlet was submerged by 1.8 m. The steam discharge rate into the PPOOLEX vessel was controlled with the help of the pressure level of the steam source (PACTEL steam generator) and a remote-operated control valve (S2002) in the DN50 steam line.

The tests were started from atmospheric conditions in PPOOLEX. After the correct initial steam generator pressure (0.6 MPa) had been reached, the remote-controlled cut-off valve (X2100) in the DN50 steam line was opened. To remove air from the steam line and to heat up the piping structures from the PACTEL steam generators to the PPOOLEX vessel, steam mass flow rate was at first adjusted to a higher level (slightly above 200 g/s) for about 200-250 seconds. The pool bulk temperature rose approximately 3-5 °C during this clearing phase.

The stratification process was initiated by reducing the steam flow rate to the desired level (130 g/s in SPA-T8R and 30 g/s in SPA-T9). In SPA-T8R, the erosion and mixing phases were started by increasing the steam flow rate into the test vessel after the predetermined temperature difference between the bottom and surface layers of the pool had been reached (20 °C for erosion to start and 85 °C for mixing to start). In SPA-T9, the steam flow rate was increased in steps of 15-20 g/s every time the pool top temperature had risen by 15 °C until the pool was mixed.

The main parameters of the SPA-T8, SPA-T8R and SPA-T9 tests are listed in Table 2, correspondingly. The path of the tests defined by steam mass flux and pool bulk temperature is marked on the condensation mode map for a sparger of Chan and Lee [20] in Figure 4. In the map steam mass flux is determined as the flow rate through the injection holes of the sparger head divided by the cross-sectional area of the holes.

Table 2. Parameter values of the sparger tests SPA-T8, SPA-T8R and SPA-T9.

Test	Initial water level [m]	Initial water temperature [°C]	Steam flow rate [g/s]		
			Stratification	Erosion/Mixing phase(s)	Final mixing phase
SPA-T8	3.0	~14	~110*	~120*	~280*
SPA-T8R	3.0	~13	~128	~140	~250
SPA-T9	3.0	~15	~29	~45/65/85	-

*Estimated values because the flow meter was broken

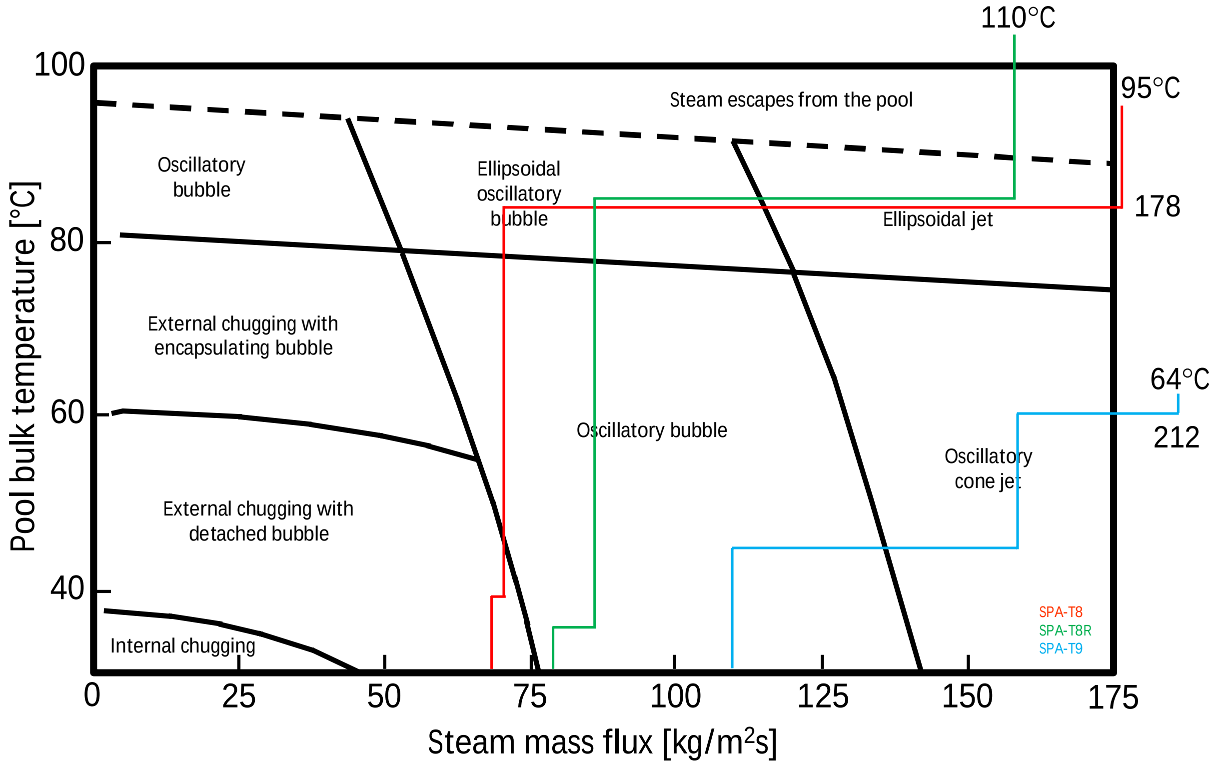

Figure 4. Paths of the SPA-T8, SPA-T8R and SPA-T9 tests marked on the direct condensation mode map for pure steam discharge of Chan and Lee [20].

4 TEST RESULTS

The following chapters give a more detailed description of the SPA-T8R and SPA-T9 tests and present the observed phenomena. Because the original SPA-T8 test was somewhat of poor quality due to the faulty flow measurement it is not analysed in more detail here.

4.1 SPA-T8R

Water was expelled out of the sparger pipe as soon as steam injection was initiated. In SPA-T8R, all the injection holes of the sparger head were open and as a result 32 horizontal and radially directed steam jets developed around the lower end of the sparger. The pipe was practically full of steam during the rest of the test. This can be seen from the three temperature measurements from inside the sparger pipe plotted in Figure 5. Measurement T4077 shows that the steam temperature in the upper part of the sparger pipe was higher than at the sparger head throughout the test. T4073 indicates that slight temperature oscillations were present above the region of the injection holes during the second half of the erosion phase, while there were no oscillations at the lower end of the sparger (T4070).

The steam mass flow rate during the stratification phase was about ~128 g/s (corresponding to the mass flux of about 79.6 kg/m^{2}s). According to the direct condensation mode map for pure steam discharge of Chan and Lee the dominant flow mode is then oscillatory bubble, Figure 4. With this kind of mass flux steam flows through the injection holes of the sparger as small jets and condenses mainly outside the sparger pipe. Because no chugging kind of phenomenon exists and the steam jets are too weak to create much turbulence in the pool, suitable conditions for thermal stratification to occur prevail. During the erosion phase the steam flow rate was only slightly higher (~140 g/s, 87.0 kg/m^{2}s). At the end of erosion phase the pool water temperature increased above 80 °C and the flow mode changed from oscillatory bubble to ellipsoidal oscillatory bubble (Figure 4). For the final mixing phase the steam mass flow rate was increased to ~250 g/s (155.4 kg/m^{2}s). As a result the flow mode changed to ellipsoidal jet (Figure 4). Figure 6 shows the steam mass and volumetric flow rate curves in the SPA-T8R test.

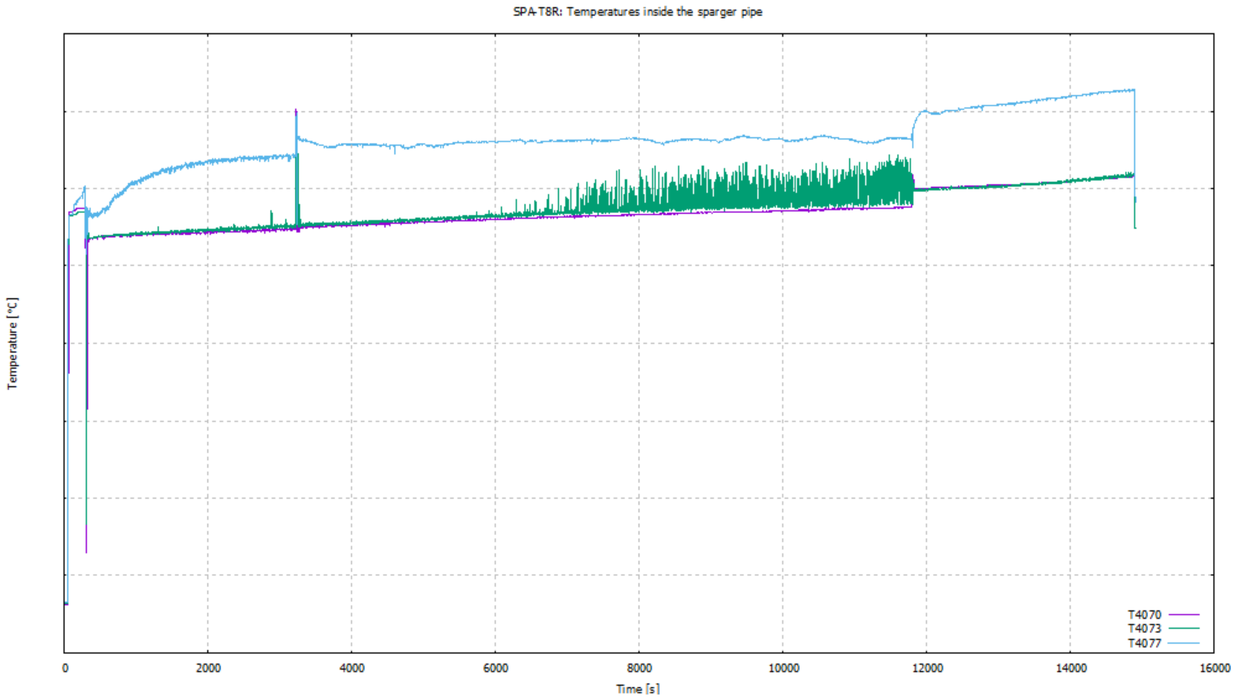

Figure 5. Temperatures inside the sparger pipe in the SPA-T8R test.

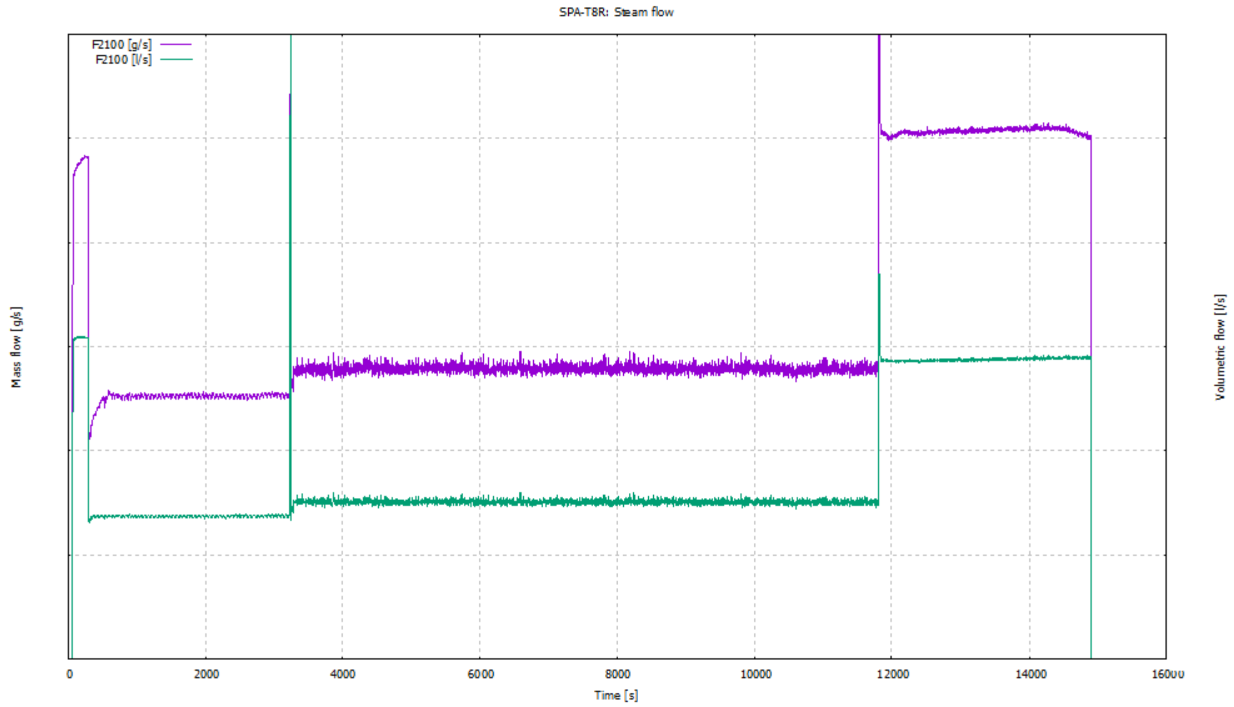

Figure 6. Mass and volumetric steam flow rates in the SPA-T8R test.

The stratification phase continued until 3235 seconds into the experiment. Two regions with clearly different water temperatures developed in the pool. The region close to the pool bottom, where the steam jets had no effect, remained at the temperature established after the clearing phase in the beginning of the test. The rest of the pool volume heated up instead quite uniformly. The heat-up process was driven by flow of warm condensed water upwards from the sparger outlet as well as by conduction through the pipe wall. The temperature measurements attached to the vertical rods in the pool indicate that the thermocline between the cold and warm water was just below the TC measurements at the elevation of 672 mm. Measurements at that elevation show slightly lower temperatures than all the other measurements above them. The next TCs downwards at the elevation of 522 mm and 472 mm indicate only 1-2 °C higher temperatures than all the other TCs in the cold water region (Figure 7). The exact elevation of the thermocline and its width is hard to determine due to missing measurements between the 522 mm and 672 mm elevations. However, it seems that the estimated elevation of the thermocline at 670 mm on the basis of the pre-test simulation was quite accurate. The oscillating behaviour of the temperature curve measured by the TC at the 672 mm elevation further confirms that the thermocline was around that elevation. However, it seems that the width of the thermocline was not as narrow as it was thought to be.

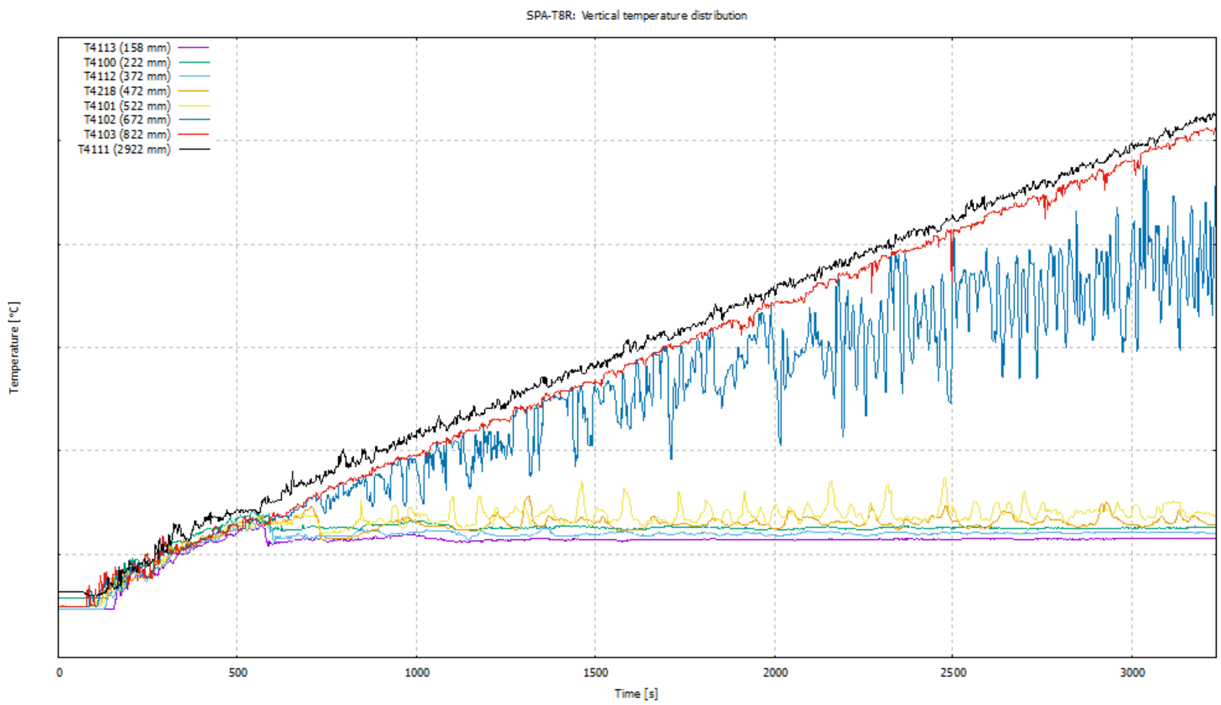

Figure 7. Vertical temperature distribution in wetwell pool during the clearing phase (0-300 s) and stratification phase (300-3235 s) in the SPA-T8R test.

On the basis of the pre-test simulation it was believed that even a small increase in the steam flow rate could somewhat erode the thermocline and at least partly mix the pool. To verify this assumption the steam mass flow rate was increased to about 140 g/s for the erosion phase in the SPA-T8R test. Figure 8 shows how the elevation of the thermocline moved downwards as some of the TCs in the cold region first started to indicate elevated readings and later the same readings as all the other TCs above the thermocline. At the end of this phase the thermocline seemed to be between the elevations of 372 mm and 472 mm according to the TC readings.

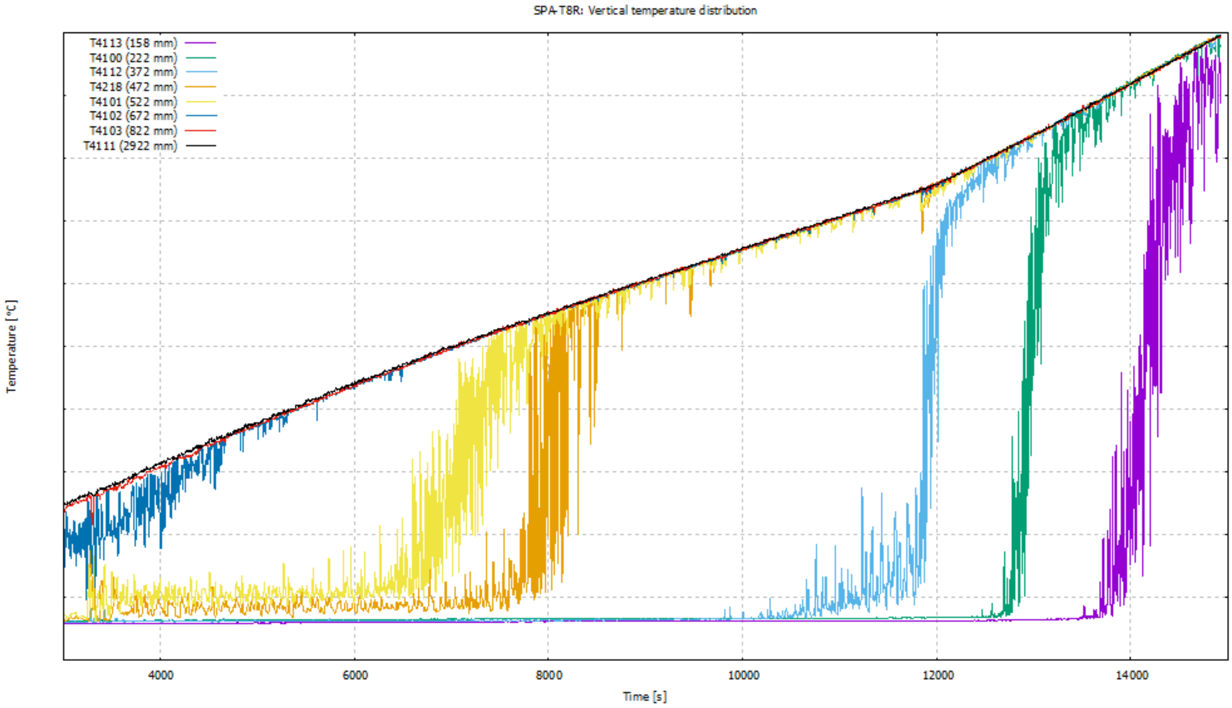

Figure 8. Vertical temperature distribution in wetwell pool during the erosion phase (3235-11800 s) and final mixing phase (11800-14920 s) in the SPA-T8R test.

For the final mixing phase the steam mass flow rate was increased to about 250 g/s at 11800 seconds into the experiment (Figure 6). The aim was to mix the pool completely and see how long it would take. The mixing process speeded up considerably compared to the erosion phase but it took still over 3000 seconds to mix the pool (Figure 8). This is three times the estimate obtained in the pre-test simulation. At the end the pool bulk temperature was about 110 °C.

The development of the vertical temperature profile of pool water over the whole SPA-T8R test can be seen from Figure 9. The initial uniform temperature profile first changes to a stratified situation and eventually back to a uniform and mixed situation at the end of the final mixing phase. Even during the stratified phase the temperature curves are almost straight vertical lines outside the thermocline region indicating rather constant water temperature distribution elsewhere in the pool. The slow movement of the thermocline downwards as the test proceeded can also be seen from Figure 9. The thickness of the thermocline region in case of a sparger pipe is small compared to the previous stratification/mixing experiments done in PPOOLEX with a straight blowdown pipe. However, the thermocline region wasn't as narrow as expected on the basis of pre-test simulations.

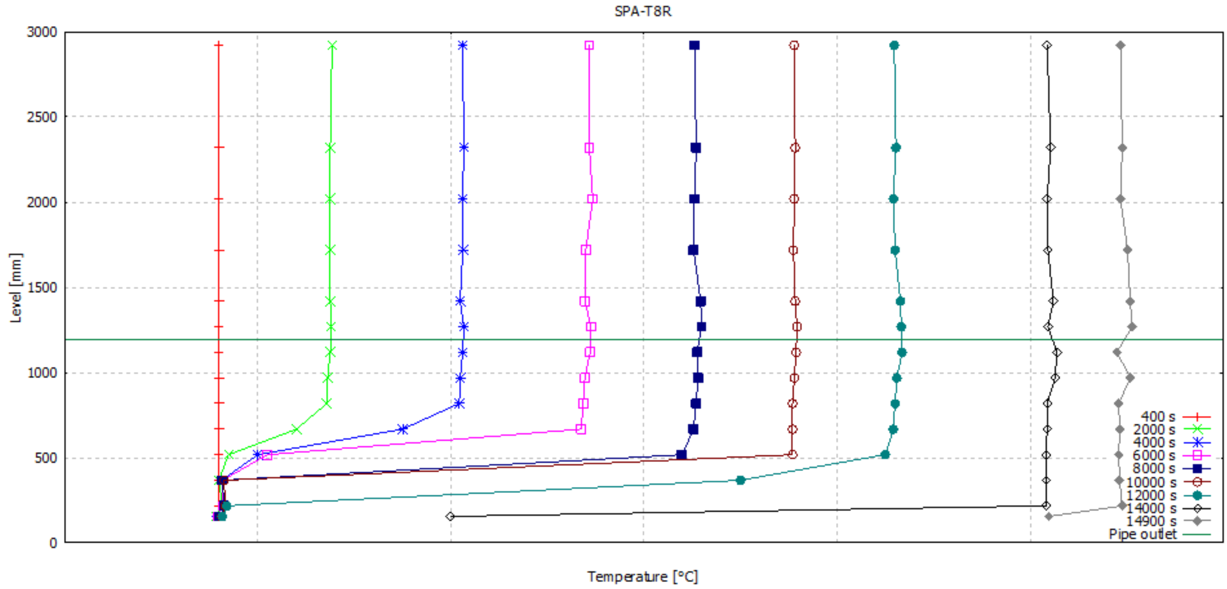

Figure 9. Development of vertical temperature profile of pool water in the SPA-T8R test.

4.2 SPA-T9

In SPA-T9, only the lowest row of the injection holes of the sparger head were open. Steam flow was thus through 8 horizontally oriented holes. The objective was to find out if the elevation of the thermocline changes and how the erosion/mixing process differs from the case where all the injection holes were open.

Again water was expelled out of the sparger pipe as soon as steam injection was initiated and suitable conditions for thermal stratification to occur prevailed since no chugging kind of phenomenon existed. In SPA-T9, the steam flow rate was increased in steps of 15-20 g/s. During the first (stratification) step the flow rate was about 29 g/s (corresponding to the mass flux of about 72.1 kg/m^{2}s). This step is not plotted on the flow mode map of Chan and Lee in Figure 4 because it is outside the lower temperature range of the chart. In the next step the flow rate was increased to 45 g/s. This corresponds to the mass flux of about 111.9 kg/m^{2}s the dominant flow mode being oscillatory bubble (Figure 4). During the next step the flow rate was about 65 g/s (~161.6 kg/m^{2}s). The flow mode now changed to oscillatory cone jet (Figure 4). The final flow step in SPA-T9 was at 85 g/s (211.4 kg/m^{2}s, Figure 4) because with this flow rate the pool mixed completely. Figure 10 shows the steam mass and volumetric flow rate curves in the SPA-T89 test.

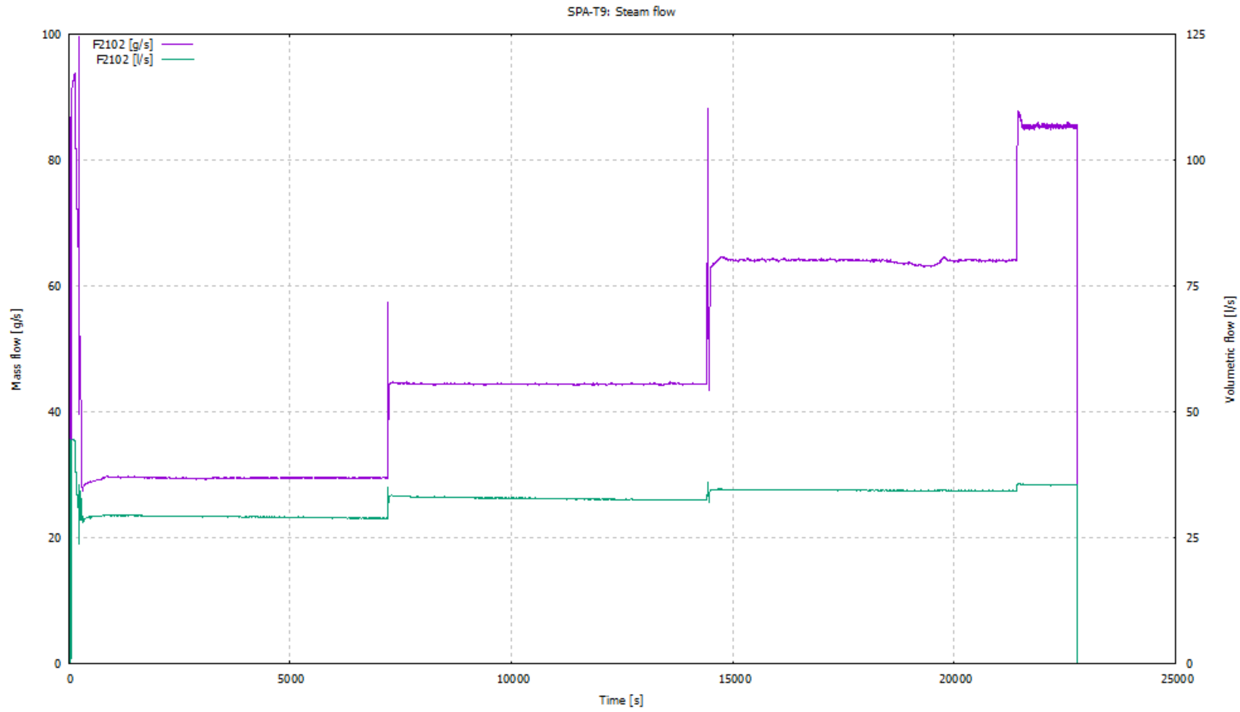

Figure 10. Mass and volumetric steam flow rates in the SPA-T9 test.

Figure 11 presents the vertical temperature distribution in the wetwell pool during the whole SPA-T9 test. It seems that the thermocline first settles on a slightly higher elevation than in the SPA-T8R test despite the fact that the lowest elevation used for steam injection both in SPA-T8R and SPA-T9 was the bottom row of injection holes at the sparger head. Temperature measurements at the elevations of 972 mm and 1072 mm indicate that the thermocline is now between them while in SPA-T8R it was just below the 670 mm elevation. In both cases the flow mode is oscillatory bubble although the steam mass flux values aren't exactly the same. The thickness of the thermocline also seems to be slightly narrower when the steam injection is only through one row of injection holes.

As the steam flow rate was increased in steps the elevation of the thermocline shifted downwards due to the erosion/mixing process. During the step with a 45 g/s flow rate the thermocline seemed to be somewhere between the TC measurements at the elevations of 672 mm and 772 mm. When the flow rate was increased to 65 g/s the thermocline passed through the TC measurements at the elevations of 572 mm, 522 mm, 472 mm and finally 372 mm. It moved further downwards and beyond the measurement at the elevation of 222 mm when the flow rate was once more increased to 85 g/s. At about 22750 seconds into the experiment the last TC measurements at the elevation of 158 mm started to indicate the same temperatures as the rest of the measurements meaning that the pool was completely mixed. No further flow steps were needed.

The complete mixing of the pool with quite a small steam injection mass flow rate is understandable if we take into account the fact that 65 g/s corresponds to about 162 kg/m^2s and 85 g/s to about 212 kg/m^2s. These are both bigger values than the figure 155 kg/m^2s corresponding to the 250 g/s flow rate used during the final mixing phase in the SPA-T8R test when all the injection holes in the sparger head were open.

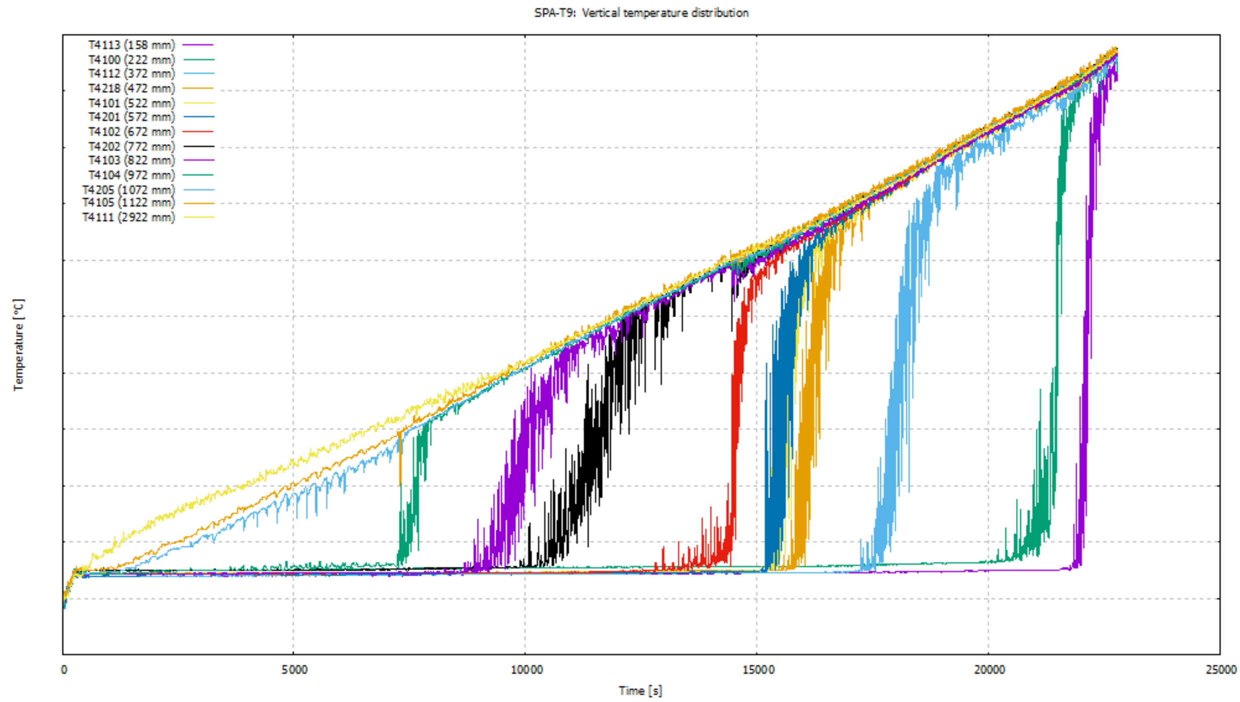

Figure 11. Vertical temperature distribution in the wetwell pool during the different flow rate steps in the SPA-T9 test.

Figure 12 shows the development of the vertical temperature profile of pool water over the whole SPA-T9 test. Again, the initial uniform temperature profile first changes to a stratified situation and eventually back to a uniform and mixed situation at the end. It can be clearly seen that along the test the thermocline moves downwards thus verifying that erosion is the prevailing process rather than mixing via internal circulation.

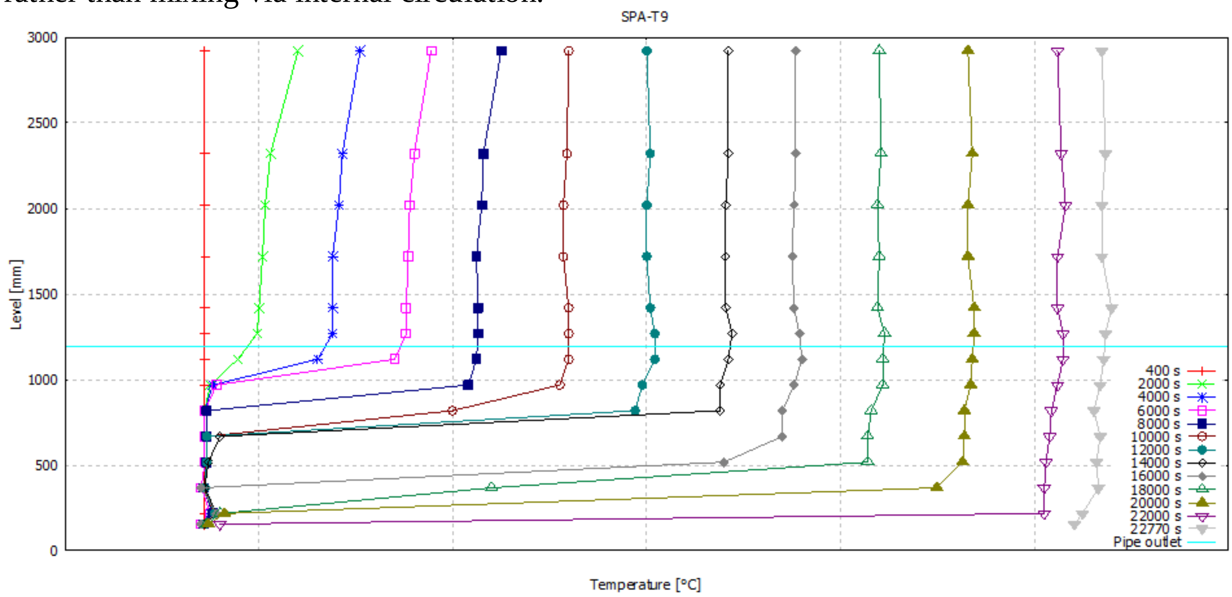

Figure 12. Development of vertical temperature profile of pool water in the SPA-T9 test.

4.3 PIV MEASUREMENTS

PIV measurements were conducted in the SPA-T8, SPA-T8R and SPA-T9 tests. The idea was to get detailed velocity field data from the vicinity of the thermocline to help in the development work of the EMS and EHS models by KTH.

4.3.1 PIV measurement parameters

The parameters for the PIV measurements done in the SPA-T8R and SPA-T9 tests were decided on the basis of the trial PIV measurements carried out during the SPA-T8 test, the results of which were otherwise disregarded due to the faulty flow meter.

In our PIV system the maximum amount of image pairs with the maximum measuring frequency of 7 Hz is around 350. After 350 image pairs the frequency drops to roughly 1-2 Hz depending on how fast the main computer can write the data files to the hard drive. 350 image pairs was chosen for the sample size to be used in the SPA-T8R and SPA-t9 tests.

The camera aperture was closed to the f-number value of 8 to increase the depth-of-field in order to achieve sharper particle images because the cameras were filming in angle towards the measurement plane and focusing the plane was not possible even with Scheimpflug adjustment. Closing the aperture more was not possible as the laser power would not have been enough.

The time between the images or laser pulses, *dt*, was set to 68490 µs. This resulted in a pixel displacement of around 5 pixels in SPA-T8R. That is also the maximum possible *dt* for the system. The laser was shot with maximum power in pulse A and with 95% power in pulse B to achieve equal intensity.

Rhodamin-doped fluorescent tracer particles were chosen because non-condensable gas has been a problem in the past experiments. The cameras were equipped with red filters to avoid reflections from non-condensable gas bubbles which can act as tracer particles if traditional tracers e.g. glass hollow spheres are used.

Nine different PIV measurement series of 350 image pairs were recorded during the SPA-T8R test and eleven series during the SPA-T9 test. The times spans of the PIV measurement series expressed with the help of time running from the start of recording of all the other measurements are presented in Table 3 for SPA-T8R and in Table 4 for SPA-T9.

Table 3. Time intervals of the PIV measurements for SPA-T8R

PIV series	Time from start of test
Test1	1363 s – 1413 s
Test2	1680 s – 1730 s
Test3	2100 s – 2150 s
Test4	3115 s – 3165 s
Test5	3496 s – 3546 s
Test6	3900 s – 3950 s
Test7	4185 s – 4235 s
Test8	4617 s – 4667 s
Test9	5370 s – 5420 s

Table 4. Time intervals of the PIV measurements for SPA-T9

PIV series	Time from start of test
Test1	2155 s – 2205 s
Test2	4949 s – 4999 s
Test3	7765 s – 7815 s
Test4	9954 s – 10004 s
Test5	10284 s – 10334 s
Test6	10549 s – 10599 s
Test7	10857 s – 10907 s
Test8	14835 s – 14885 s
Test9	18420 s – 18470 s
Test10	20450 s – 20500 s
Test11	21963 s – 22013 s

4.3.2 Quality of results

The quality of the PIV measurement results varied depending on the optical circumstances. Particle images of reasonable quality considering particle movement were obtained from velocity fields in the SPA-T8R test before the optical refractive index changed at the level of the laser window and made the image blurred. In the SPA-T9 test, particle movement seemed to be almost stagnant in those few measurement series where there were no other problems that prevented us from getting good quality images. Reason for the small particle movement and thus for low velocities at the elevation of the PIV measurement windows is the fact that in SPA-T9 the thermocline was on a higher elevation after the stratification phase than in SPA-T8R.

The system's maximum *dt* is 68490 microseconds. The PIV system's manufacturer states that PIV can measure with shifts between 0.2-0.5 pixels which is the case for the almost stagnant series in SPA-T9. But when pixel movement is so low, possible misalignment of the laser sheets can also have an effect on the results because the misalignment in pixels can be in the same range or even more in some parts of the measurement area.

After processing the PIV images, all vector fields were inspected. Also the particle images were inspected to find the sequences of the measurement series where the particle images were mostly aberration free and the respective vector fields had not missing vectors or were affected by spurious vectors to high numbers. The following Tables from 5 to 8 list all the sequences with recognized flow patterns from the SPA-T8R test. The time span of each measurement sequence is given within a decimal accuracy.

Table 5. PIV Test1 measurement sequences with recognized flow patterns from SPA-T8R

Measurement number	Time span of measurement	Number of image pairs
SPA-8R Test1-1	1363 s – 1367,7 s	33
SPA-8R Test1-2	1380,1 s – 1383,7 s	25
SPA-8R Test1-3	1386,6 s – 1390,9 s	30
SPA-8R Test1-4	1405,9 s – 1411,6 s	40

Table 6. PIV Test2 measurement sequences with recognized flow patterns from SPA-T8R

Measurement number	Time span of measurement	Number of image pairs
SPA-8R Test2-1	1680 s – 1684,3 s	30
SPA-8R Test2-2	1688,6 s – 1695,7 s	50
SPA-8R Test2-3	1703,6 s – 1707,1 s	25
SPA-8R Test2-4	1717,1 s – 1721,4 s	30

Table 7. PIV Test3 measurement sequences with recognized flow patterns from SPA-T8R

Measurement number	Time span of measurement	Number of image pairs
SPA-8R Test3-1	2100 s – 2104,3 s	30
SPA-8R Test3-2	2137,1 s – 2141,4 s	30
SPA-8R Test3-3	2140 s – 2145,7 s	40

Table 8. PIV Test4 measurement sequences with recognized flow patterns from SPA-T8R

Measurement number	Time span of measurement	Number of image pairs
SPA-8R Test4-1	3115 s – 3120 s	35
SPA-8R Test4-2	3127,1 s – 3130 s	25
SPA-8R Test4-3	3132,1 s – 3135,7 s	25
SPA-8R Test4-4	3152,1 s – 3156,4	30
SPA-8R Test4-5	3156,6 s – 3160,7 s	30
SPA-8R Test4-6	3162,1 s – 3165 s	20

For the SPA-T9 test, averaged vector fields can’t be presented due to different of problems that occurred throughout the whole measurement. For the tests 1-3 the particle movement was below a single pixel which allows errors in the alignment of the laser sheet to dominate the result. For the tests 4-8 the aberrations for cameras or/and for laser were dominating thus leaving particle images blurred. Tests 9-11 produced better quality particle images but the seeding density of particles had become too low due to increased water temperature along the test and therefore most particles had fallen to the bottom of the wetwell pool of PPOOLEX. To overcome this problem in future different sets of particles with different densities should be used and fed to the wetwell pool if notable increase in pool temperature is expected over the duration of the test.

4.3.3 PIV results

In this chapter the PIV measurement results of the SPA-T8R Test1-1 are presented with uncertainty quantification for all vector components. In Figure 13 the averaged vector field of the flow pattern that existed for 33 consecutive image pairs is presented. The vertical axis refers to the distance from the pool bottom in millimetres. The zero point of the horizontal axis is at the centre line of the calibration plate.

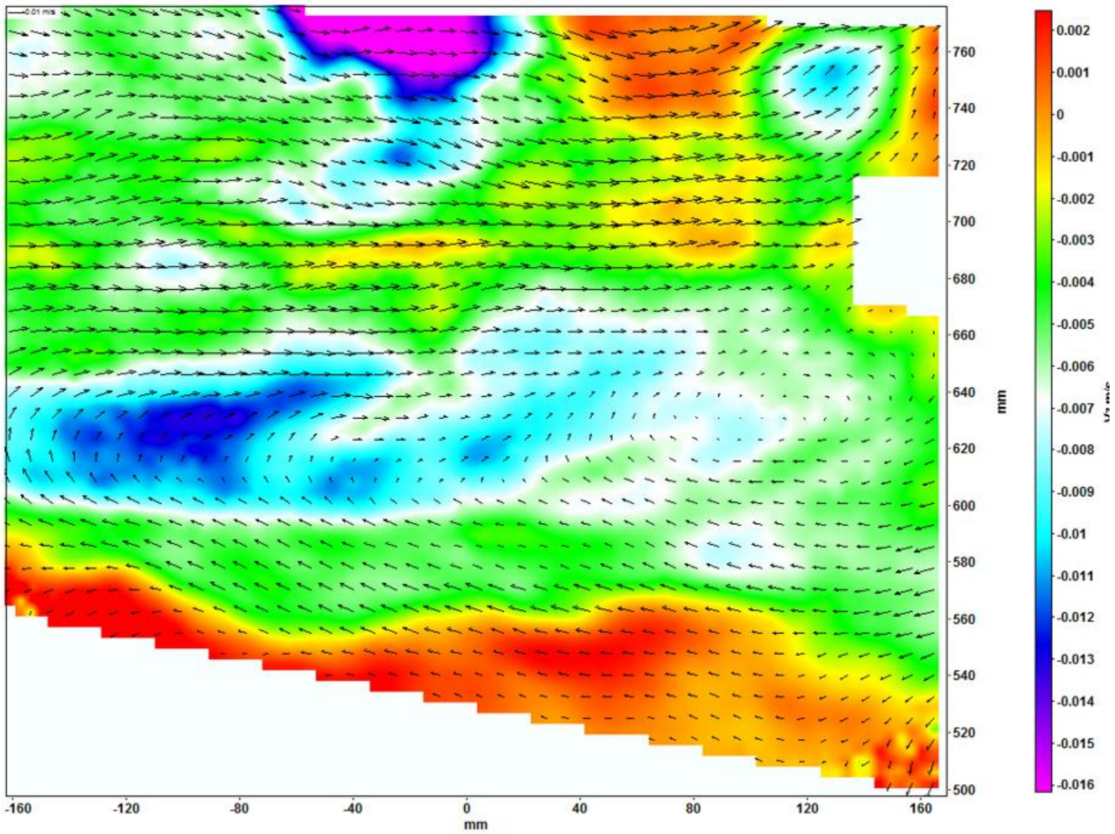

Figure 13. Averaged vector field of PIV Test1-1 measurement from SPA-T8R.

The vector represents the x and y components and the background colour the z component. Every other vector horizontally and vertically has been removed for easier interpretation of the averaged vector field. Camera 1 in Figure 2 was affected by a reflection from a support rig of the thermocouple train and thus a rectangular area above the centre line on the right side has been masked out. The reference vector of 0.01 m/s is shown on the top left corner of the vector field. The averaged vector field components and respective uncertainty fields are presented in Figures 14-16.

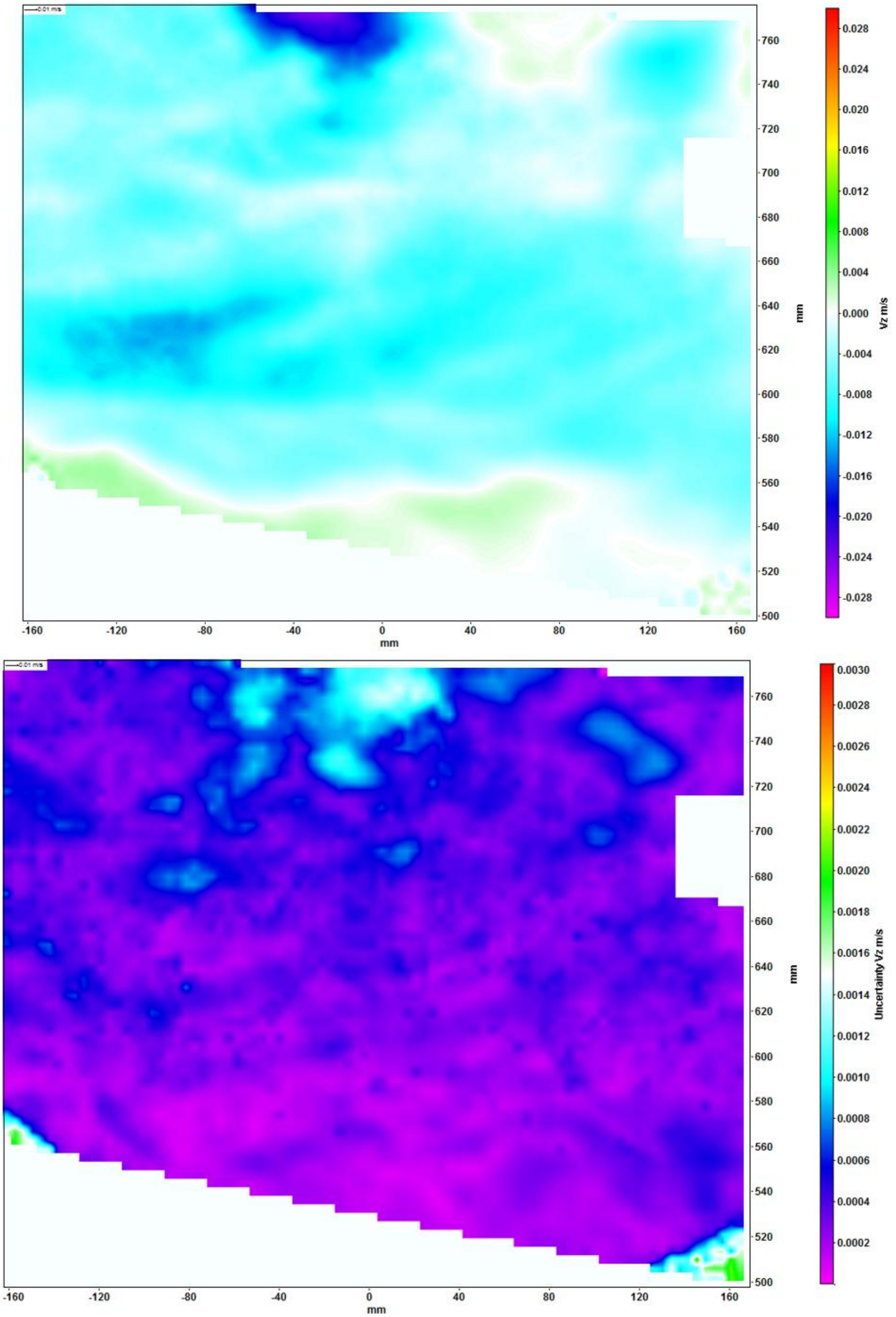

Figure 14. On top the V_z component and below the uncertainty field of V_z.

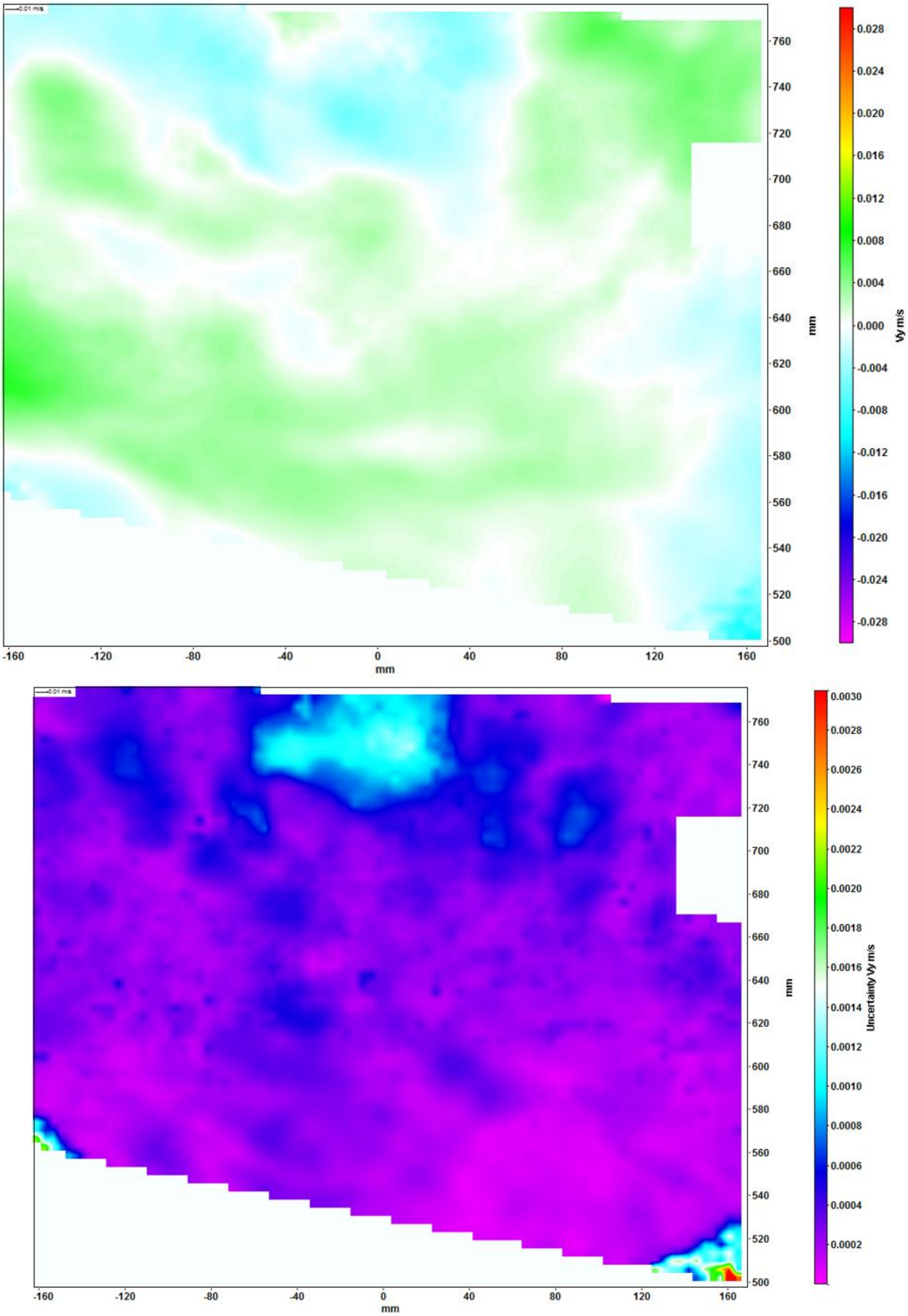

Figure 15. On top the V_y component and below the uncertainty field of V_y.

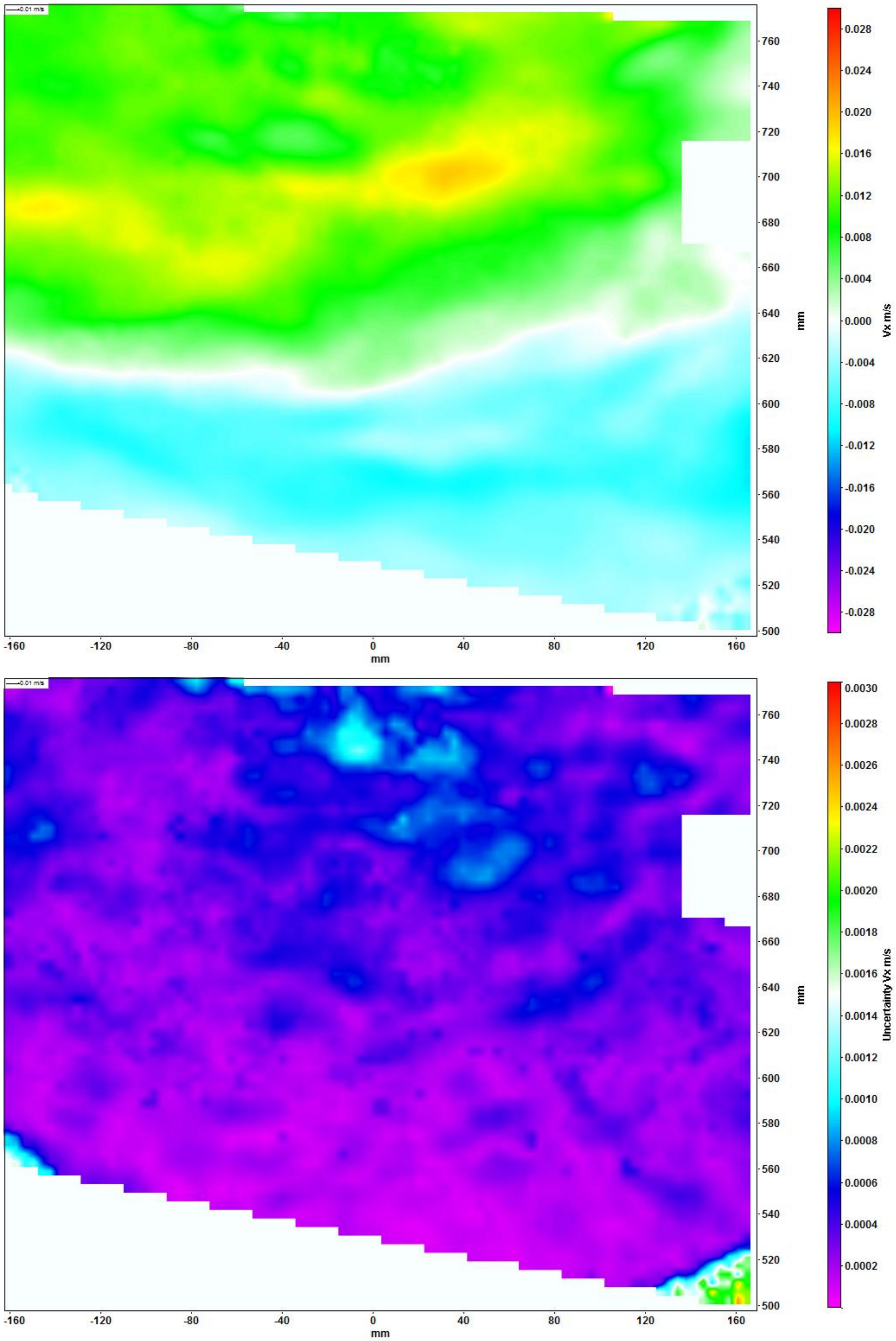

Figure 16. On top the V_x component and below the uncertainty field of V_x.

The averaged vector fields and uncertainty fields for the other PIV measurements sequences from SPA-T8R listed in Tables 5-8 are presented in the Appendix 4.

4.3.4 Conclusions from PIV measurements

The few sequences with recognized flow patterns from the SPA-T8R test indicate that some kind of swirls could exist at the elevation of the thermocline. The flow direction just under the thermocline can also be opposite to that just above the thermocline. Due to the limited number of good quality flow pattern data obtained from the tests it is no use trying to conclude in detail on the basis of the PIV measurements how the erosion process actually proceeds. However, some flow field information from the short duration measurement sequences might be useful in the development work of simulation tools and models, particularly the EMS and EHS models, and therefore all the data with recognized flow patterns are included as an appendix to this report.

The exact quality of the PIV results is hard to define. The software used for processing were able to analyse vector fields in most cases when the aberrations were at a minimal level. For the SPA-T9 test the movement of the particles was almost non-existent before the optical environment became too harsh to execute PIV measurement successfully. Going through all the vector field data and estimating overall quality of the particle images is very time consuming when the conditions are optically as challenging as they were in SPA-T8R and SPA-T9.

The somewhat chaotic nature of the investigated phenomenon also creates problems when measuring with a slow-speed PIV system. The amount of data that can be gathered from individual short lasting flow patterns is limited. Time-averaging without good statistics is questionable although DaVis is offering Uncertainty quantification to give indication of the uncertainties within the results. Getting comparable data would give more reliability to the results as the overall measurement environment is very challenging and the nature of the flow is more or less chaotic. Also creating measurement schemes that could give indications of how one parameter affects the results is nearly impossible in PPOOLEX due to the complexity of the set-up. Thus the results are advised to be treated as qualitative instead of quantitative.

One option to overcome these problems would be to measure with a high-speed system to either to gather more data on the short-lived flow patterns or obtaining time-resolved data in general (more particle images from shorter turbulent flow patterns). But that would require an update to the laser of the system. Optically PIV measurements might benefit if the elevation of the thermocline and the measurement area were changed to an even more optimal place for the PIV cameras. For the almost stagnant flow field case reducing the measurement area might be beneficial by chancing the camera lenses. Thus there would be more pixels per mm and the particle shift would be more distinctive. Although the harsh optical environment would still exist.

5 SUMMARY AND CONCLUSIONS

This report summarizes the results of the two sparger pipe tests (SPA-T8R and SPA-T9) carried out in the PPOOLEX facility at LUT in 2016. The test facility is a closed stainless steel vessel divided into two compartments, drywell and wetwell. In the SPA tests the drywell compartment was bypassed i.e. the sparger pipe in the wetwell was connected directly to the steam line coming from the PACTEL facility which acted as a steam source.

The main objective of the tests was to obtain data for the development of the Effective Momentum Source (EMS) and Effective Heat Source (EHS) models to be implemented in GOTHIC code by KTH. Originally the models were developed for straight blowdown pipes but KTH plans to extend the EMS and EHS models to cover also situations where steam injection into the pool is via a sparger pipe. The test parameters were selected by KTH on the basis of pre-test simulations and analysis of the results of the earlier sparger tests in PPOOLEX. Particularly the behaviour of the thermocline between the cold and warm water volumes was of interest. For this purpose also PIV measurements were tried during the tests.

In both tests steam injection into the pool was only through the holes at the sparger head because the holes of the LRR were blocked. In SPA-T8R all the 32 injection holes in four rows at the sparger head were open while in SPA-T9 only the eight holes in the bottom row were open and the rest were blocked. In SPA-T8R there was a stratification phase and an erosion phase with a moderate steam flow rate and then a final mixing phase with a clearly higher flow rate. In SPA-T9 a stratified situation was first created with a suitable steam flow rate and then the flow rate was increased in small steps until the whole pool was mixed.

In SPA-T8R the thermocline seemed to be around the elevation of 670 mm at the end of the stratification phase just as predicted by the pre-test simulations. However, the thickness of the thermocline was larger than expected. The thermocline moved downwards as the erosion process progressed. The prevailing mixing mechanism during the final mixing phase was also erosion rather than internal circulation.

In SPA-T9 the thermocline was at first clearly at a higher elevation than in SPA-T8R. It then started to shift downwards as the flow rate was increased in small steps. Complete mixing of the pool was achieved with quite a small steam mass flow rate, i.e. 85 g/s. Looking at the direct condensation mode map for pure steam discharge of Chan and Lee reveals that corresponding mass flux value is about 212 kg/m^{2}s. This is a bigger value than the figure 155 kg/m^{2}s corresponding to the 250 g/s flow rate used during the final mixing phase in the SPA-T8R test when all the injection holes in the sparger head were open. Erosion was again the prevailing mechanism in the mixing process of SPA-T9.

The few sequences with recognized flow patterns from the PIV measurements from SPA-T8R indicate that some kind of swirls could exist at the elevation of the thermocline. The flow direction just under the thermocline can also be opposite to that just above the thermocline. The somewhat chaotic nature of the investigated phenomenon creates problems when measuring with a slow-speed PIV system and therefore definitive conclusions on the detailed behaviour of the thermocline can’t be made. However, certain flow field information from the obtained short duration measurement sequences may be useful in the development work of simulation tools and models.

The mixing mechanism in the SPA-T8R and SPA-T9 tests was somewhat different than in many previous tests done in PPOOLEX either with a straight blowdown pipe or with a sparger pipe. Now, the layers of cold water slowly eroded rather than mixed through internal circulation as has been the case in most of the tests carried out before. As a result the thermocline region shifted slowly downwards as the mixing process proceeded. These tests in PPOOLEX verified that mixing of a thermally stratified water pool can happen through an erosion process instead of internal circulation if suitable flow conditions prevail.

6 REFERENCES

1. Puustinen, M., Laine, J., Räsänen, A., PPOOLEX Experiments on Thermal Stratification and Mixing. Lappeenranta University of Technology. 2009. Research Report CONDEX 1/2008.
2. Laine, J., Puustinen, M., PPOOLEX Experiments on Wall Condensation. Lappeenranta University of Technology. 2009. Research Report CONDEX 3/2008.
3. Laine, J., Puustinen, M., Räsänen, A., PPOOLEX Experiments with a Modified Blowdown Pipe Outlet. Lappeenranta University of Technology. 2009. Research Report CONDEX 2/2008.
4. Laine, J., Puustinen, M., Räsänen, A., PPOOLEX Experiments with Two Parallel Blowdown Pipes. Lappeenranta University of Technology. 2010. Research Report CONDEX 1/2009.
5. Puustinen, M., Laine, J., Räsänen, A., PPOOLEX Experiments on Dynamic Loading with Pressure Feedback. Lappeenranta University of Technology. 2010. Research Report CONDEX 2/2009.
6. Laine, J., Puustinen, M., Räsänen, A., Tanskanen, V., PPOOLEX Experiments on Stratification and Mixing in the Wet Well Pool. Lappeenranta University of Technology. 2011. Research Report CONDEX 1/2010.
7. Puustinen, M., Laine, J., Räsänen, A., Multiple Blowdown Pipe Experiment with the PPOOLEX Facility. Lappeenranta University of Technology. 2011. Research Report CONDEX 2/2010.
8. Puustinen, M., Laine, J., Räsänen, A., PPOOLEX Experiments with a Blowdown Pipe Collar. Lappeenranta University of Technology. 2012. Research Report EXCOP 1/2011.
9. Laine, J., Puustinen, M., Räsänen, A., PPOOLEX Experiments on the Dynamics of Free Water Surface in the Blowdown Pipe. Lappeenranta University of Technology. 2013. Research Report EXCOP 2/2012.
10. Laine, J., Puustinen, M., Räsänen, A., PPOOLEX Mixing Experiments. Lappeenranta University of Technology. 2014. Research Report EXCOP 1/2013.
11. Gamble, R. E., Nguyen, T. T., Peterson, P. F., Pressure suppression pool mixing in passive advanced BWR plants. Nuclear Engineering and Design, 204, 321-336, 2000.
12. Li, H., Villanueva, W., Kudinov, P., Effective Models for Simulation of Thermal Stratification and Mixing Induced by Steam Injection into a Large Pool of Water. Division of Nuclear Power Safety, Royal Institute of Technology (KTH), NORTHNET Roadmap 3 Research report, Stockholm, 2014.
13. Laine, J. Puustinen, M. Räsänen, A., PPOOLEX Experiments with a Sparger. Lappeenranta University of Technology. 2015. Research Report EXCOP 1/2014.
14. Puustinen, M., Laine, J., Räsänen, A., Additional Sparger Tests in PPOOLEX with Reduced Number of Injection Holes. Lappeenranta University of Technology. 2016. Research Report INSTAB 1/2015.
15. Puustinen, M., Partanen, H., Räsänen, A., Purhonen, H., PPOOLEX Facility Description. Lappeenranta University of Technology. 2007. Technical Report POOLEX 3/2006.
16. Tuunanen, J., Kouhia, J., Purhonen, H., Riikonen, V., Puustinen, M., Semken, R. S., Partanen, H., Saure, I., Pylkkö, H., General Description of the PACTEL Test Facility. Espoo: VTT. 1998. VTT Research Notes 1929. ISBN 951-38-5338-1.
17. Räsänen, A., Mittausjärjestelmä lauhtumisilmiöiden tutkimukseen. Lappeenranta University of Technology. 2004. Master's Thesis. In Finnish.
18. Kudinov, P., PPOOLEX-SPA T8 test specifications. Email from KTH, November 23rd 2016.
19. Kudinov, P., PPOOLEX-SPA T9 test specifications, Email form KTH, December 9th 2106.
20. Chan, C. K., Lee, C. K. B., A Regime Map for Direct Contact Condensation. Int. J. Multiphase Flow. 1982.

APPENDIX 1: PPOOLEX drawings

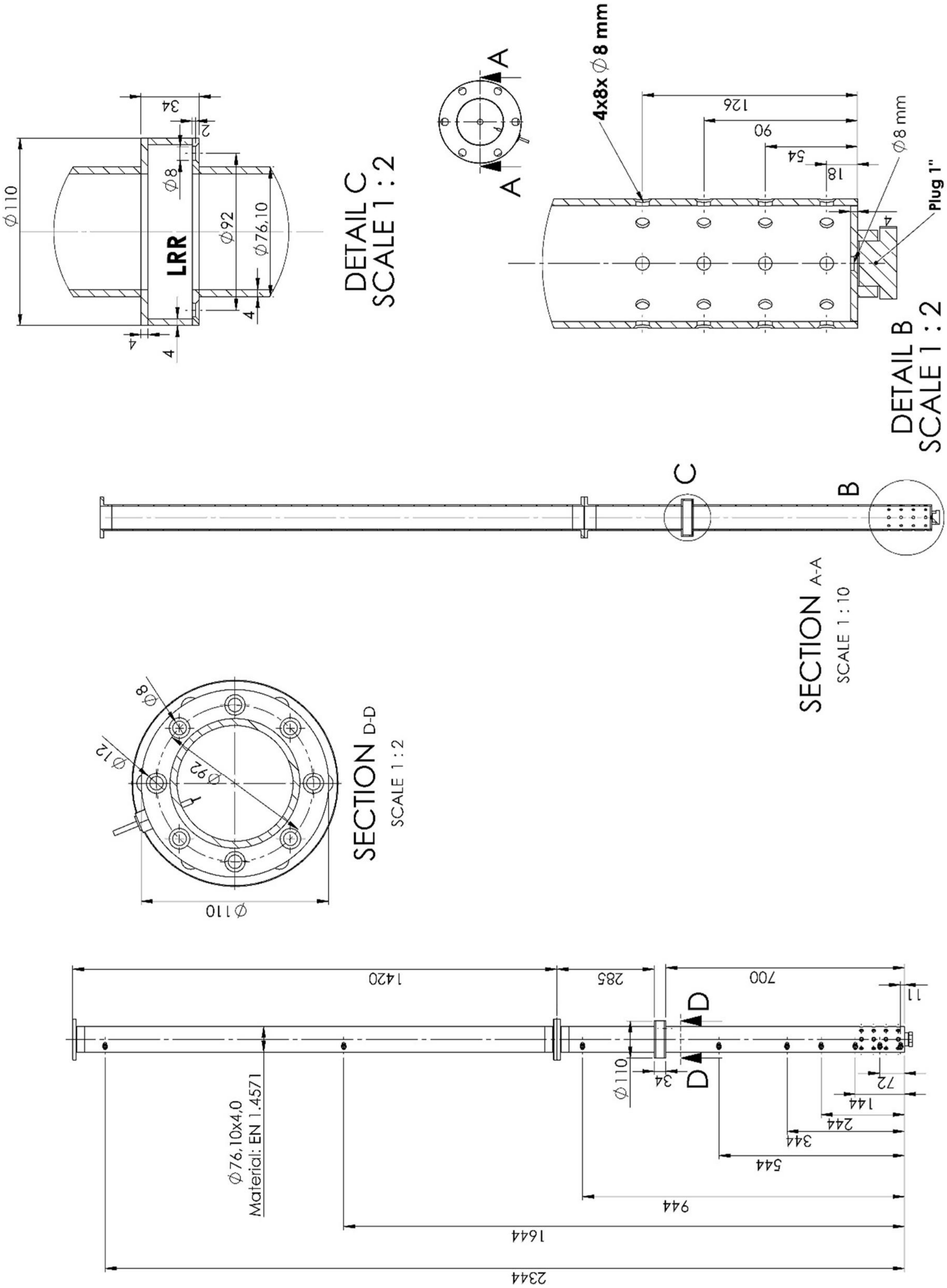

DN65 sparger pipe.

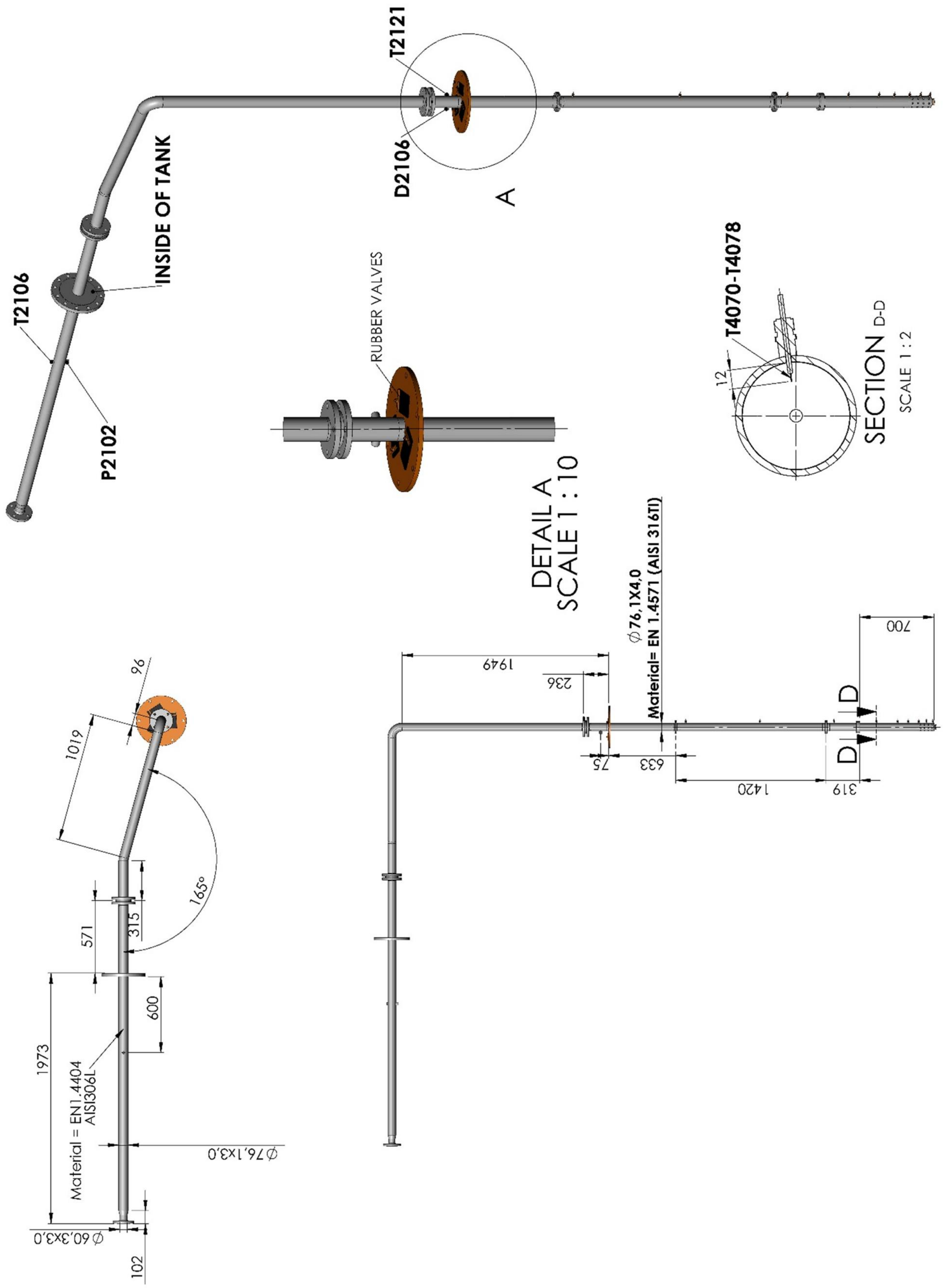

DN65 steam line.

APPENDIX 2: PPOOLEX instrumentation

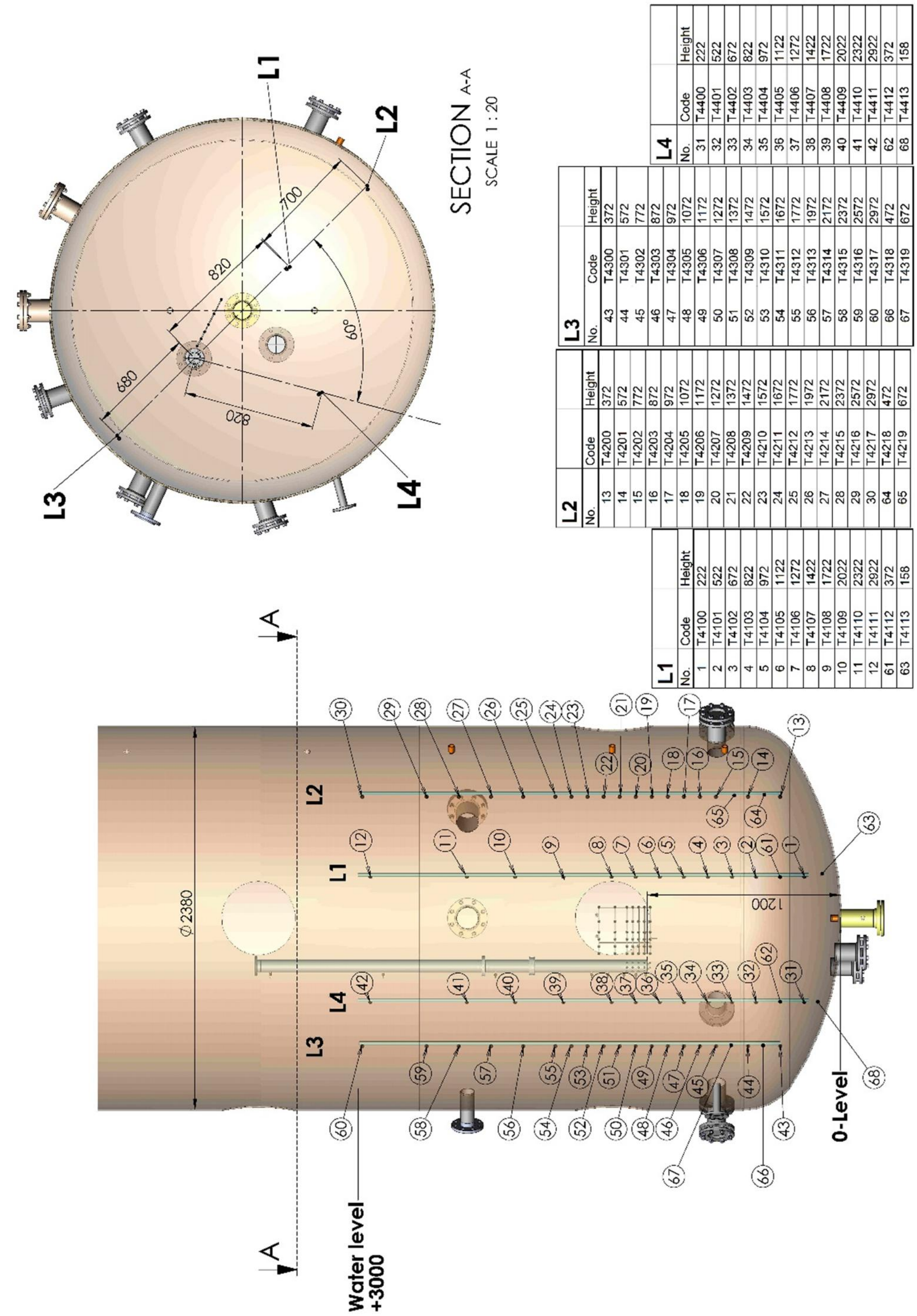

L1 No.	Code	Height
1	T4100	222
2	T4101	522
3	T4102	672
4	T4103	822
5	T4104	972
6	T4105	1122
7	T4106	1272
8	T4107	1422
9	T4108	1722
10	T4109	2022
11	T4110	2322
12	T4111	2922
61	T4112	372
63	T4113	158

L2 No.	Code	Height
13	T4200	372
14	T4201	572
15	T4202	772
16	T4203	872
17	T4204	972
18	T4205	1072
19	T4206	1172
20	T4207	1272
21	T4208	1372
22	T4209	1472
23	T4210	1572
24	T4211	1672
25	T4212	1772
26	T4213	1972
27	T4214	2172
28	T4215	2372
29	T4216	2572
30	T4217	2972
64	T4218	472
65	T4219	672

L3 No.	Code	Height
43	T4300	372
44	T4301	572
45	T4302	772
46	T4303	872
47	T4304	972
48	T4305	1072
49	T4306	1172
50	T4307	1272
51	T4308	1372
52	T4309	1472
53	T4310	1572
54	T4311	1672
55	T4312	1772
56	T4313	1972
57	T4314	2172
58	T4315	2372
59	T4316	2572
60	T4317	2972
66	T4318	472
67	T4319	672

L4 No.	Code	Height
31	T4400	222
32	T4401	522
33	T4402	672
34	T4403	822
35	T4404	972
36	T4405	1122
37	T4406	1272
38	T4407	1422
39	T4408	1722
40	T4409	2022
41	T4410	2322
42	T4411	2922
62	T4412	372
68	T4413	158

Four trains of temperature measurements in the wetwell.

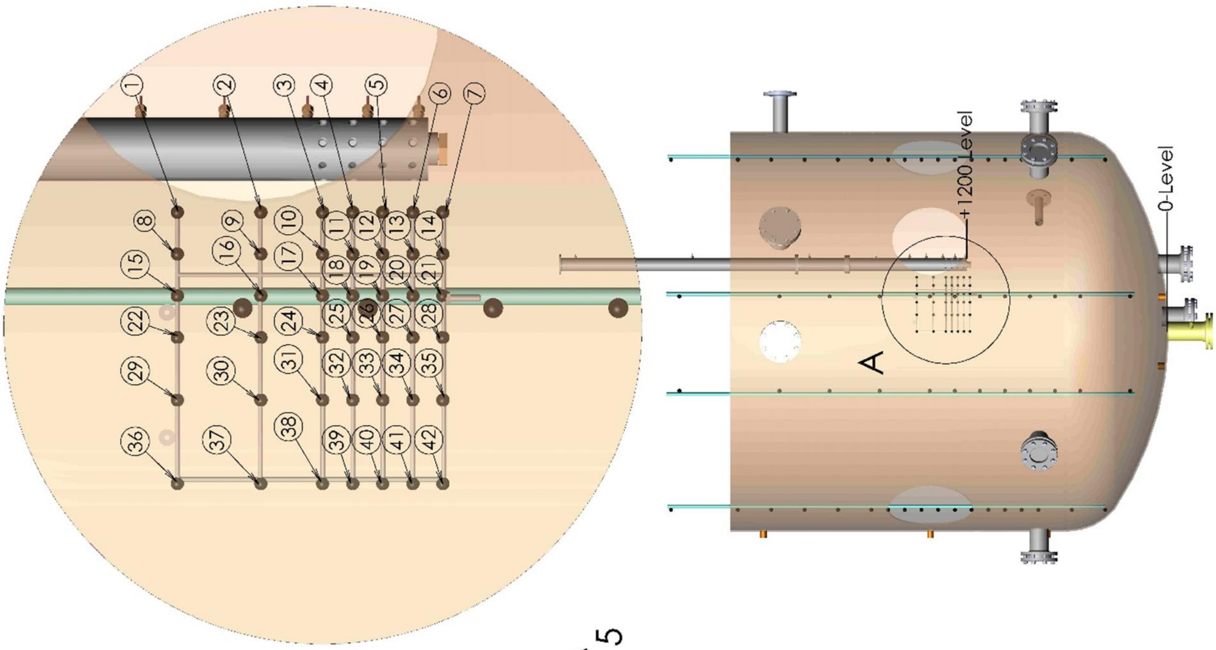

No.	Code	No.	Code	No.	Code
1	T4000	16	T4021	31	T4042
2	T4001	17	T4022	32	T4043
3	T4002	18	T4023	33	T4044
4	T4003	19	T4024	34	T4045
5	T4004	20	T4025	35	T4046
6	T4005	21	T4026	36	T4050
7	T4006	22	T4030	37	T4051
8	T4010	23	T4031	38	T4052
9	T4011	24	T4032	39	T4053
10	T4012	25	T4033	40	T4054
11	T4013	26	T4034	41	T4055
12	T4014	27	T4035	42	T4056
13	T4015	28	T4036		
14	T4016	29	T4040		
15	T4020	30	T4041		

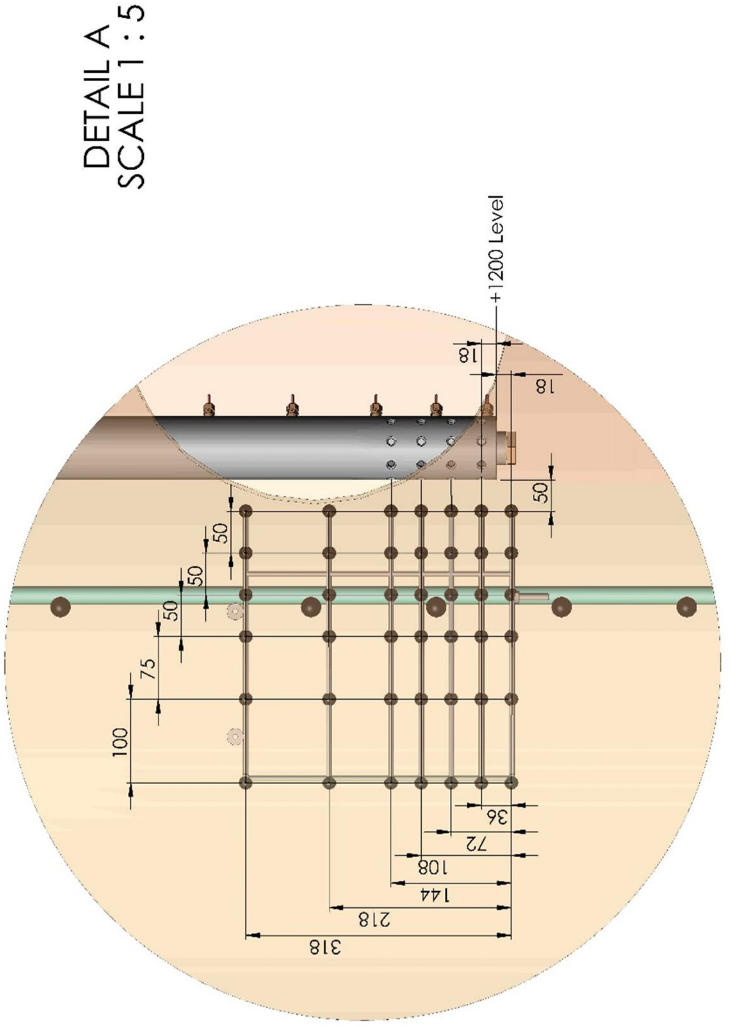

6x7 grid of temperature measurements in the wetwell.

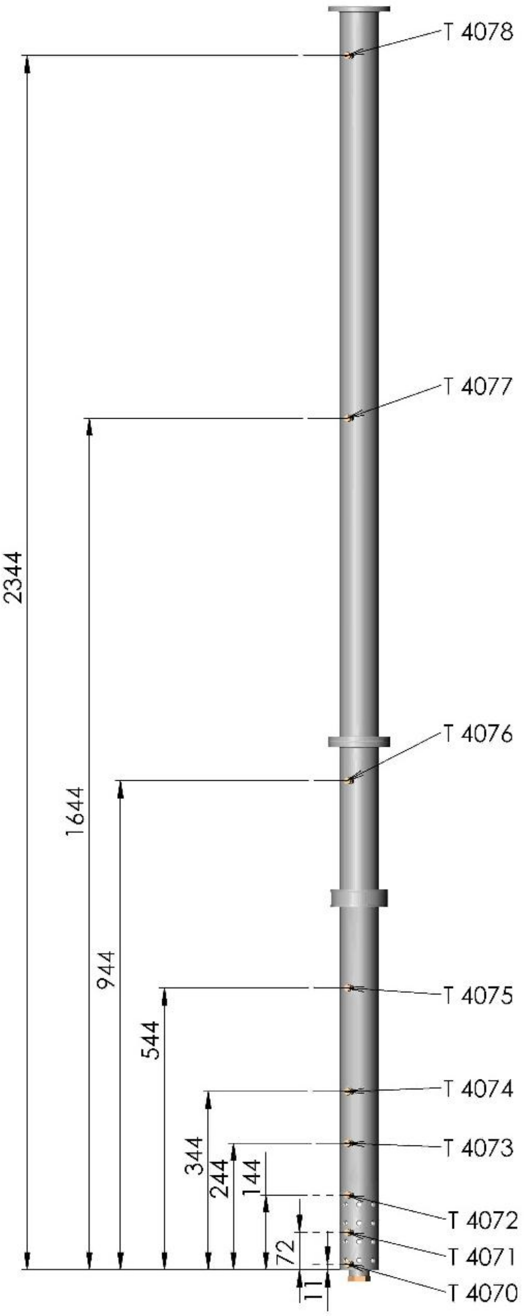

Temperature measurements inside the sparger pipe.

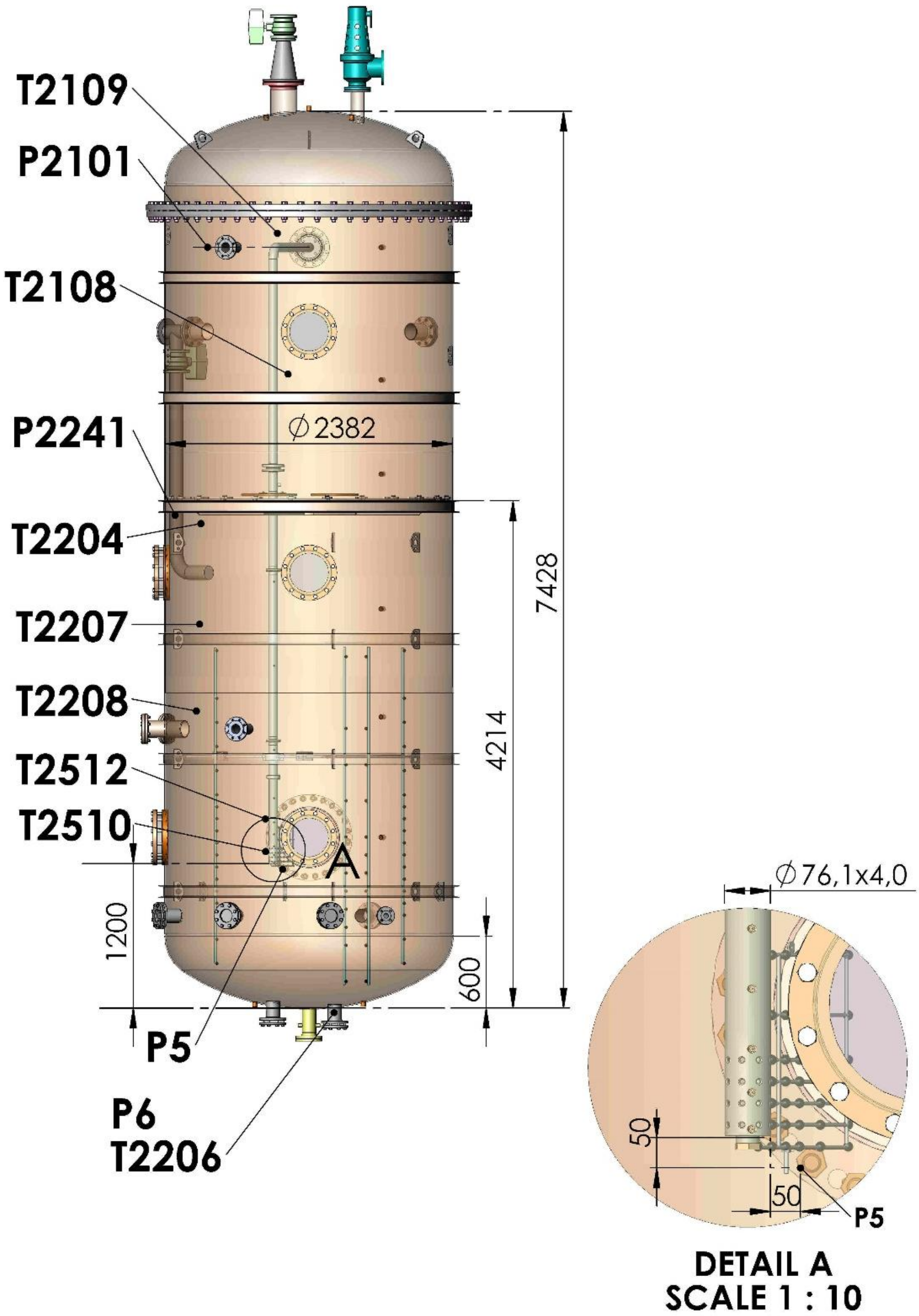

Test vessel measurements.

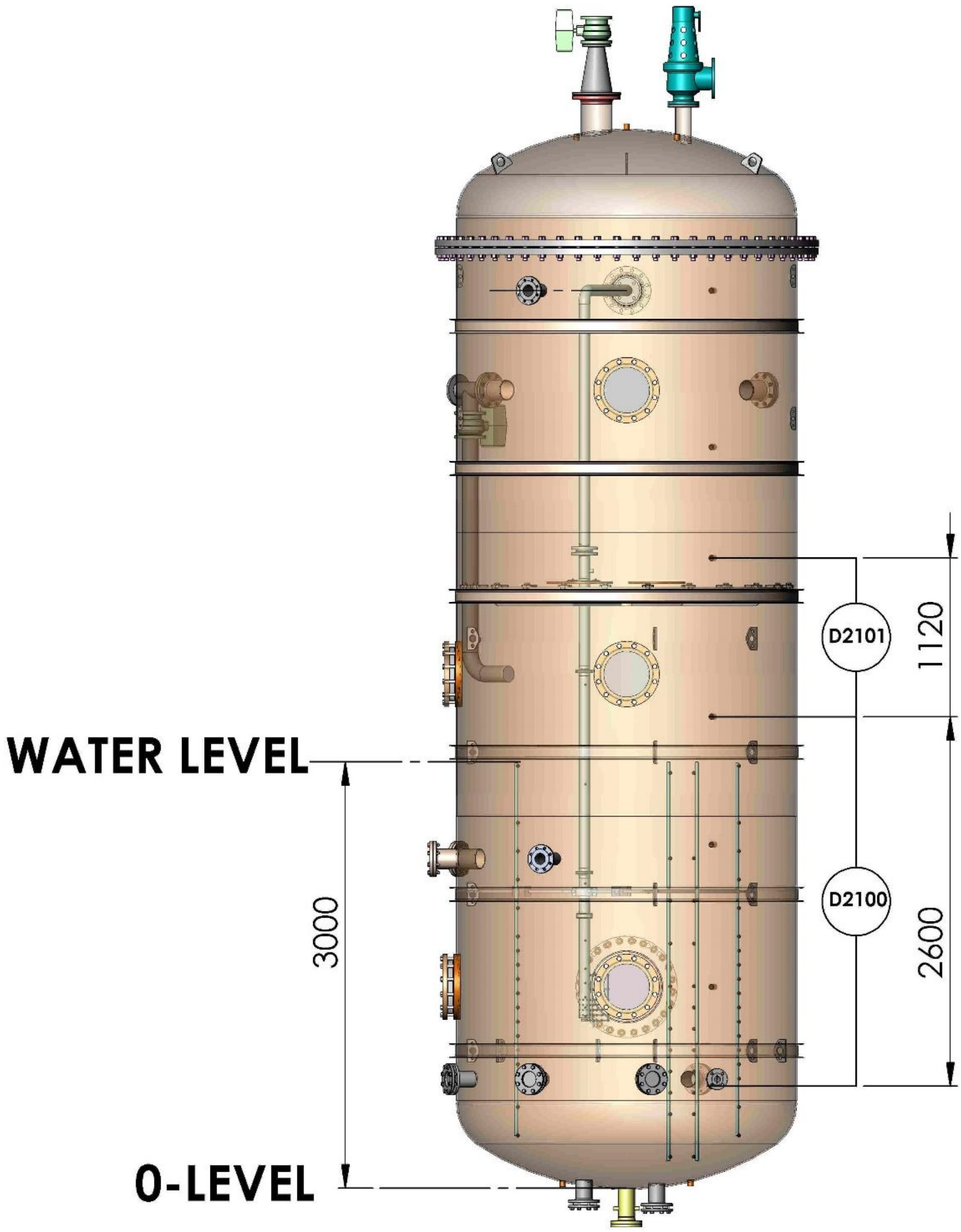

Pressure difference measurements. Nominal water level is 3.0 m.

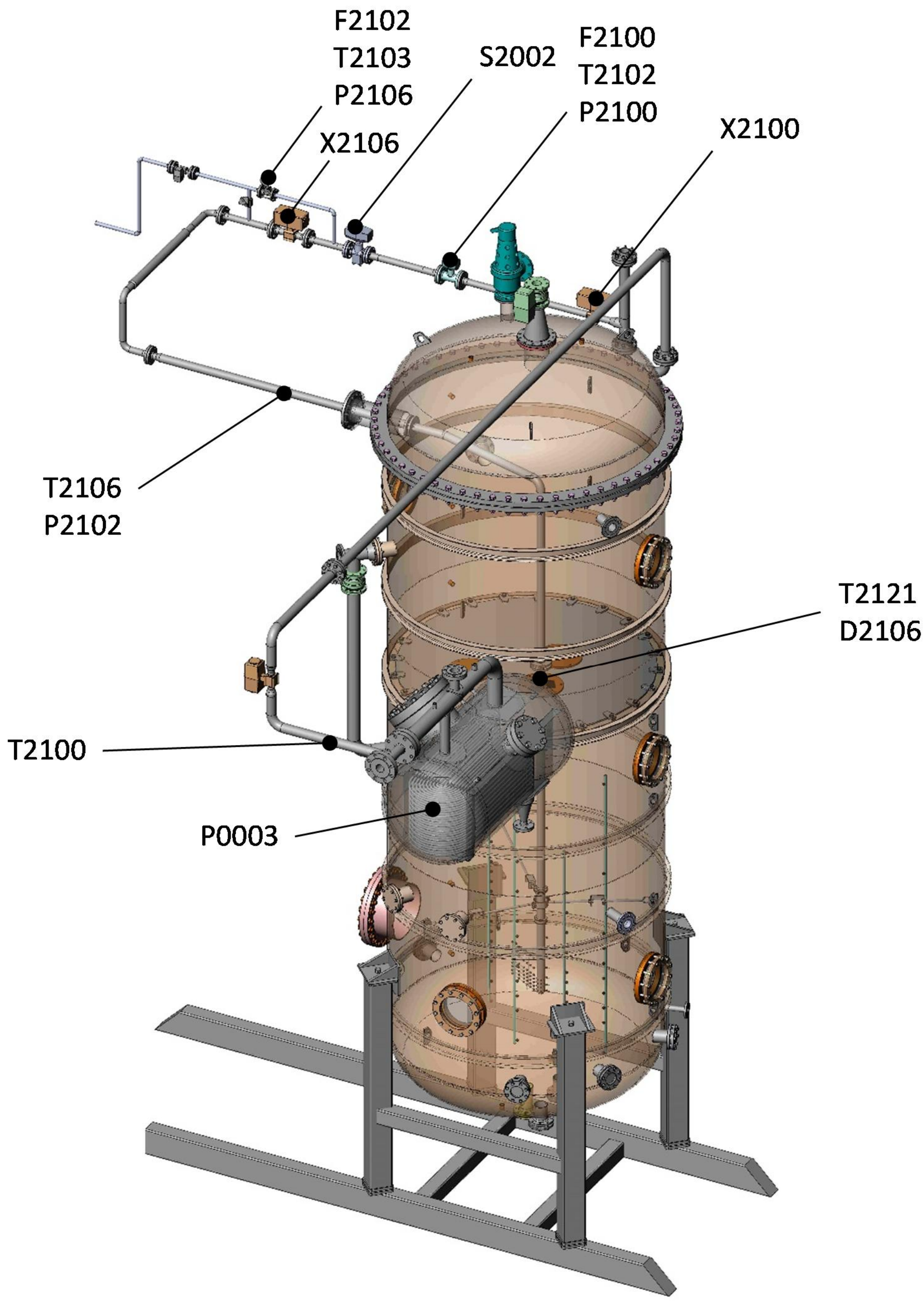

Measurements in the steam line.

Open your mind. LUT.
Lappeenranta University of Technology

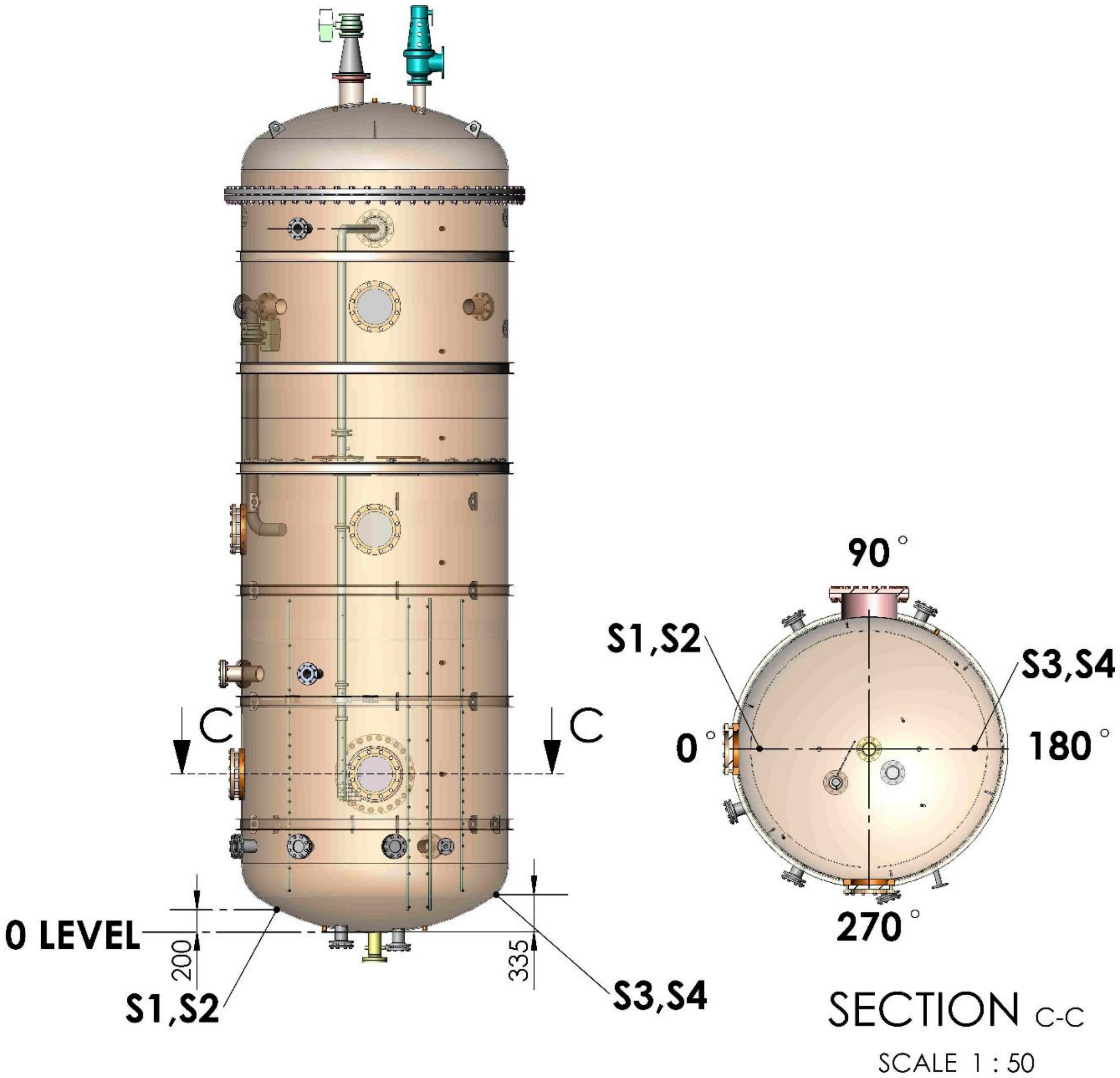

Strain gauges on the outer wall of the pool bottom.

Measurement	Code	Elevation	Location	Error estimation	Measurement software
Camera trigger	C1	-	Wetwell	Not defined	LabView
Pressure difference	D2100	700–3300	Wetwell	±0.05 m	FieldPoint
Pressure difference	D2101	3300–4420	Wetwell–drywell	±4 000 Pa	FieldPoint
Pressure difference	D2106	4347	Blowdown pipe–drywell	±3 000 Pa	FieldPoint
Flow rate	F2100	-	DN50 steam line	±5 l/s	FieldPoint
Flow rate	F2102	-	DN25 steam line	±0.7 l/s	FieldPoint
Pressure	P0003	-	Steam generator 1	±0.3 bar	FieldPoint
Pressure	P0004	-	Steam generator 2	±0.3 bar	FieldPoint
Pressure	P0005	-	Steam generator 3	±0.3 bar	FieldPoint
Pressure	P5	1150	Blowdown pipe outlet	±0.7 bar	LabView
Pressure	P6	-15	Wetwell bottom	±0.5 bar	LabView
Pressure	P2100	-	DN50 steam line	±0.2 bar	FieldPoint
Pressure	P2101	6300	Drywell	±0.03 bar	FieldPoint
Pressure	P2102	-	Inlet plenum	±0.03 bar	FieldPoint
Pressure	P2106	-	DN25 steam line	±0.06 bar	FieldPoint
Pressure	P2241	4200	Wetwell gas space	±0.05 bar	FieldPoint
Control valve position	S2002	-	DN50 Steam line	Not defined	FieldPoint
Strain	S1	200	Bottom segment	Not defined	LabView
Strain	S2	200	Bottom segment	Not defined	LabView
Strain	S3	335	Bottom segment	Not defined	LabView
Strain	S4	335	Bottom segment	Not defined	LabView
Temperature	T1279	-3260	Laboratory	±0.1 °C	FieldPoint
Temperature	T1280	-1260	Laboratory	±0.1 °C	FieldPoint
Temperature	T1281	740	Laboratory	±1.8 °C	FieldPoint
Temperature	T1282	2740	Laboratory	±0.1 °C	FieldPoint
Temperature	T1283	4740	Laboratory	±0.1 °C	FieldPoint
Temperature	T1284	6740	Laboratory	±0.1 °C	FieldPoint
Temperature	T1285	8740	Laboratory	±0.1 °C	FieldPoint
Temperature	T2100	-	DN80 steam line	±3 °C	FieldPoint
Temperature	T2102	-	DN50 steam line	±2 °C	FieldPoint
Temperature	T2103	-	DN25 steam line	±2 °C	FieldPoint
Temperature	T2106	-	Inlet plenum	±2 °C	FieldPoint
Temperature	T2108	5200	Drywell	±2 °C	FieldPoint
Temperature	T2109	6390	Drywell	±2 °C	FieldPoint
Temperature	T2121	4347	Blowdown pipe	±2 °C	FieldPoint
Temperature	T2204	4010	Wetwell gas space	±2 °C	FieldPoint
Temperature	T2206	-15	Wetwell bottom	±2 °C	FieldPoint
Temperature	T2207	3185	Wetwell gas space	±2 °C	FieldPoint
Temperature	T2208	2360	Wetwell gas space	±2 °C	FieldPoint
Temperature	T2510	1295	Wetwell	±2 °C	FieldPoint
Temperature	T2512	1565	Wetwell	±2 °C	FieldPoint
Temperature	T4000	1500	Wetwell	±2 °C	FieldPoint
Temperature	T4001	1400	Wetwell	±2 °C	LabView
Temperature	T4002	1326	Wetwell	±2 °C	LabView
Temperature	T4003	1290	Wetwell	±2 °C	LabView
Temperature	T4004	1254	Wetwell	±2 °C	LabView
Temperature	T4005	1218	Wetwell	±2 °C	LabView

Temperature	T4006	1182	Wetwell	±2 °C	LabView
Temperature	T4010	1500	Wetwell	±2 °C	FieldPoint
Temperature	T4011	1400	Wetwell	±2 °C	LabView
Temperature	T4012	1326	Wetwell	±2 °C	LabView
Temperature	T4013	1290	Wetwell	±2 °C	LabView
Temperature	T4014	1254	Wetwell	±2 °C	LabView
Temperature	T4015	1218	Wetwell	±2 °C	LabView
Temperature	T4016	1182	Wetwell	±2 °C	LabView
Temperature	T4020	1500	Wetwell	±2 °C	LabView
Temperature	T4021	1400	Wetwell	±2 °C	LabView
Temperature	T4022	1326	Wetwell	±2 °C	LabView
Temperature	T4023	1290	Wetwell	±2 °C	LabView
Temperature	T4024	1254	Wetwell	±2 °C	LabView
Temperature	T4025	1218	Wetwell	±2 °C	LabView
Temperature	T4026	1182	Wetwell	±2 °C	LabView
Temperature	T4030	1500	Wetwell	±2 °C	LabView
Temperature	T4031	1400	Wetwell	±2 °C	LabView
Temperature	T4032	1326	Wetwell	±2 °C	LabView
Temperature	T4033	1290	Wetwell	±2 °C	LabView
Temperature	T4034	1254	Wetwell	±2 °C	LabView
Temperature	T4035	1218	Wetwell	±2 °C	LabView
Temperature	T4036	1182	Wetwell	±2 °C	LabView
Temperature	T4040	1500	Wetwell	±2 °C	FieldPoint
Temperature	T4041	1400	Wetwell	±2 °C	LabView
Temperature	T4042	1326	Wetwell	±2 °C	LabView
Temperature	T4043	1290	Wetwell	±2 °C	LabView
Temperature	T4044	1254	Wetwell	±2 °C	LabView
Temperature	T4045	1218	Wetwell	±2 °C	LabView
Temperature	T4046	1182	Wetwell	±2 °C	LabView
Temperature	T4050	1500	Wetwell	±2 °C	FieldPoint
Temperature	T4051	1400	Wetwell	±2 °C	FieldPoint
Temperature	T4052	1326	Wetwell	±2 °C	FieldPoint
Temperature	T4053	1290	Wetwell	±2 °C	FieldPoint
Temperature	T4054	1254	Wetwell	±2 °C	FieldPoint
Temperature	T4055	1218	Wetwell	±2 °C	FieldPoint
Temperature	T4056	1182	Wetwell	±2 °C	FieldPoint
Temperature	T4070	1211	Blowdown pipe	±2 °C	FieldPoint
Temperature	T4071	1272	Blowdown pipe	±2 °C	FieldPoint
Temperature	T4072	1344	Blowdown pipe	±2 °C	FieldPoint
Temperature	T4073	1444	Blowdown pipe	±2 °C	FieldPoint
Temperature	T4074	1544	Blowdown pipe	±2 °C	FieldPoint
Temperature	T4075	1744	Blowdown pipe	±2 °C	FieldPoint
Temperature	T4076	2144	Blowdown pipe	±2 °C	FieldPoint
Temperature	T4077	2844	Blowdown pipe	±2 °C	FieldPoint
Temperature	T4078	3544	Blowdown pipe	±2 °C	FieldPoint
Temperature	T4100	222	Wetwell	±2 °C	FieldPoint
Temperature	T4101	522	Wetwell	±2 °C	FieldPoint
Temperature	T4102	672	Wetwell	±2 °C	FieldPoint
Temperature	T4103	822	Wetwell	±2 °C	FieldPoint
Temperature	T4104	972	Wetwell	±2 °C	FieldPoint
Temperature	T4105	1122	Wetwell	±2 °C	FieldPoint
Temperature	T4106	1272	Wetwell	±2 °C	FieldPoint

Open your mind. LUT.
Lappeenranta University of Technology

Temperature	T4107	1422	Wetwell	±2 °C	FieldPoint
Temperature	T4108	1722	Wetwell	±2 °C	FieldPoint
Temperature	T4109	2022	Wetwell	±2 °C	FieldPoint
Temperature	T4110	2322	Wetwell	±2 °C	FieldPoint
Temperature	T4111	2922	Wetwell	±2 °C	FieldPoint
Temperature	T4112	372	Wetwell	±2 °C	FieldPoint
Temperature	T4113	158	Wetwell	±2 °C	FieldPoint
Temperature	T4200	372	Wetwell	±2 °C	FieldPoint
Temperature	T4201	572	Wetwell	±2 °C	FieldPoint
Temperature	T4202	772	Wetwell	±2 °C	FieldPoint
Temperature	T4203	872	Wetwell	±2 °C	FieldPoint
Temperature	T4204	972	Wetwell	±2 °C	FieldPoint
Temperature	T4205	1072	Wetwell	±2 °C	FieldPoint
Temperature	T4206	1172	Wetwell	±2 °C	FieldPoint
Temperature	T4207	1272	Wetwell	±2 °C	FieldPoint
Temperature	T4208	1372	Wetwell	±2 °C	FieldPoint
Temperature	T4210	1572	Wetwell	±2 °C	FieldPoint
Temperature	T4212	1772	Wetwell	±2 °C	FieldPoint
Temperature	T4213	1972	Wetwell	±2 °C	FieldPoint
Temperature	T4214	2172	Wetwell	±2 °C	FieldPoint
Temperature	T4215	2372	Wetwell	±2 °C	FieldPoint
Temperature	T4216	2572	Wetwell	±2 °C	FieldPoint
Temperature	T4217	2972	Wetwell	±2 °C	FieldPoint
Temperature	T4218	472	Wetwell	±2 °C	FieldPoint
Temperature	T4219	672	Wetwell	±2 °C	FieldPoint
Temperature	T4300	372	Wetwell	±2 °C	FieldPoint
Temperature	T4301	572	Wetwell	±2 °C	FieldPoint
Temperature	T4302	772	Wetwell	±2 °C	FieldPoint
Temperature	T4303	872	Wetwell	±2 °C	FieldPoint
Temperature	T4304	972	Wetwell	±2 °C	FieldPoint
Temperature	T4305	1072	Wetwell	±2 °C	FieldPoint
Temperature	T4306	1172	Wetwell	±2 °C	FieldPoint
Temperature	T4307	1272	Wetwell	±2 °C	FieldPoint
Temperature	T4308	1372	Wetwell	±2 °C	FieldPoint
Temperature	T4310	1572	Wetwell	±2 °C	FieldPoint
Temperature	T4312	1772	Wetwell	±2 °C	FieldPoint
Temperature	T4313	1972	Wetwell	±2 °C	FieldPoint
Temperature	T4314	2172	Wetwell	±2 °C	FieldPoint
Temperature	T4315	2372	Wetwell	±2 °C	FieldPoint
Temperature	T4316	2572	Wetwell	±2 °C	FieldPoint
Temperature	T4317	2972	Wetwell	±2 °C	FieldPoint
Temperature	T4318	472	Wetwell	±2 °C	FieldPoint
Temperature	T4319	672	Wetwell	±2 °C	FieldPoint
Temperature	T4400	222	Wetwell	±2 °C	FieldPoint
Temperature	T4401	522	Wetwell	±2 °C	FieldPoint
Temperature	T4402	672	Wetwell	±2 °C	FieldPoint
Temperature	T4403	822	Wetwell	±2 °C	FieldPoint
Temperature	T4404	972	Wetwell	±2 °C	FieldPoint
Temperature	T4405	1122	Wetwell	±2 °C	FieldPoint
Temperature	T4406	1272	Wetwell	±2 °C	FieldPoint
Temperature	T4407	1422	Wetwell	±2 °C	FieldPoint
Temperature	T4408	1722	Wetwell	±2 °C	FieldPoint

Temperature	T4409	2022	Wetwell	±2 °C	FieldPoint
Temperature	T4410	2322	Wetwell	±2 °C	FieldPoint
Temperature	T4411	2922	Wetwell	±2 °C	FieldPoint
Temperature	T4412	372	Wetwell	±2 °C	FieldPoint
Temperature	T4413	158	Wetwell	±2 °C	FieldPoint
Cut-off valve position	V1	-	DN50 Steam line	Not defined	LabView
Cut-off valve position	X2100	-	DN50 Steam line	Not defined	FieldPoint
Steam partial pressure	X2102	5200	Drywell	Not defined	FieldPoint
Cut-off valve position	X2106	-	DN50 Steam line	Not defined	FieldPoint

Measurements of the PPOOLEX facility in the SPA experiment series.

APPENDIX 3: PPOOLEX test facility photographs

Lower part of the sparger pipe.

APPENDIX 4: Averaged vector fields and uncertainty fields from SPA-T8R

SPA-T8R Test1-2 [1380.1 s – 1383.7 s]

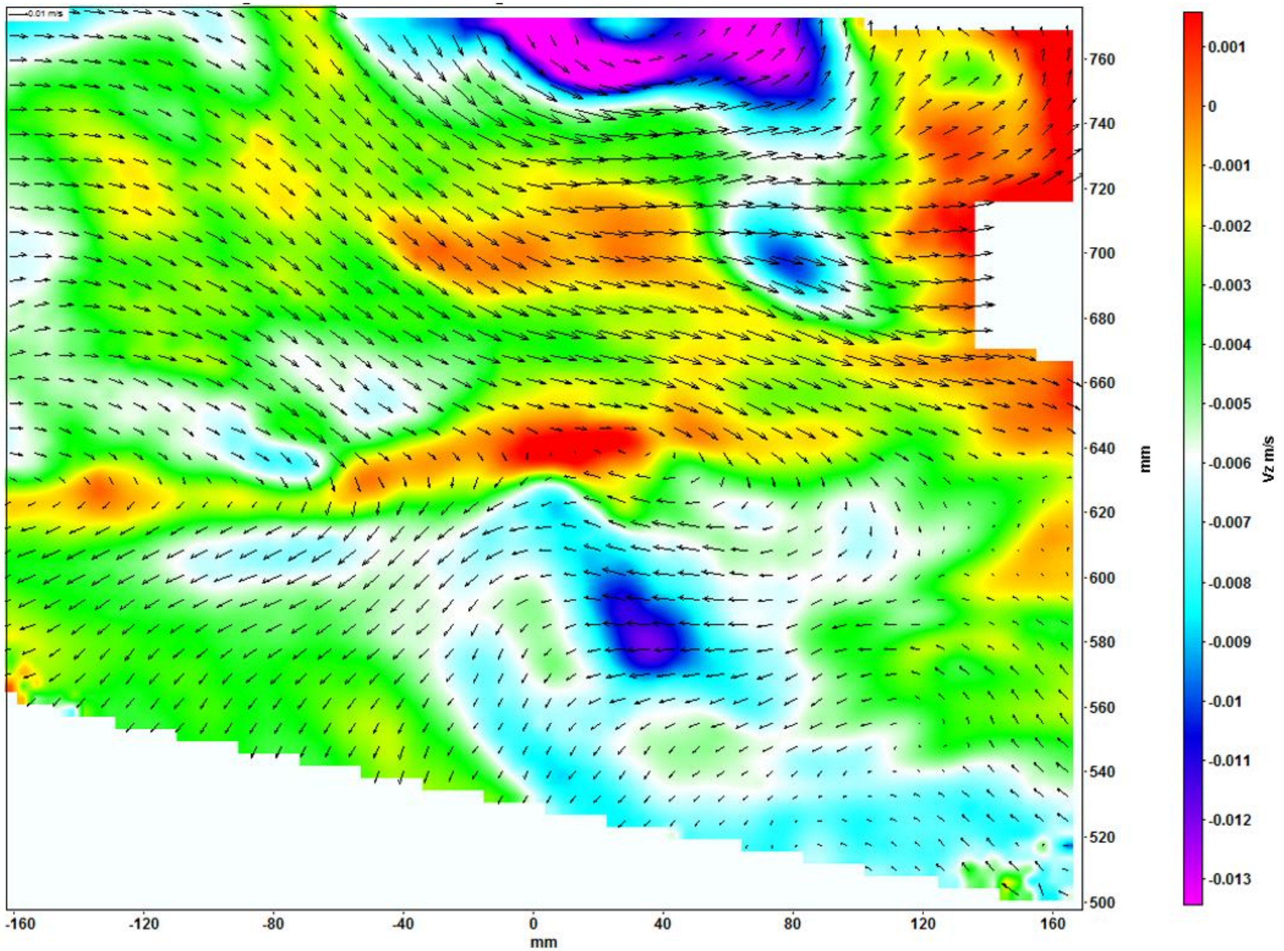

Averaged vector field from SPA-T8R Test1-2.

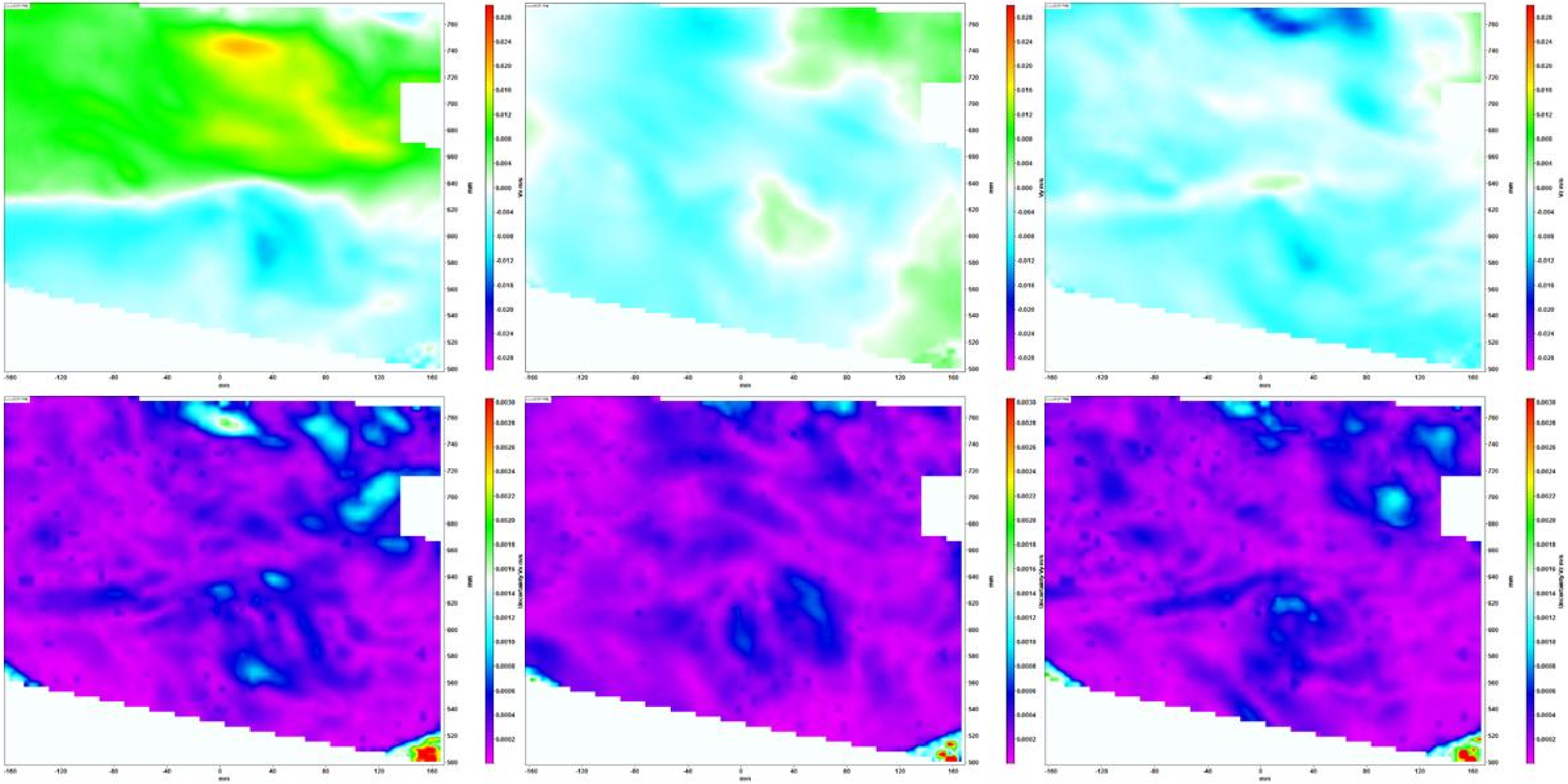

On top components of the averaged vector fields in order of x, y, z from left to right and below the uncertainty fields for respective components from SPA-T8R Test1-2.

SPA-T8R Test1-3 [1386.6 s – 1390.9 s]

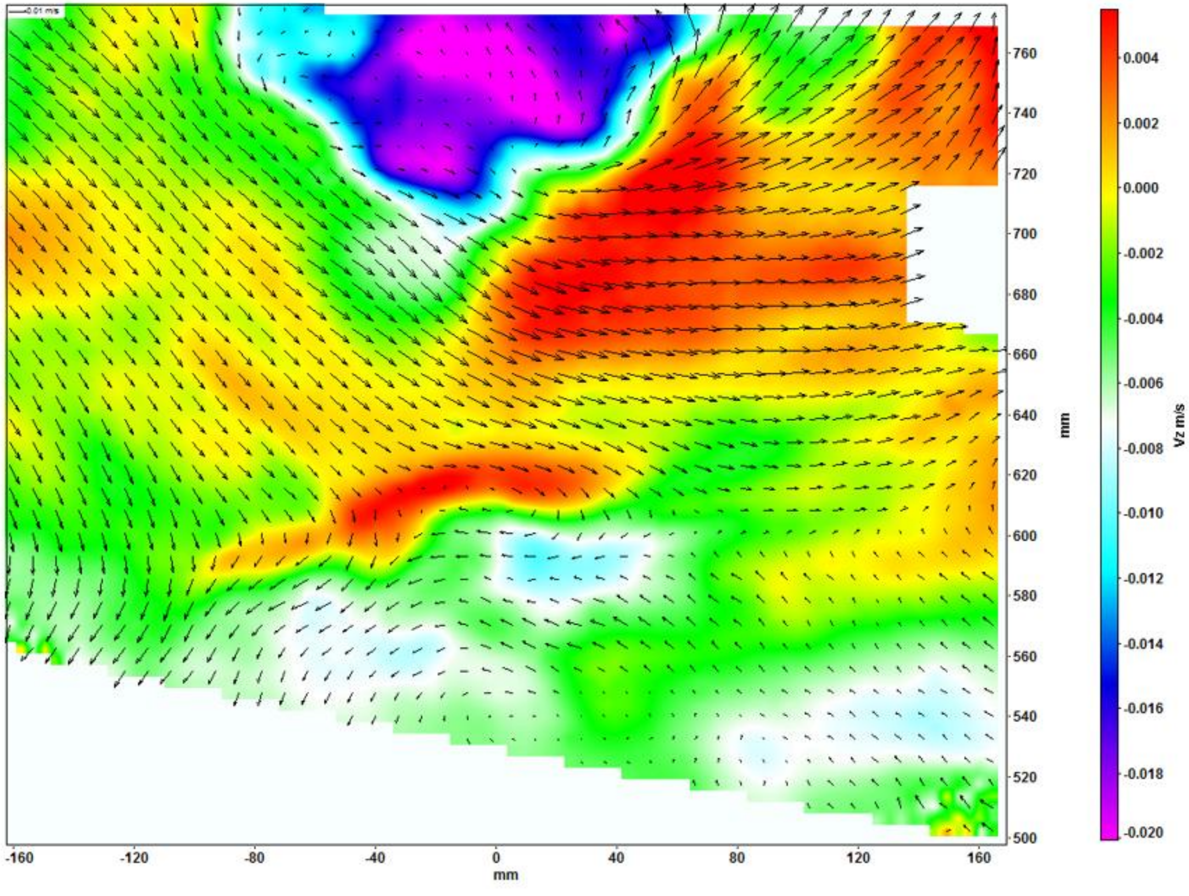

Averaged vector field from SPA-T8R Test1-3.

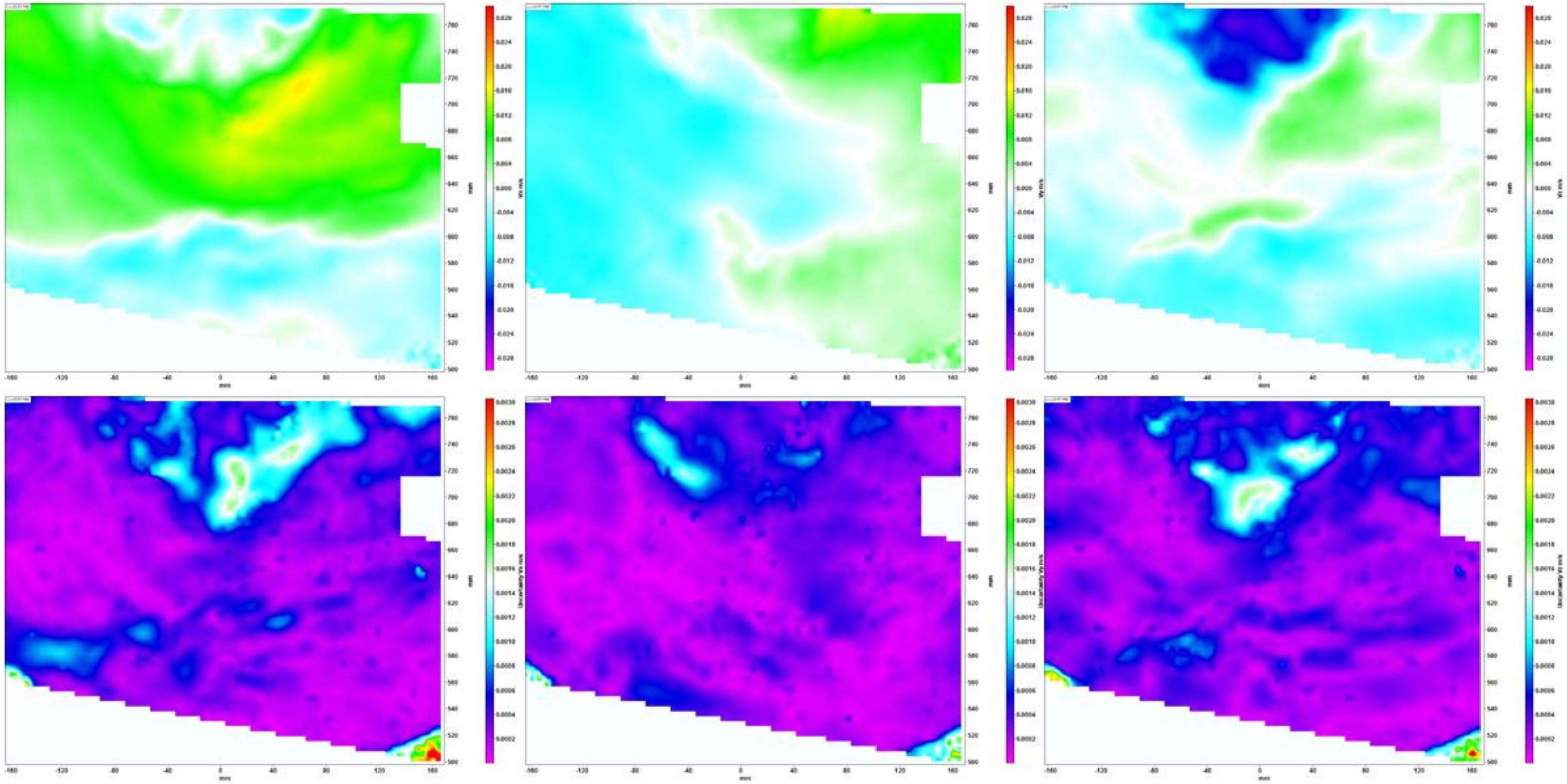

On top components of the averaged vector fields in order of x, y, z from left to right and below the uncertainty fields for respective components from SPA-T8R Test1-3.

SPA-T8R Test1-4 [1405.9 s – 1411.6 s]

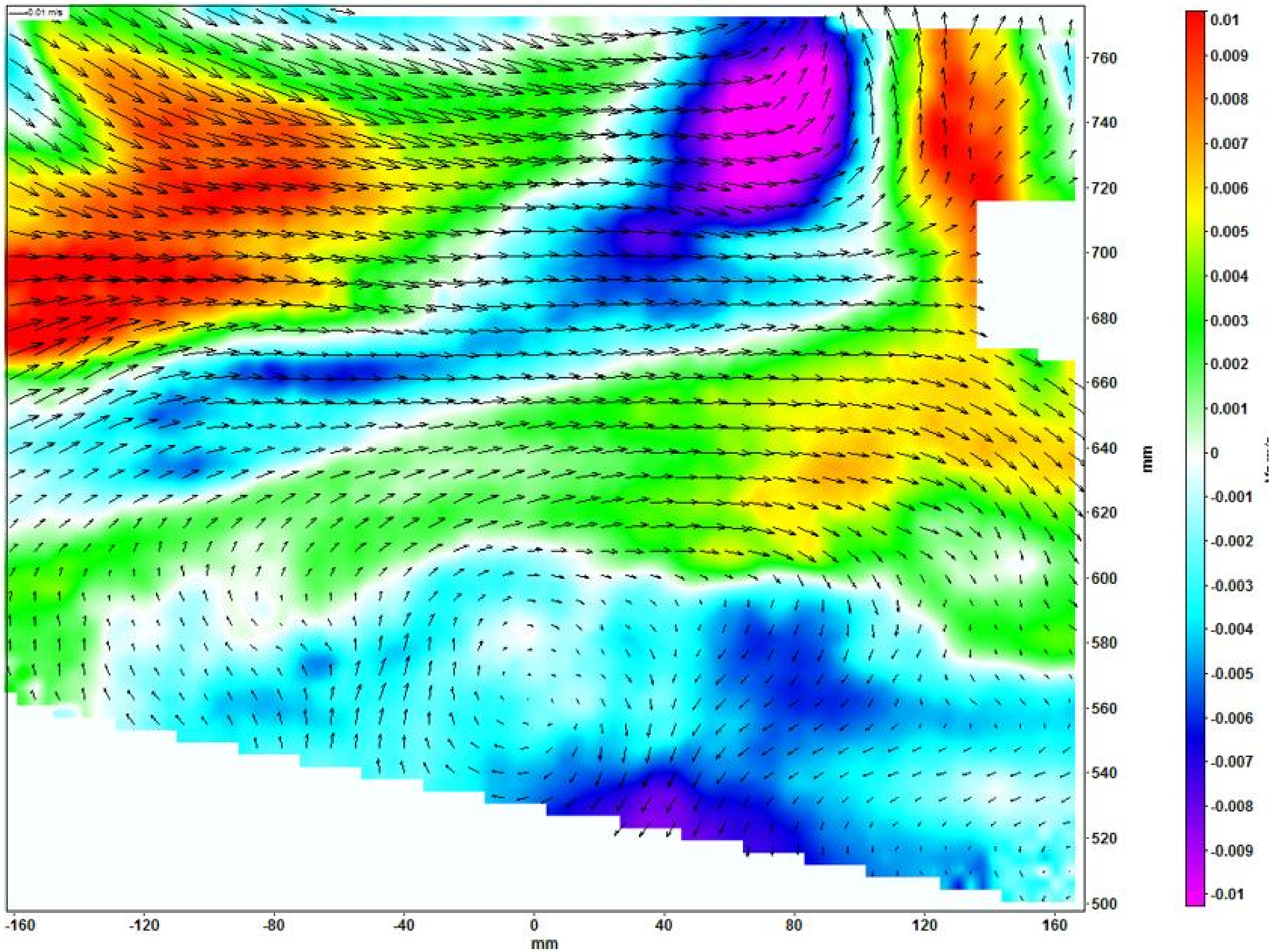

Averaged vector field from SPA-T8R Test1-4.

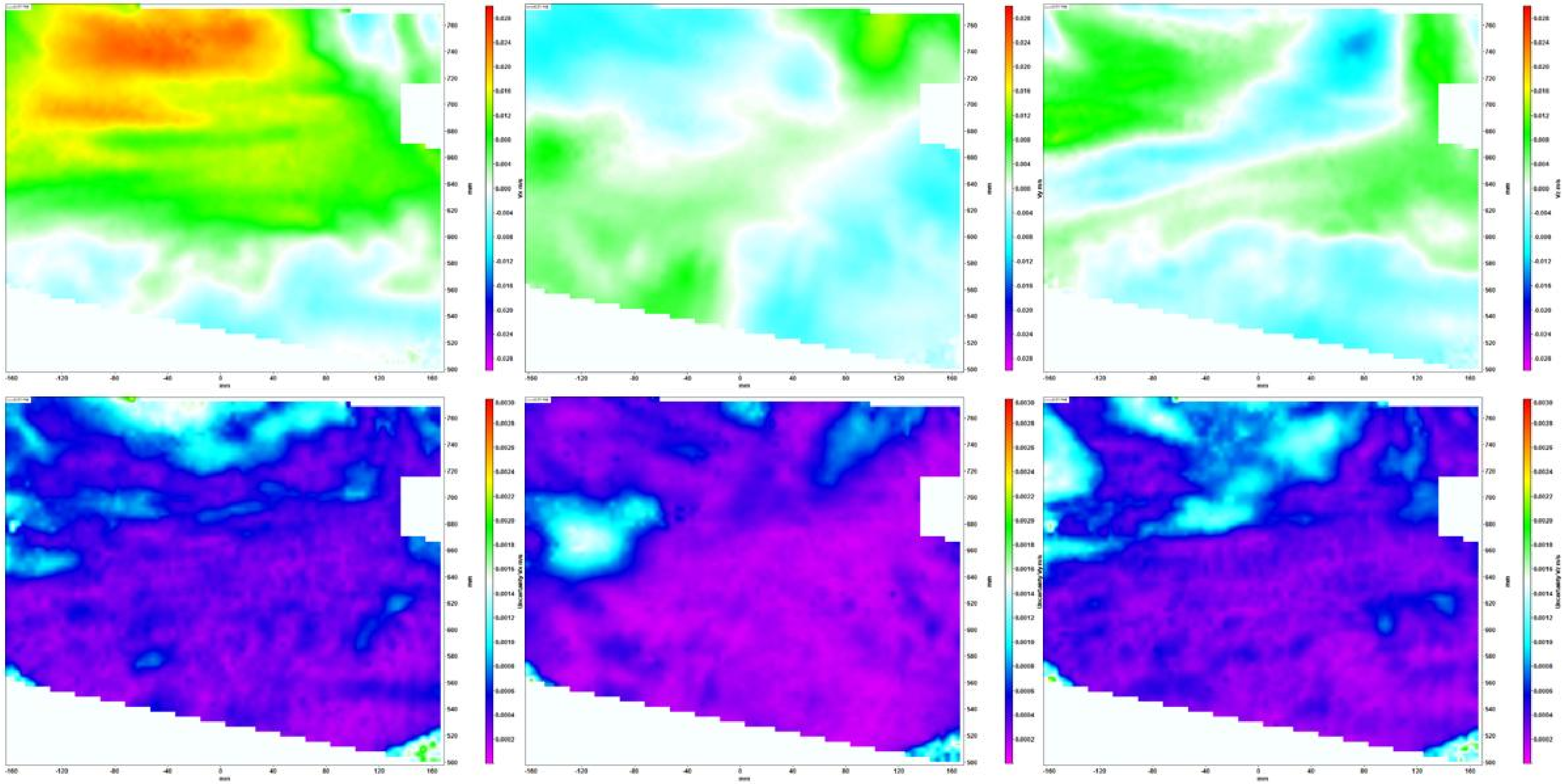

On top components of the averaged vector fields in order of x, y, z from left to right and below the uncertainty fields for respective components from SPA-T8R Test1-4.

SPA-T8R Test2-1 [1680.0 s – 1684.3 s]

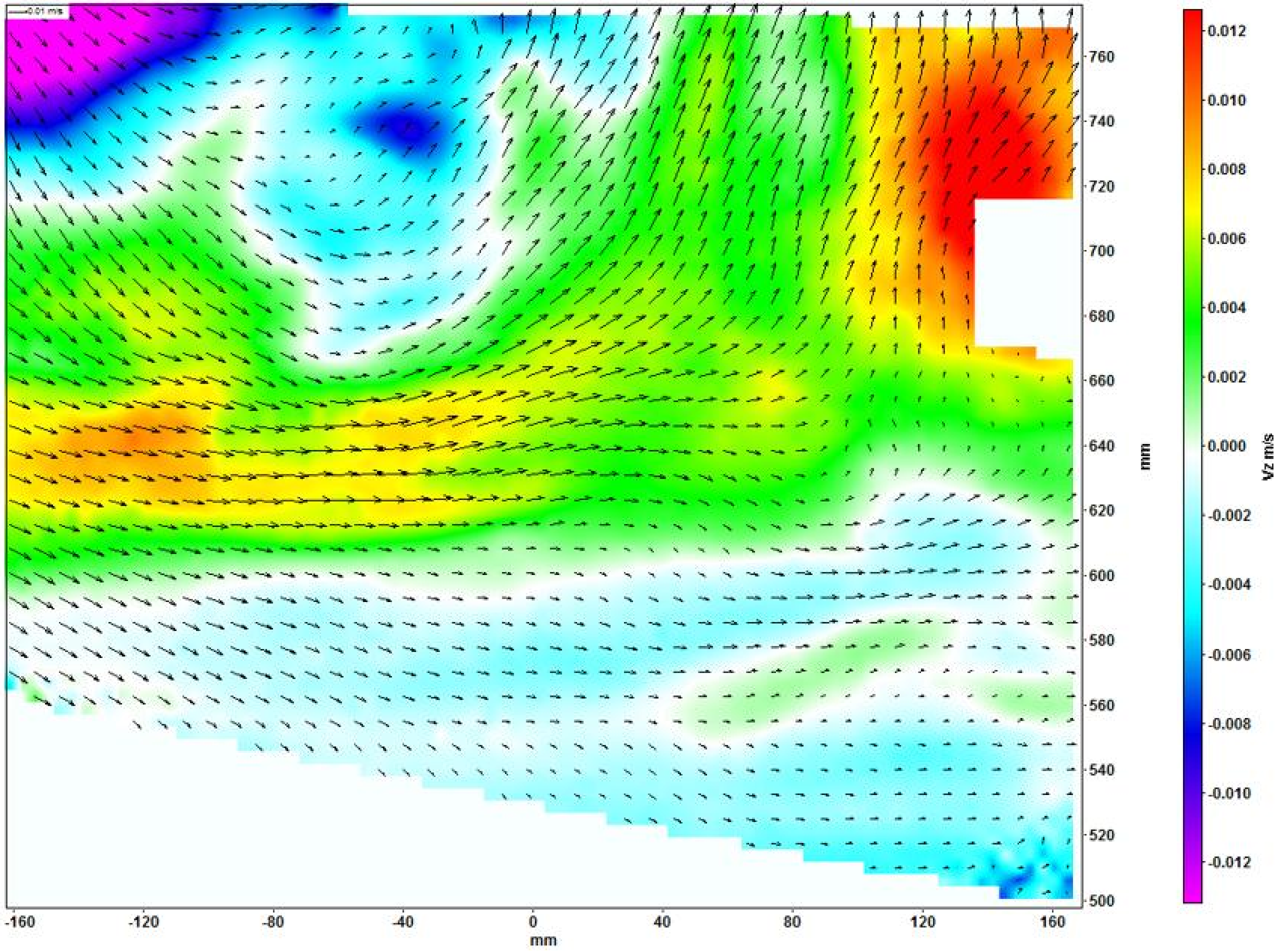

Averaged vector field from SPA-T8R Test2-1.

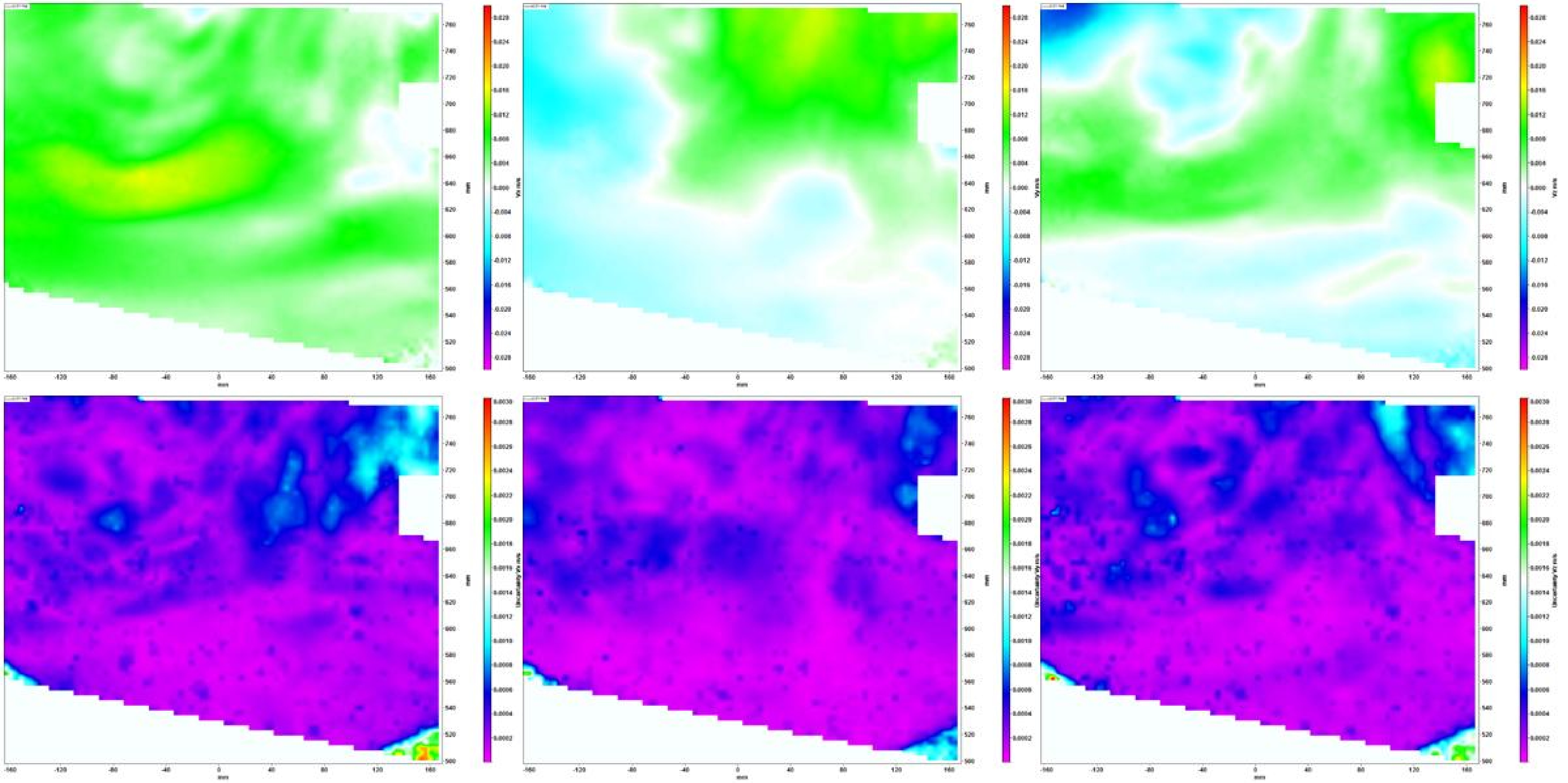

On top components of the averaged vector fields in order of x, y, z from left to right and below the uncertainty fields for respective components from SPA-T8R Test2-1.

SPA-T8R Test2-2 [1688.6 s – 1695.7 s]

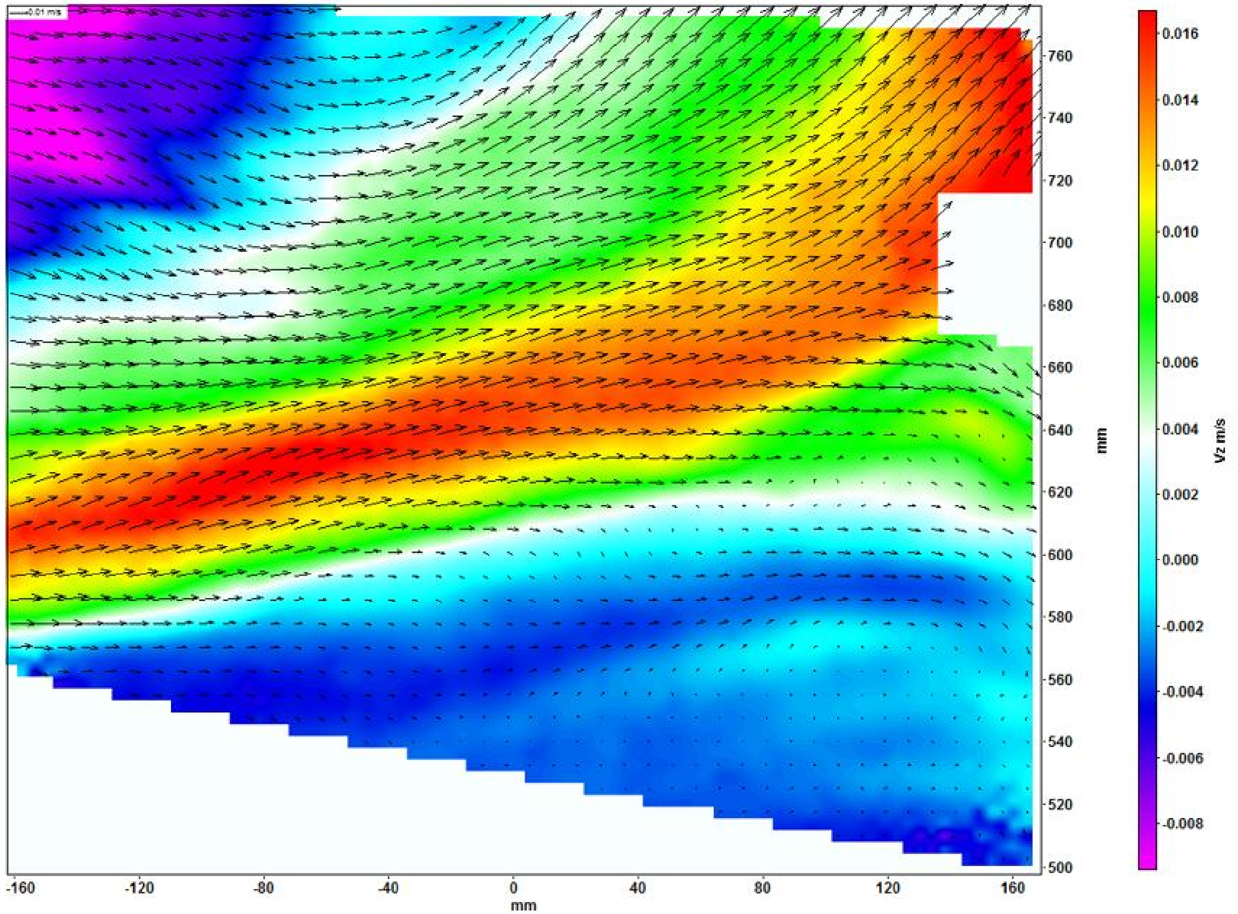

Averaged vector field from SPA-T8R Test2-2.

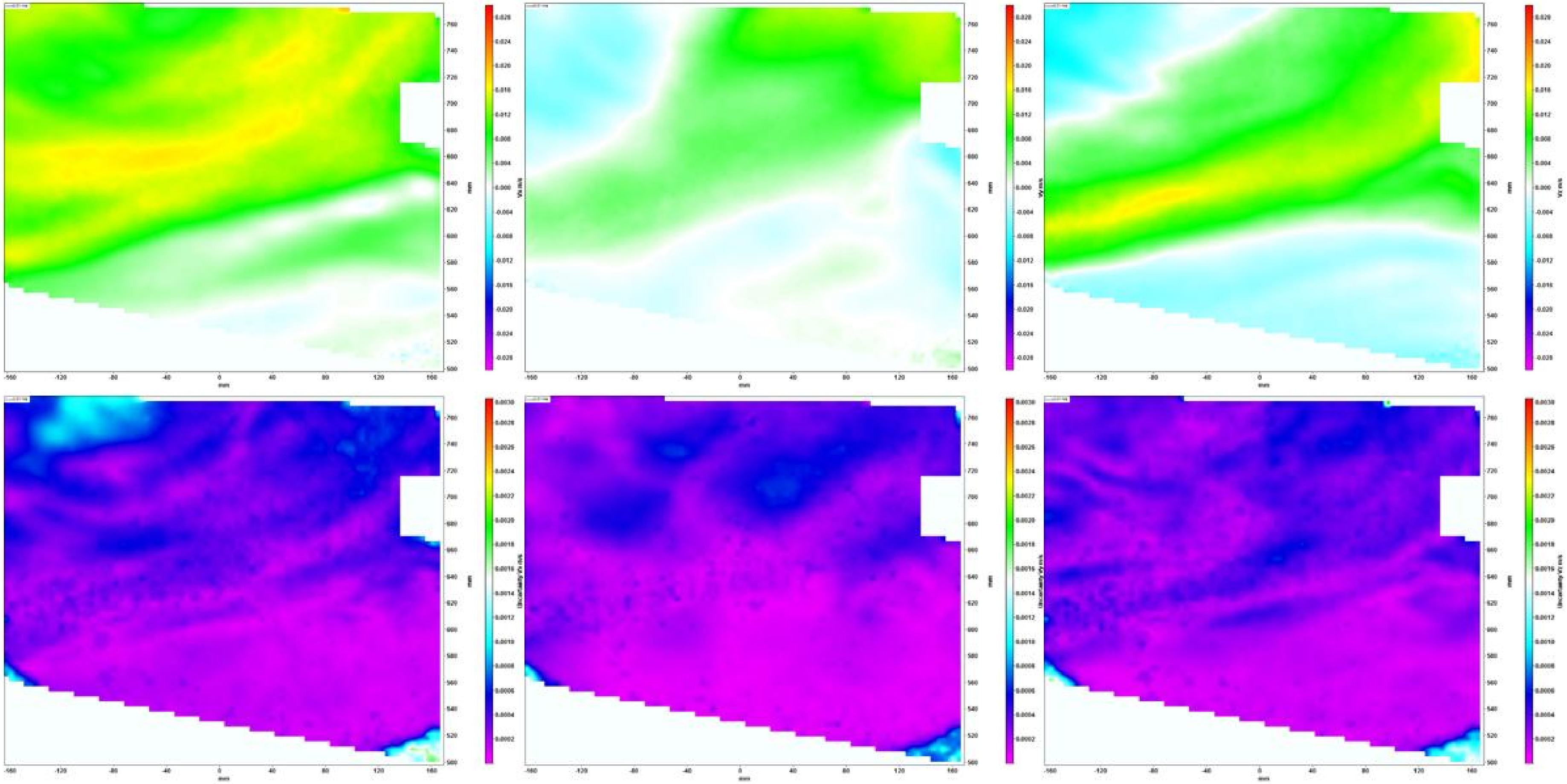

On top components of the averaged vector fields in order of x, y, z from left to right and below the uncertainty fields for respective components from SPA-T8R Test2-2.

SPA-T8R Test2-3 [1703.6 s – 1707.1 s]

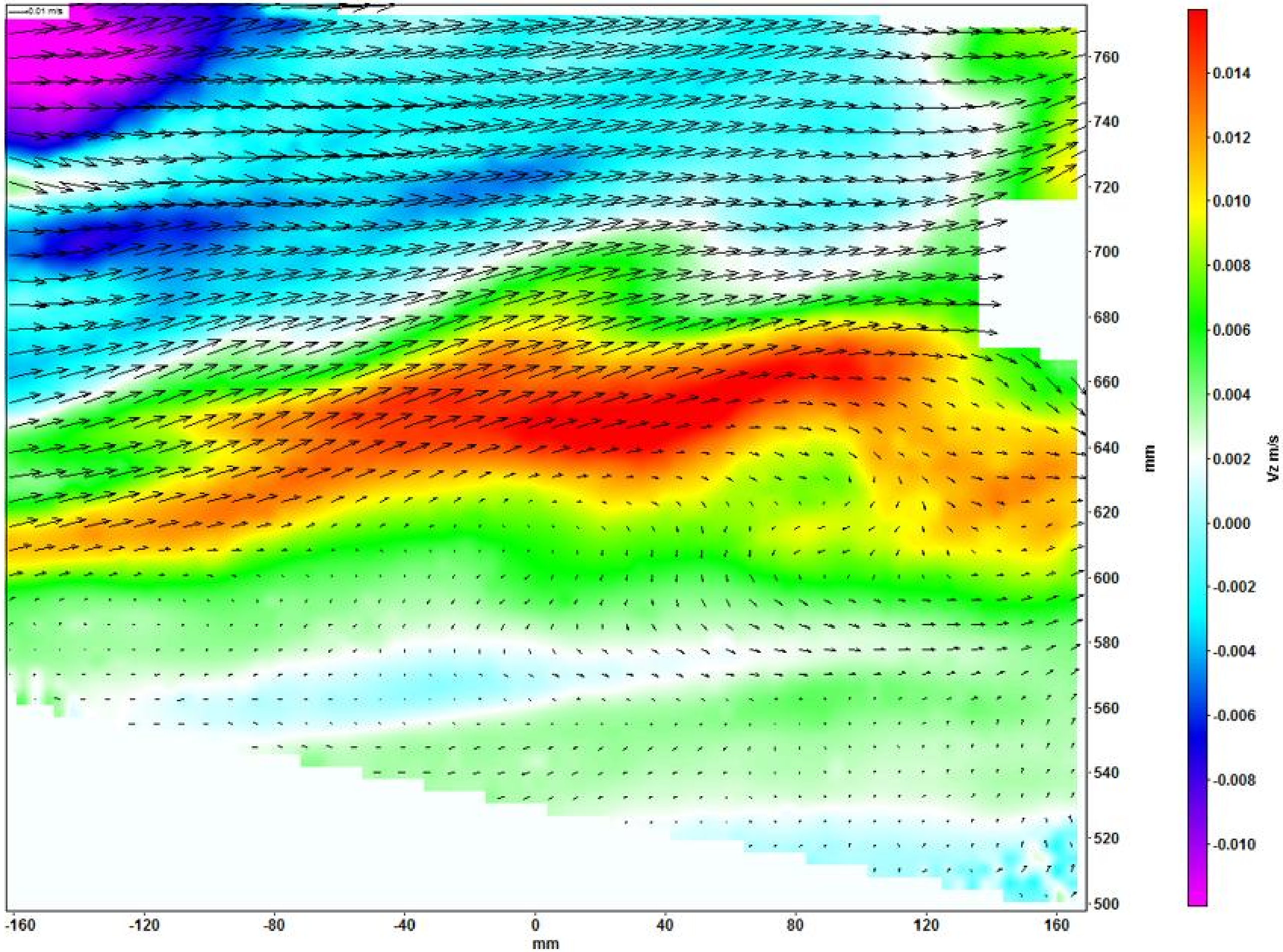

Averaged vector field from SPA-T8R Test2-3.

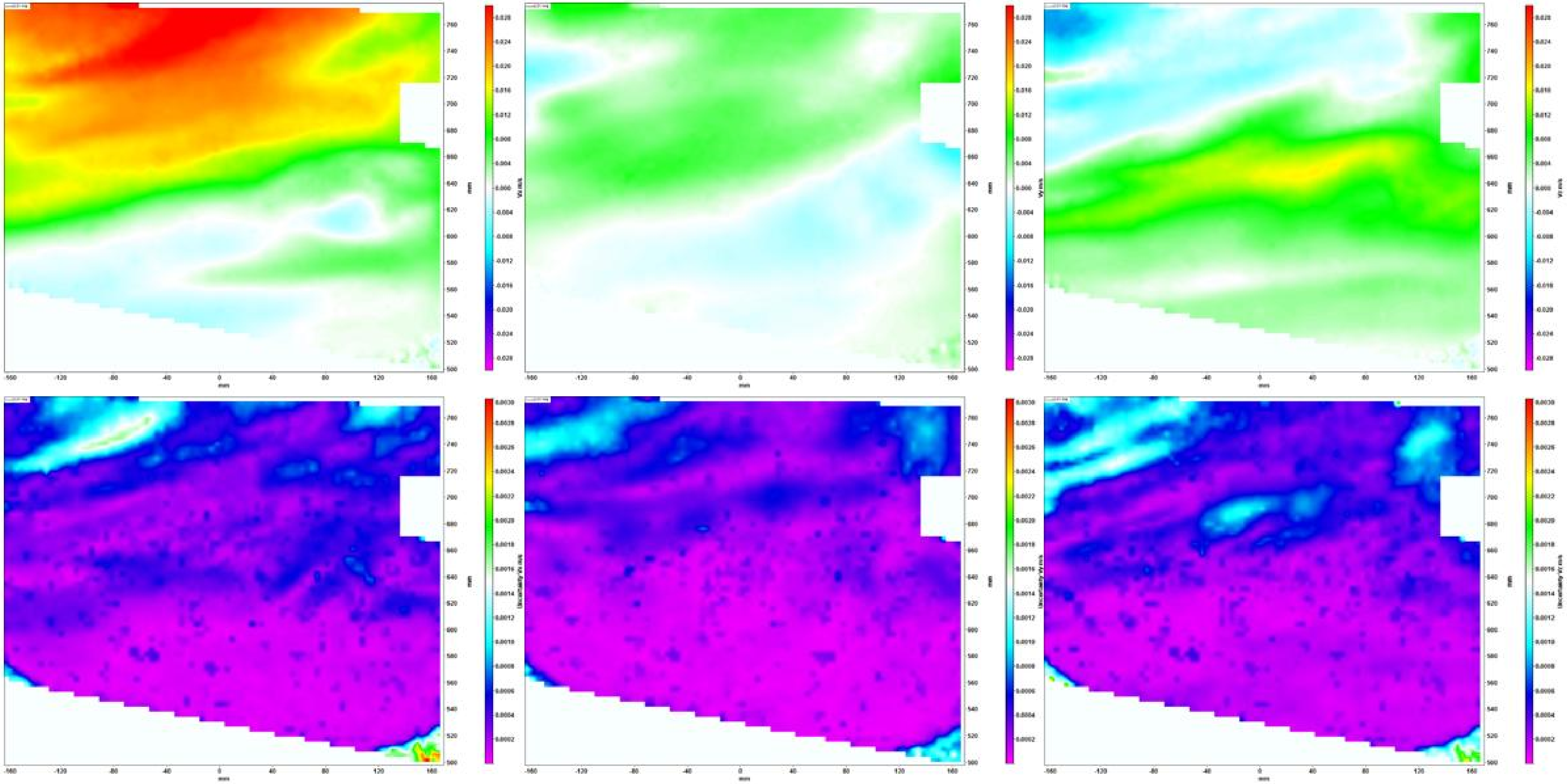

On top components of the averaged vector fields in order of x, y, z from left to right and below the uncertainty fields for respective components from SPA-T8R Test2-3.

SPA-T8R Test2-4 [1717.1 s – 1721.4 s]

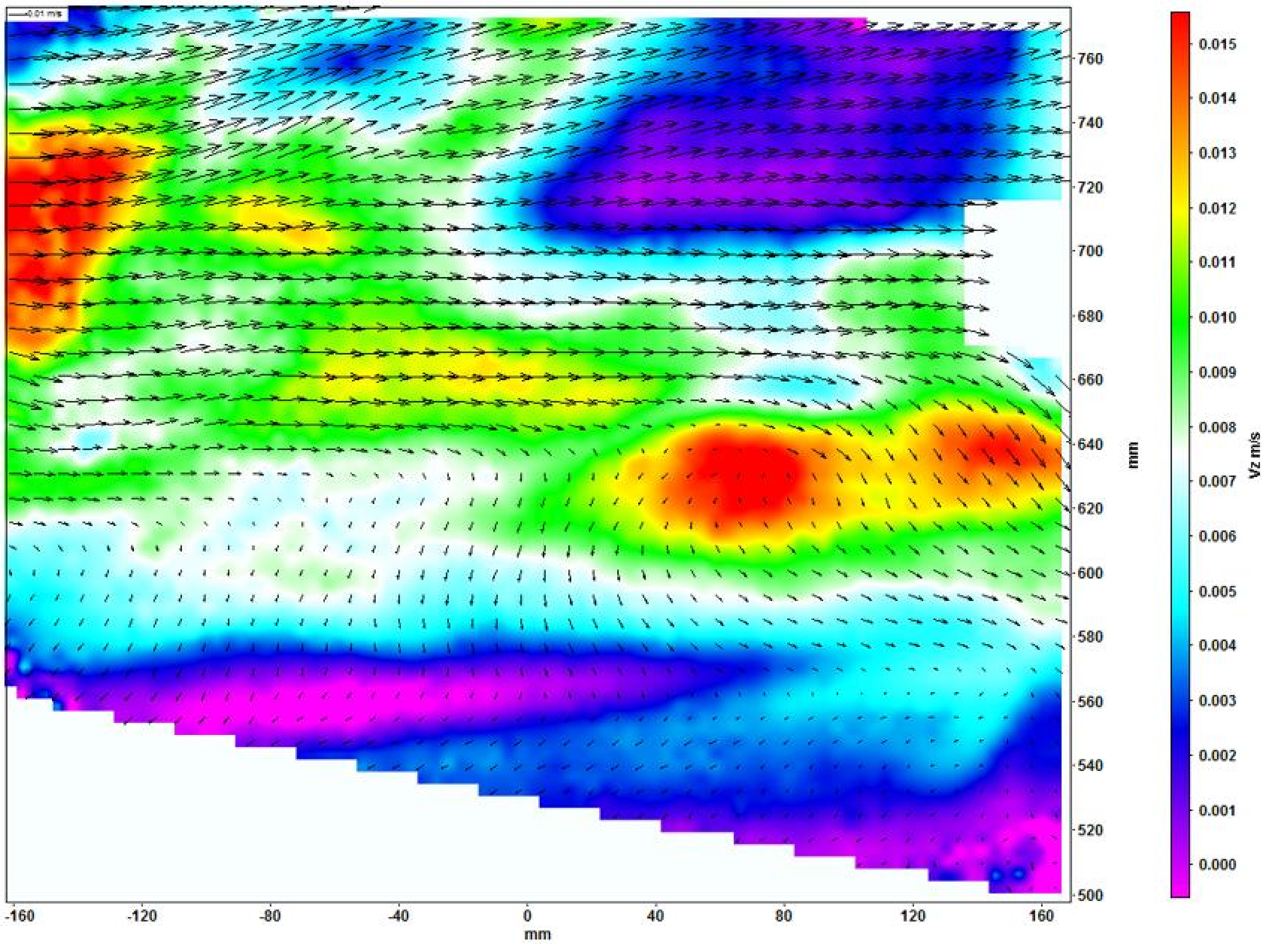

Averaged vector field from SPA-T8R Test2-4.

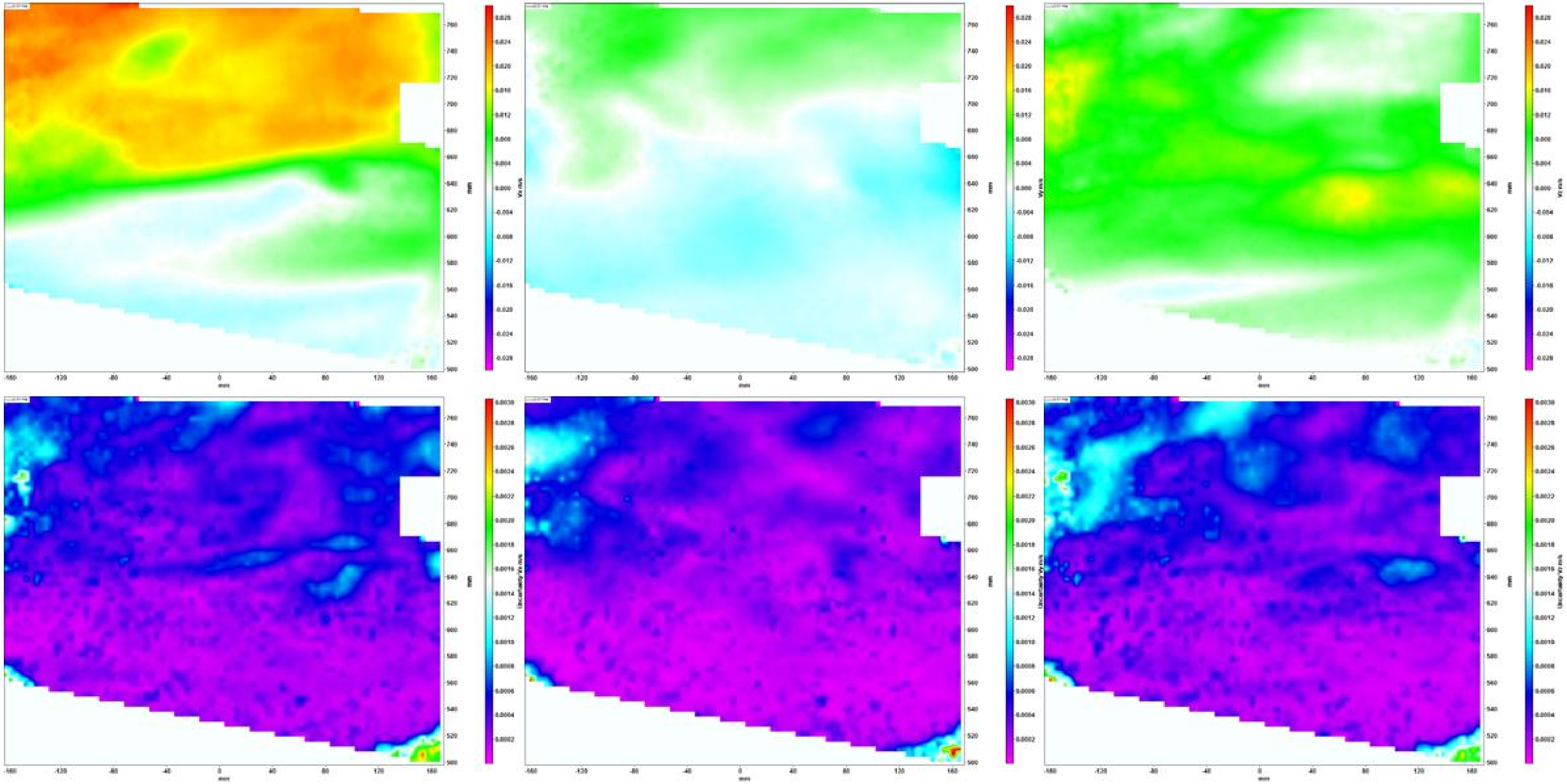

On top components of the averaged vector fields in order of x, y, z from left to right and below the uncertainty fields for respective components from SPA-T8R Test2-4.

SPA-T8R Test3-1 [2100.0 s – 2104.3 s]

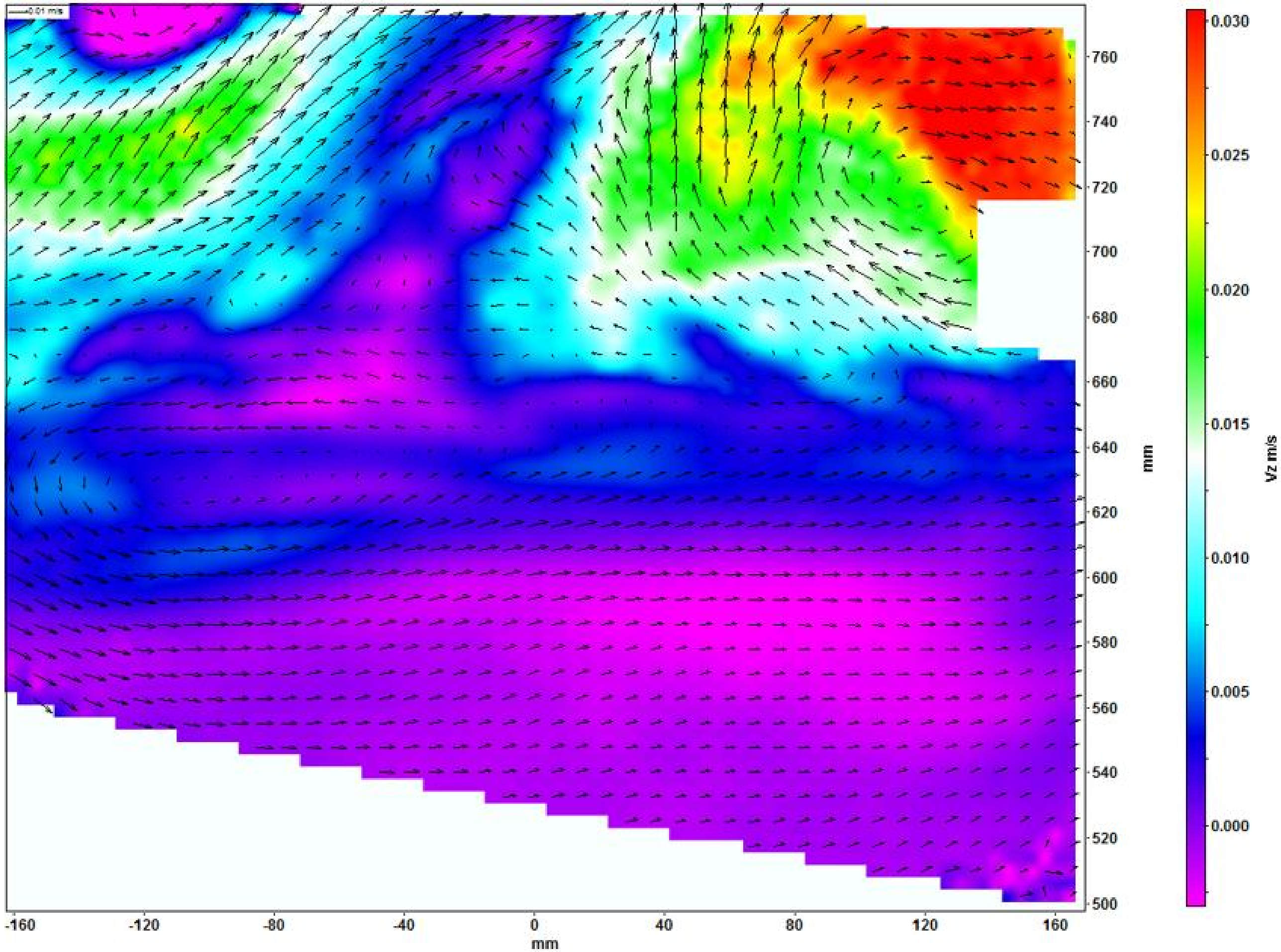

Averaged vector field from SPA-T8R Test3-1.

Open your mind. LUT.
Lappeenranta University of Technology

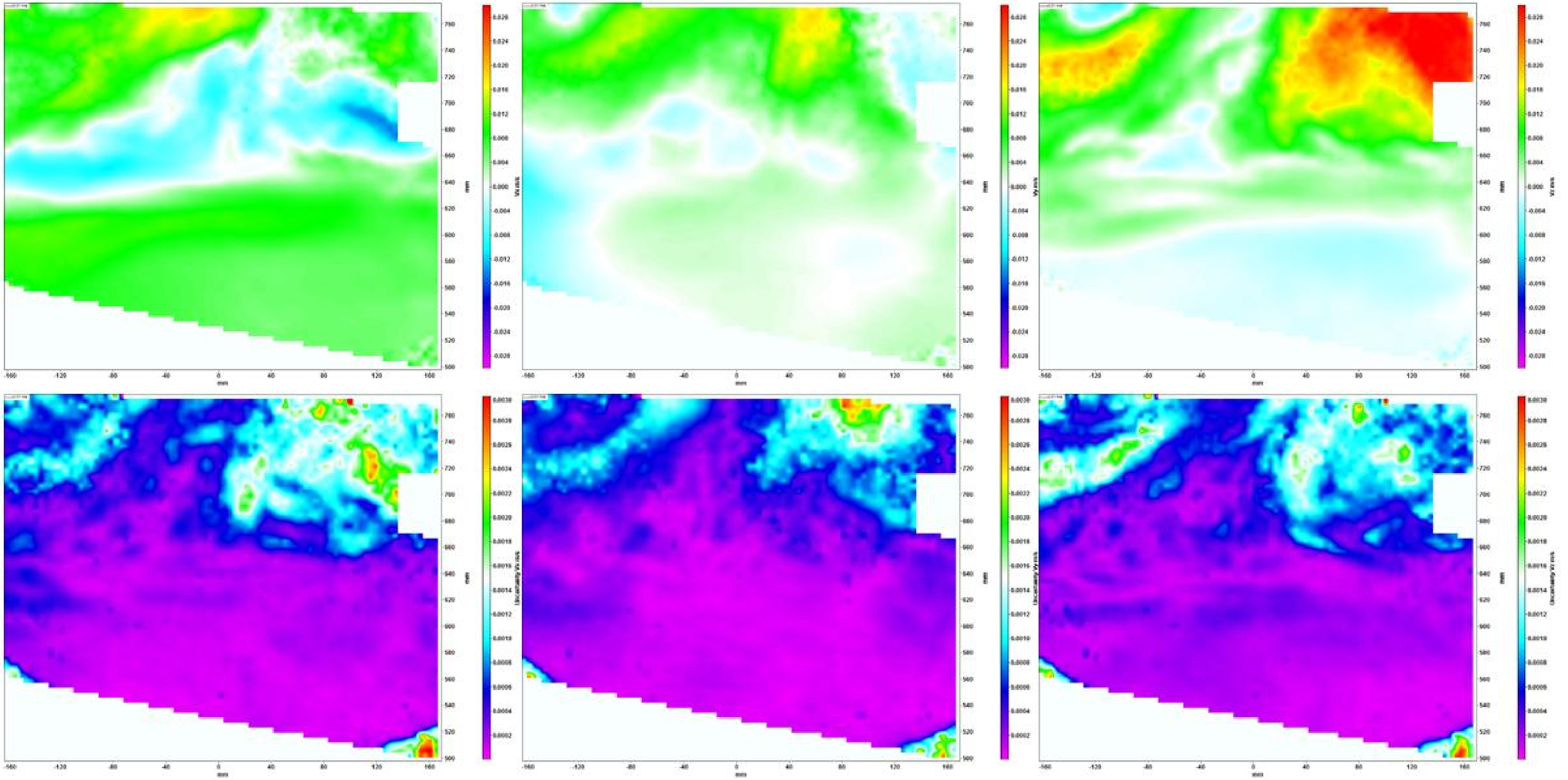

On top components of the averaged vector fields in order of x, y, z from left to right and below the uncertainty fields for respective components from SPA-T8R Test3-1.

Open your mind. LUT.
Lappeenranta University of Technology

SPA-T8R Test3-2 [2137.1 s – 2141.4 s]

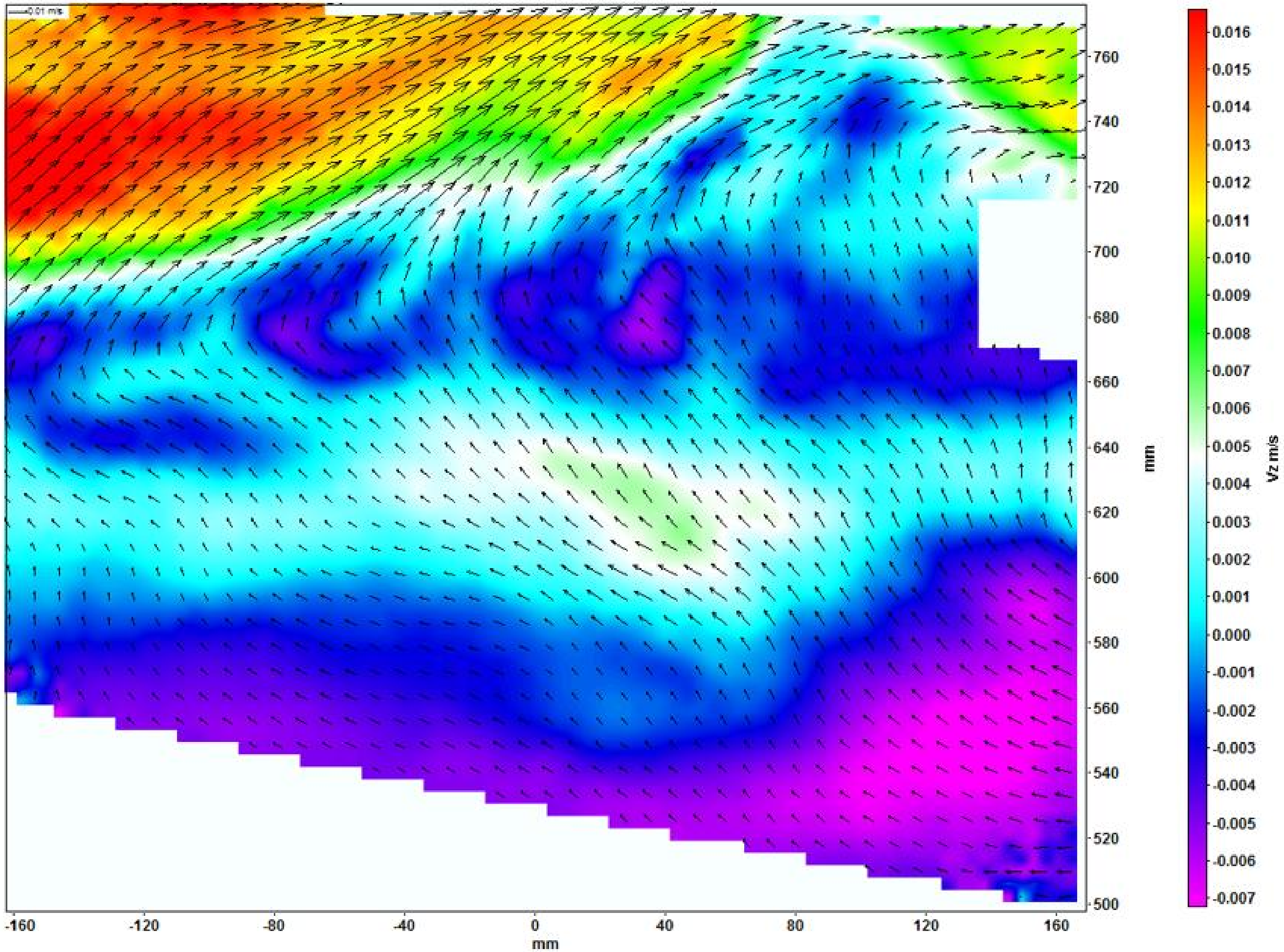

Averaged vector field from SPA-T8R Test3-2.

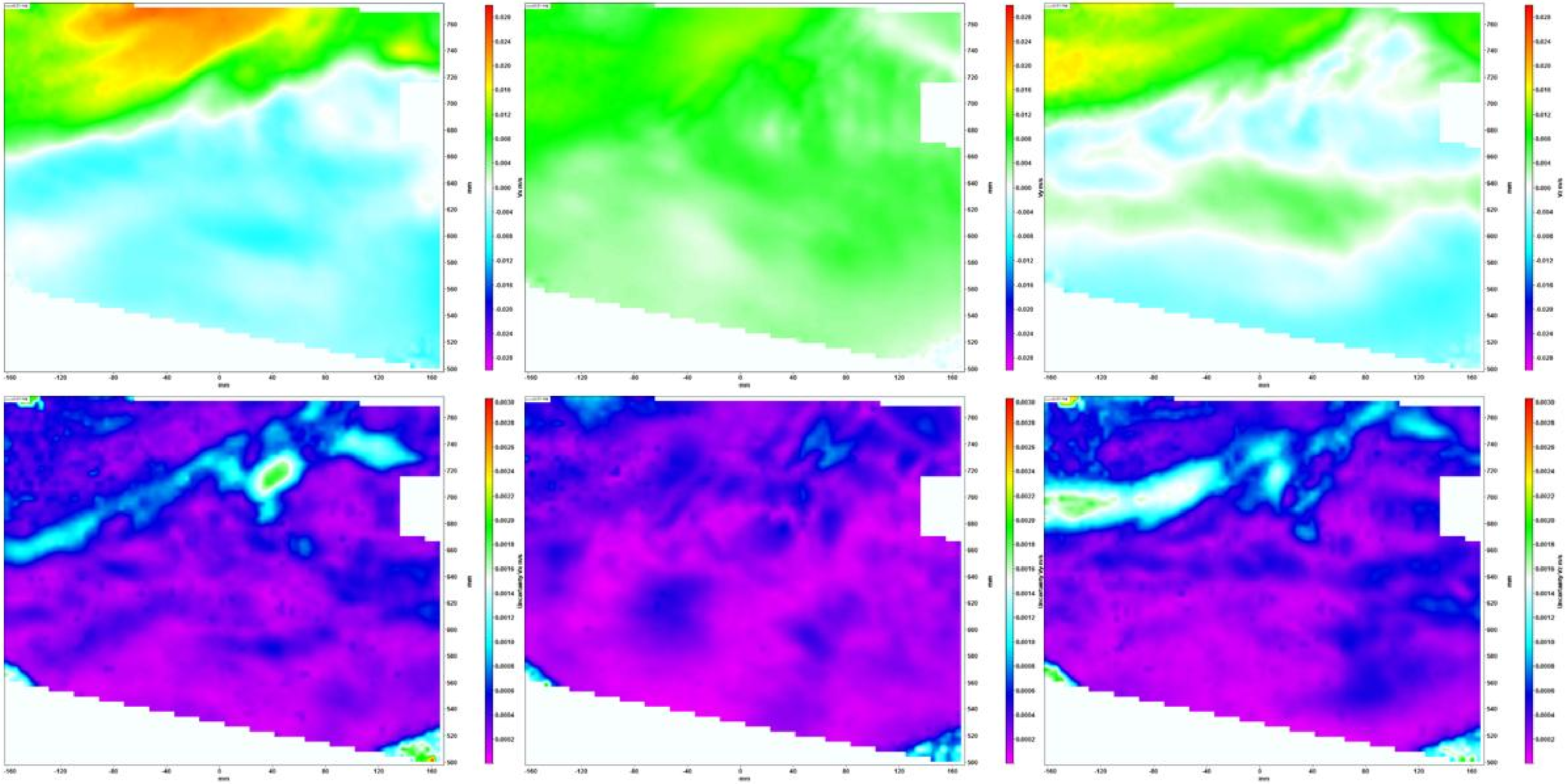

On top components of the averaged vector fields in order of x, y, z from left to right and below the uncertainty fields for respective components from SPA-T8R Test3-2.

SPA-T8R Test3-3 [2140.0 s – 2145.7 s]

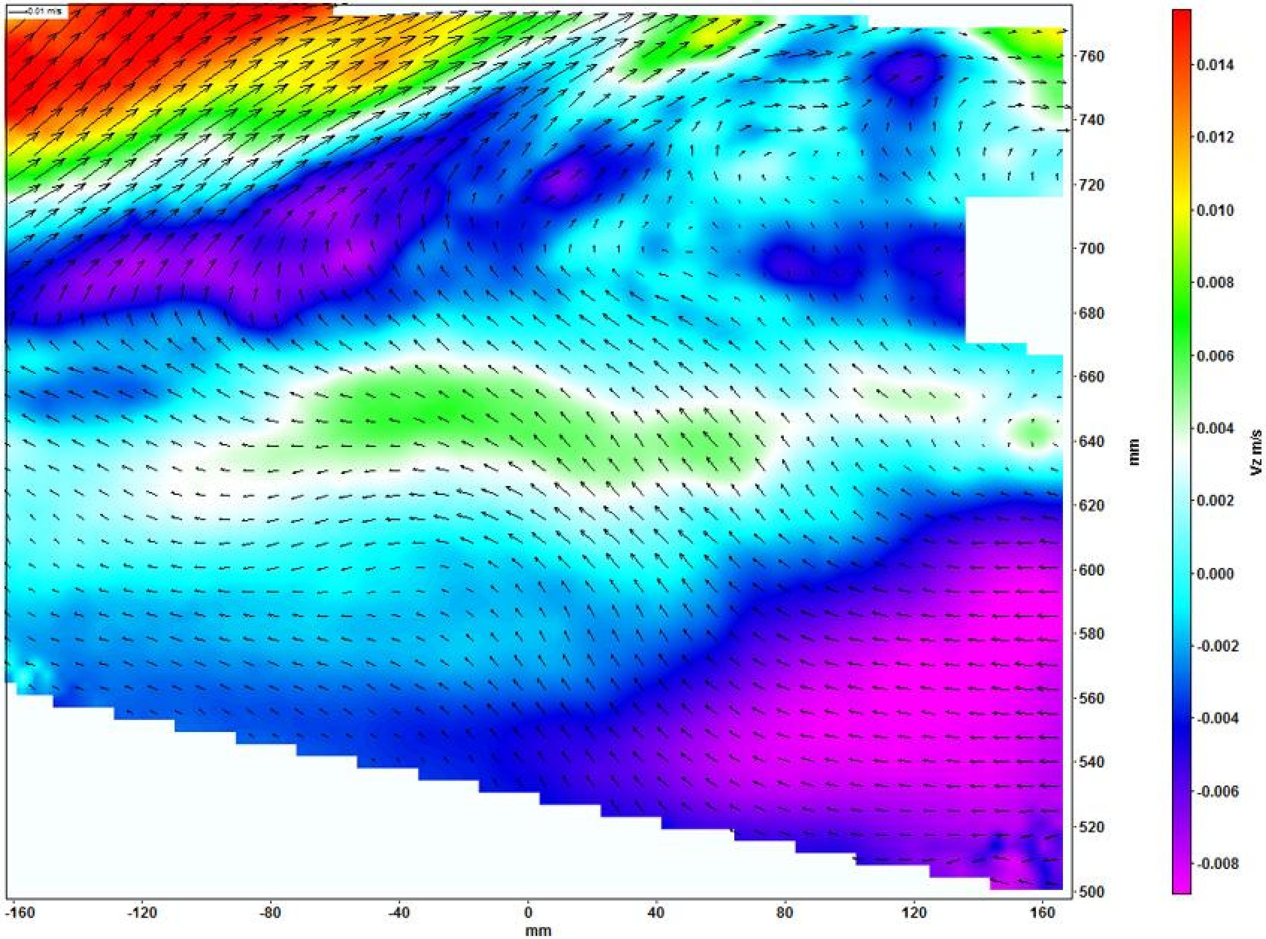

Averaged vector field from SPA-T8R Test3-3.

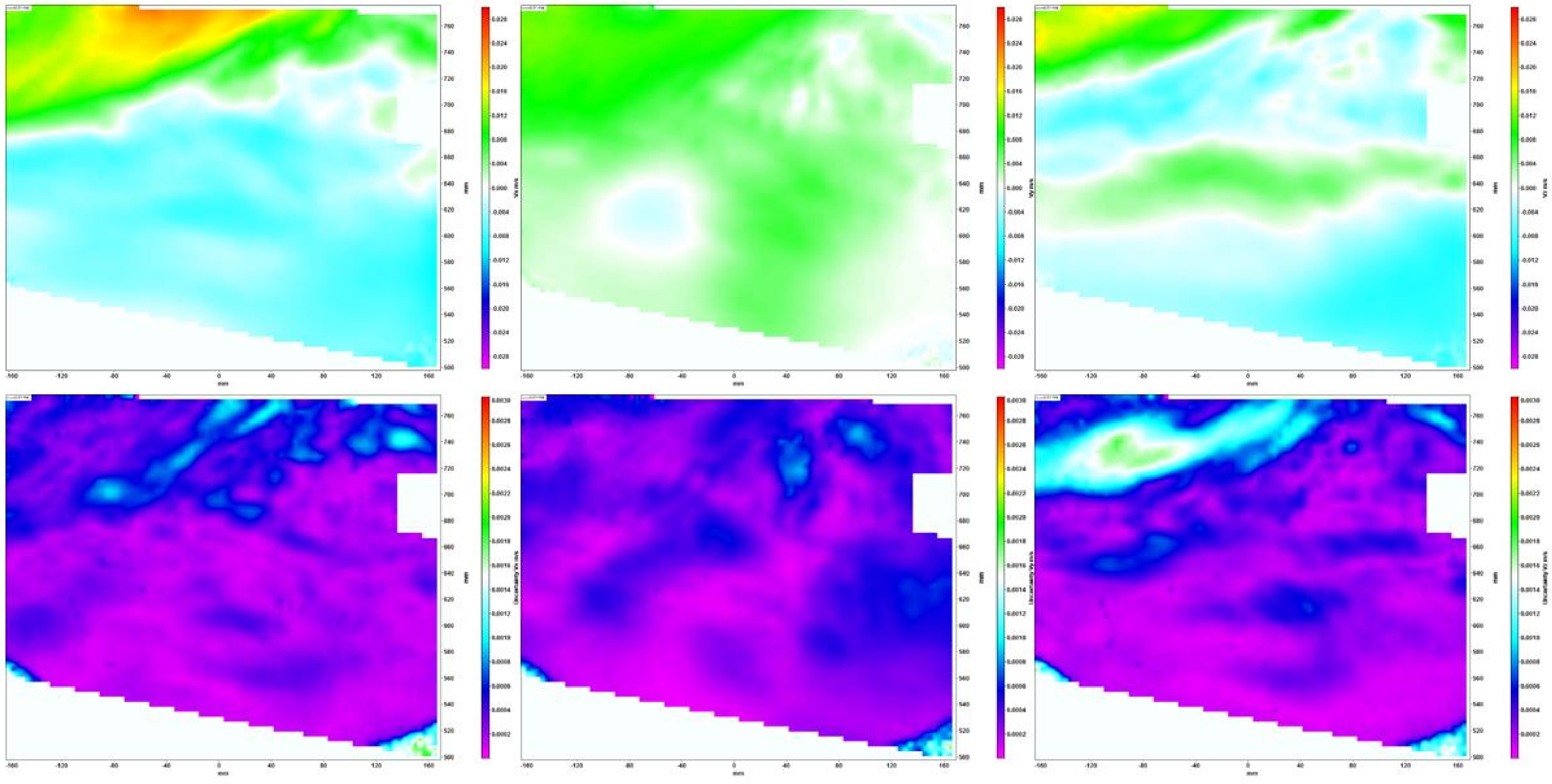

On top components of the averaged vector fields in order of x, y, z from left to right and below the uncertainty fields for respective components from SPA-T8R Test3-3.

SPA-T8R Test4-1 [3115.0 s – 3120.0 s]

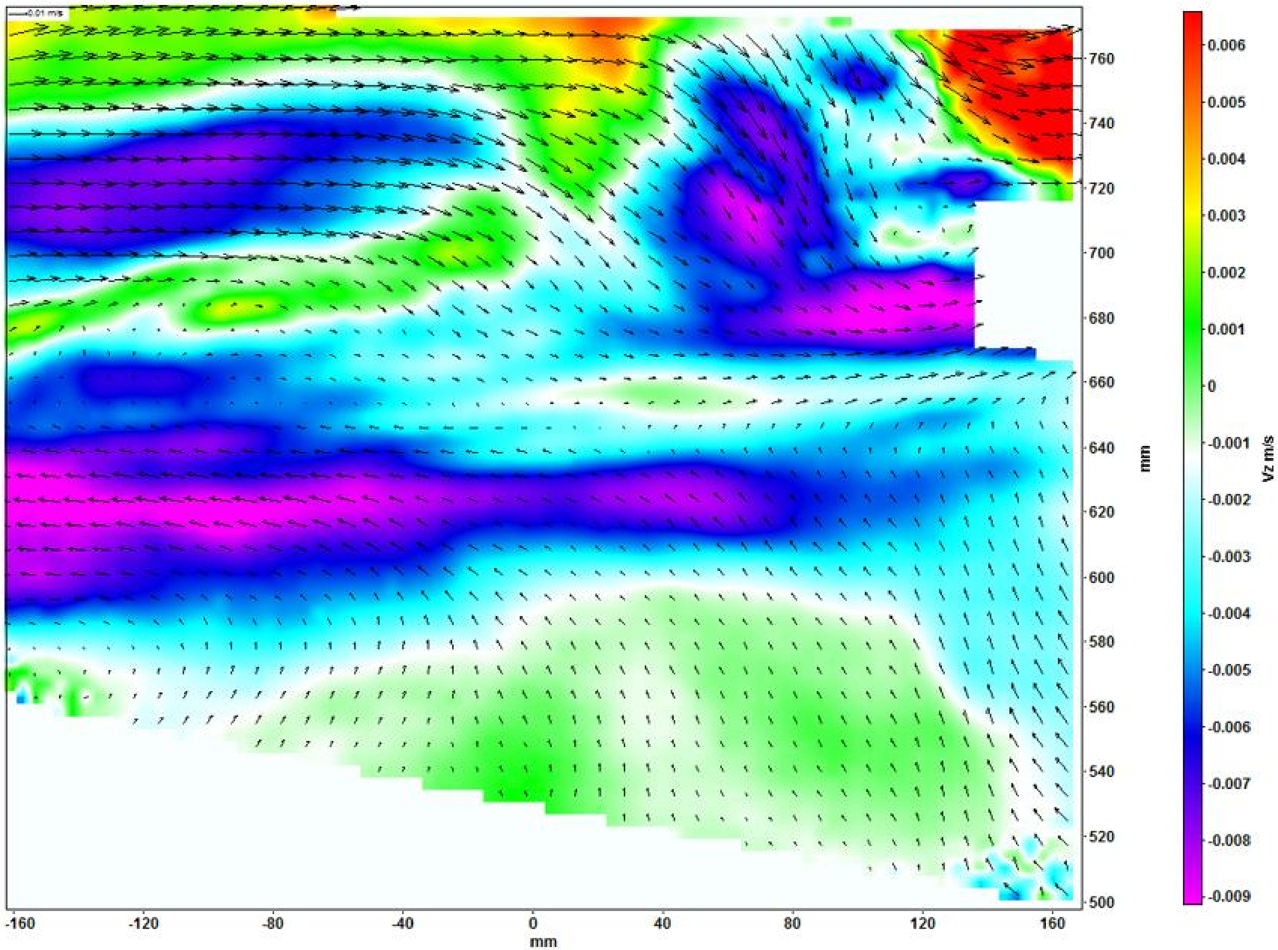

Averaged vector field from SPA-T8R Test4-1.

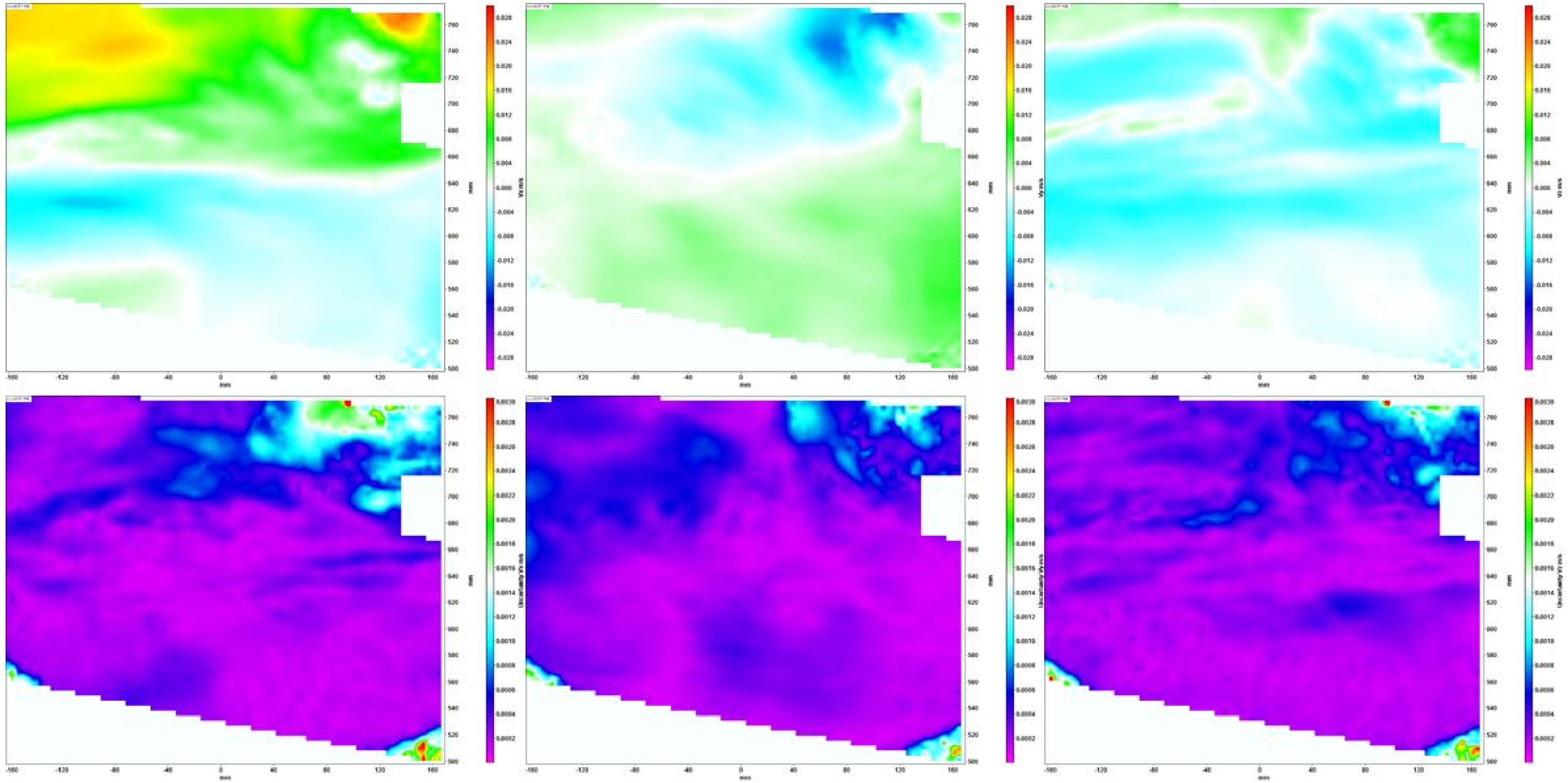

On top components of the averaged vector fields in order of x, y, z from left to right and below the uncertainty fields for respective components from SPA-T8R Test4-1.

SPA-T8R Test4-2 [3127.1 s – 3130.0 s]

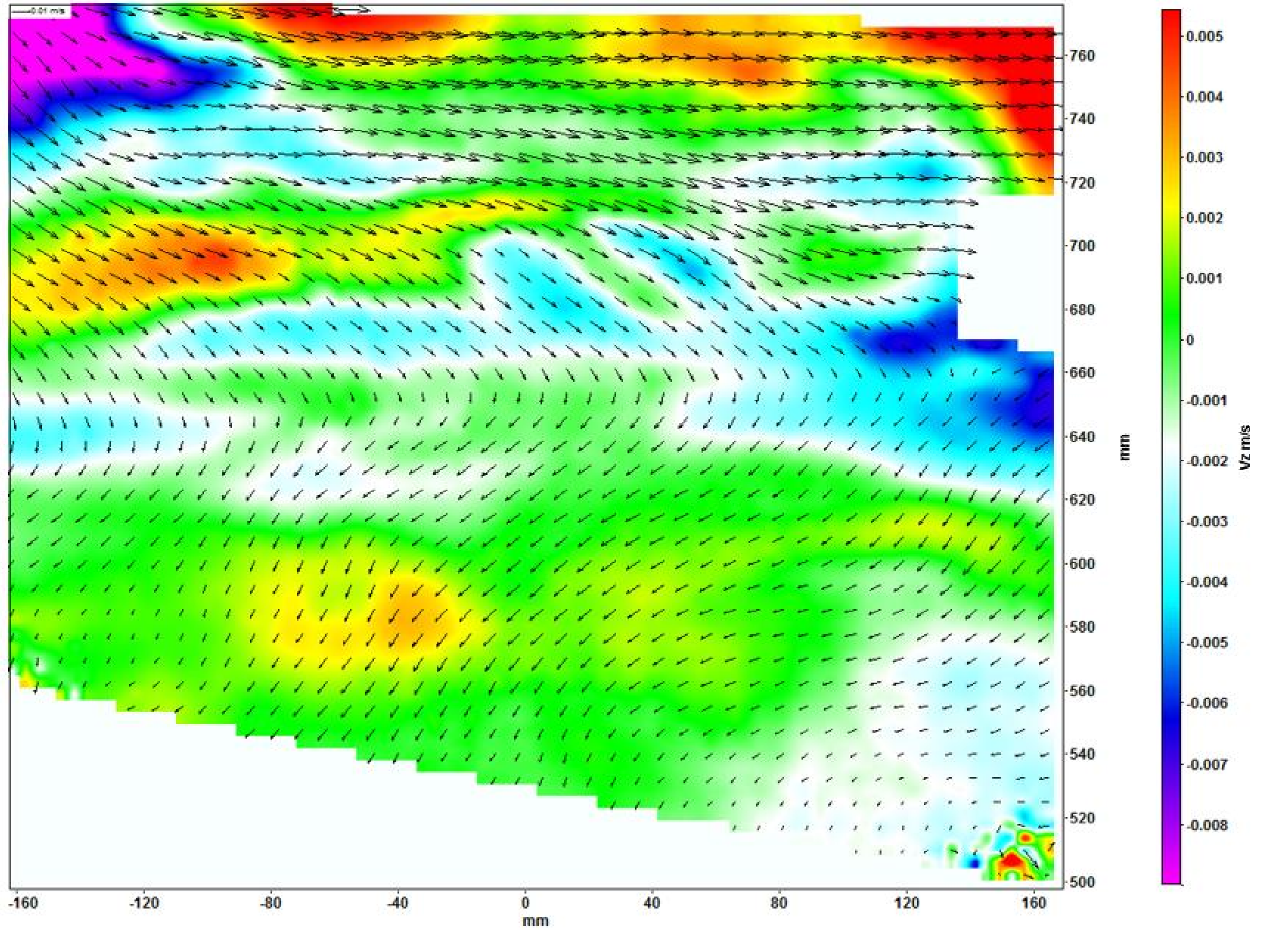

Averaged vector field from SPA-T8R Test4-2.

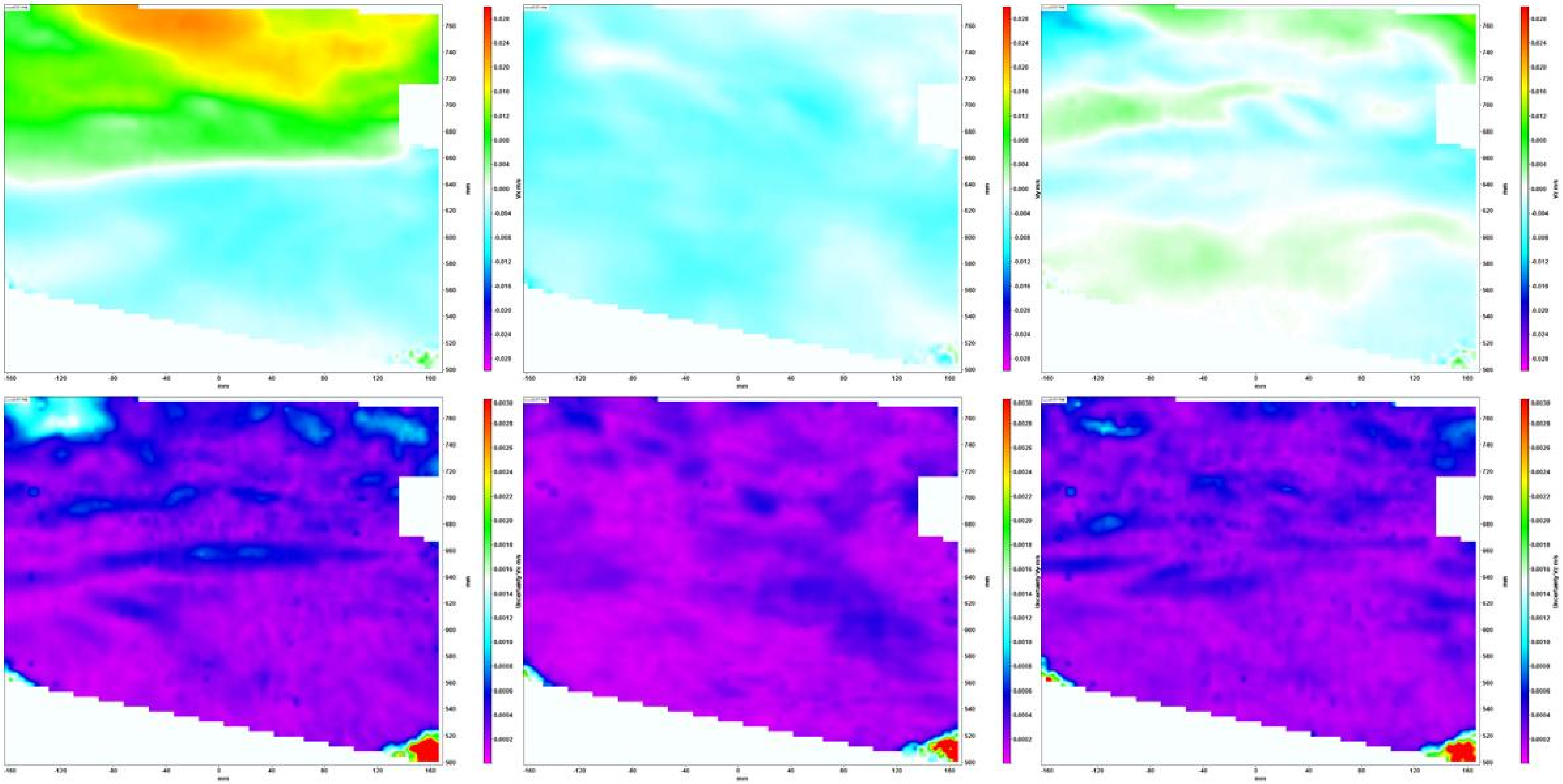

On top components of the averaged vector fields in order of x, y, z from left to right and below the uncertainty fields for respective components from SPA-T8R Test4-2.

Open your mind. LUT.
Lappeenranta University of Technology

SPA-T8R Test4-3 [3132.1 s – 3135.7 s]

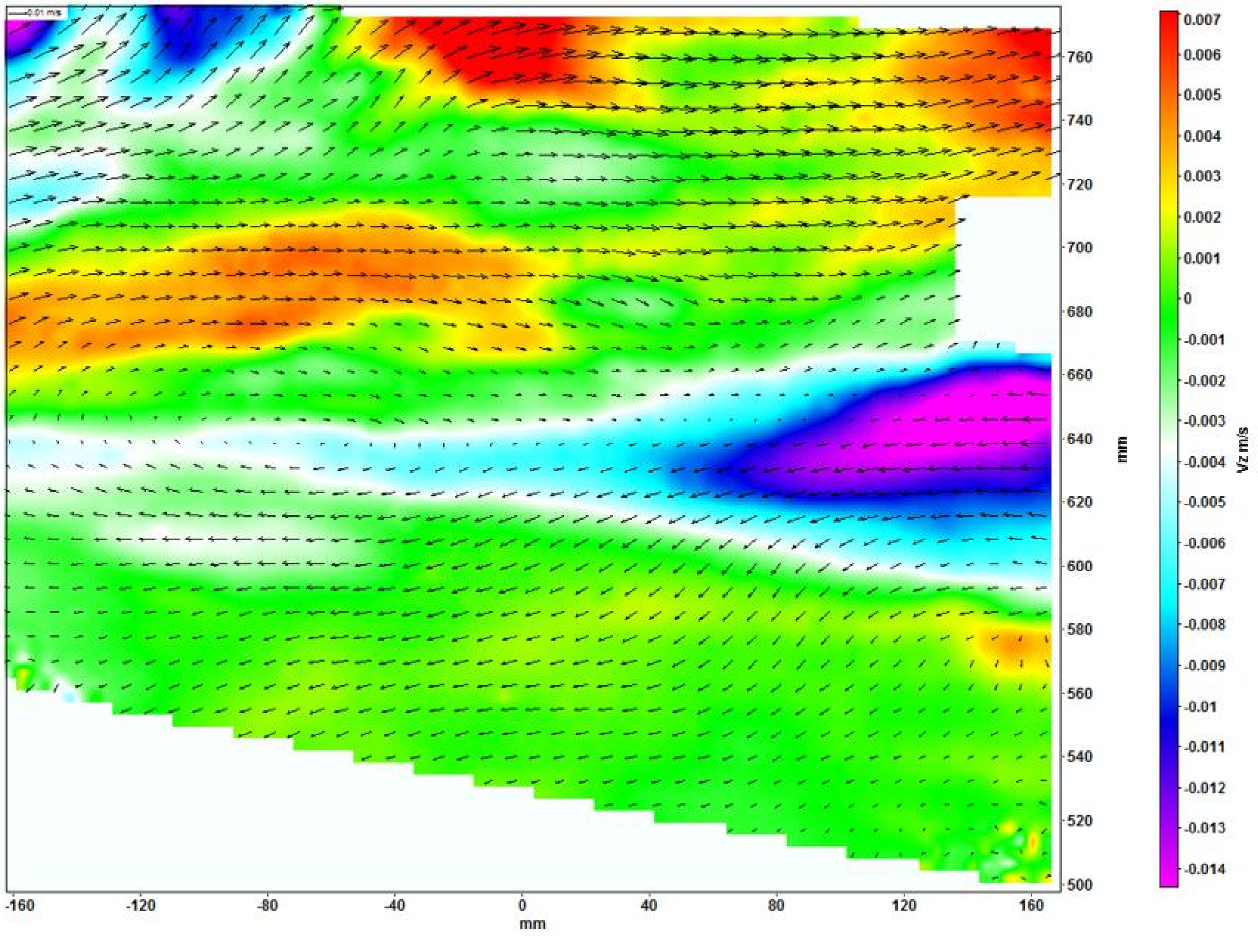

Averaged vector field from SPA-T8R Test4-3.

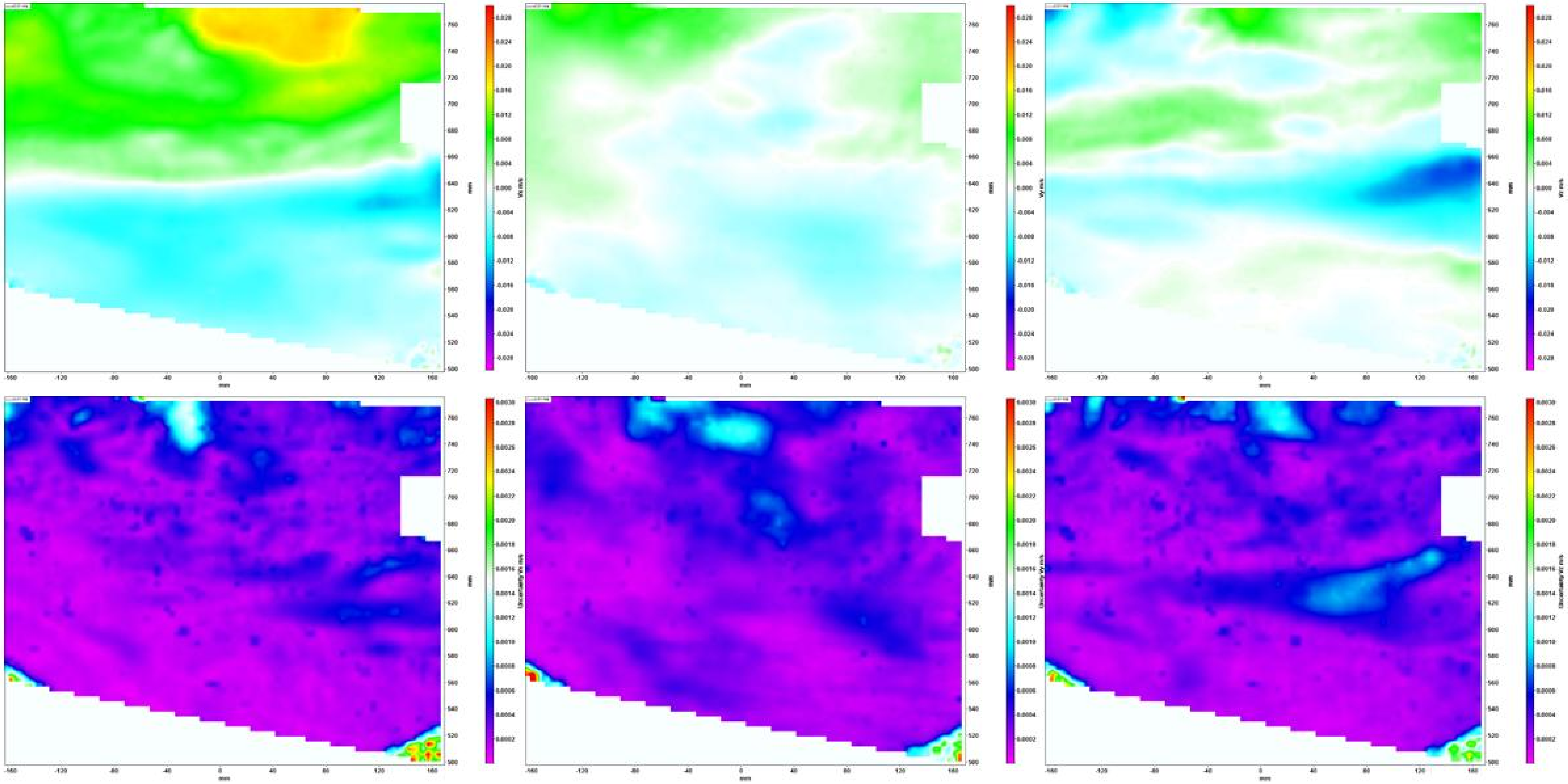

On top components of the averaged vector fields in order of x, y, z from left to right and below the uncertainty fields for respective components from SPA-T8R Test4-3.

SPA-T8R Test4-4 [3152.1 s – 3156.4 s]

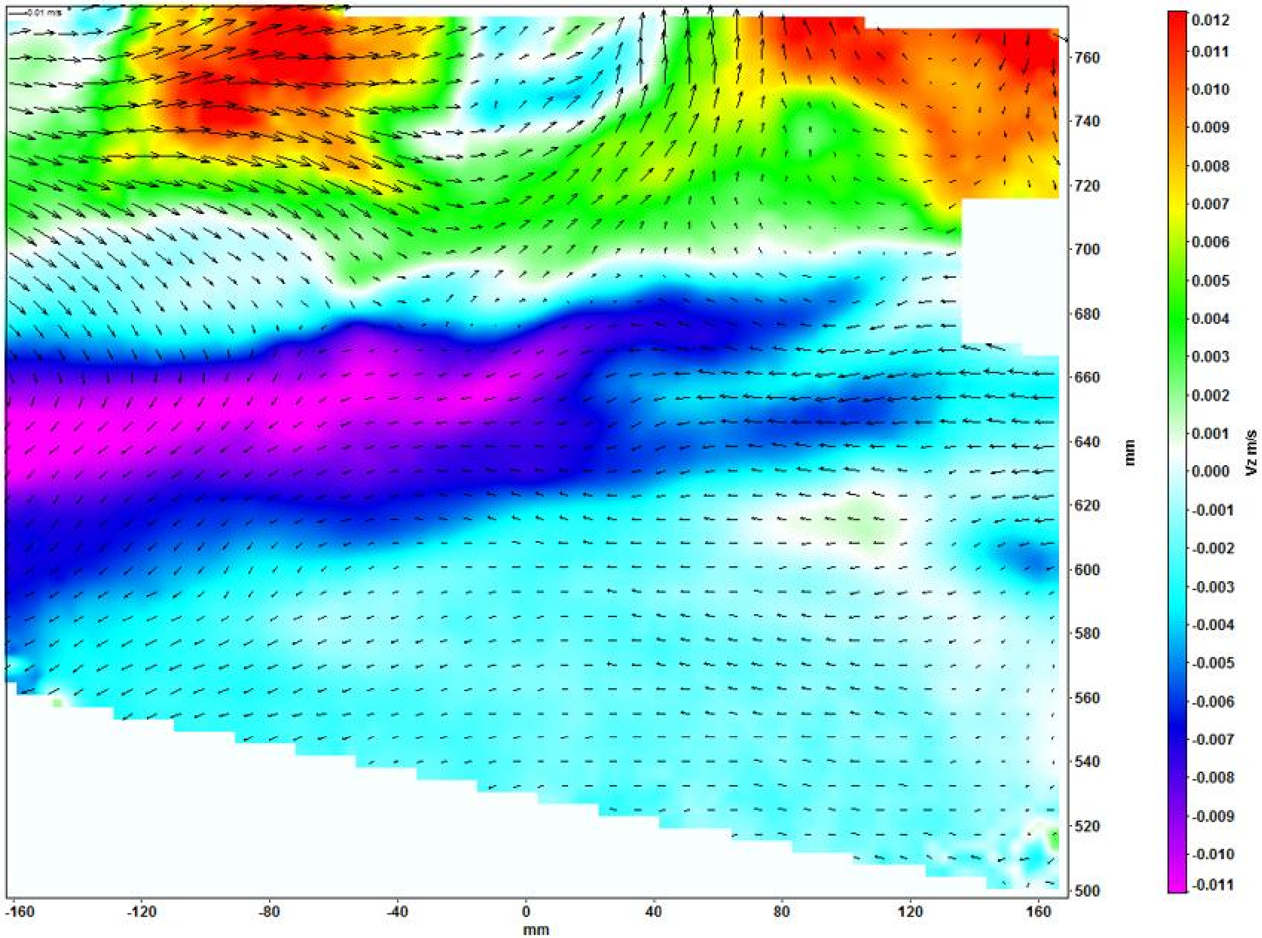

Averaged vector field from SPA-T8R Test4-4.

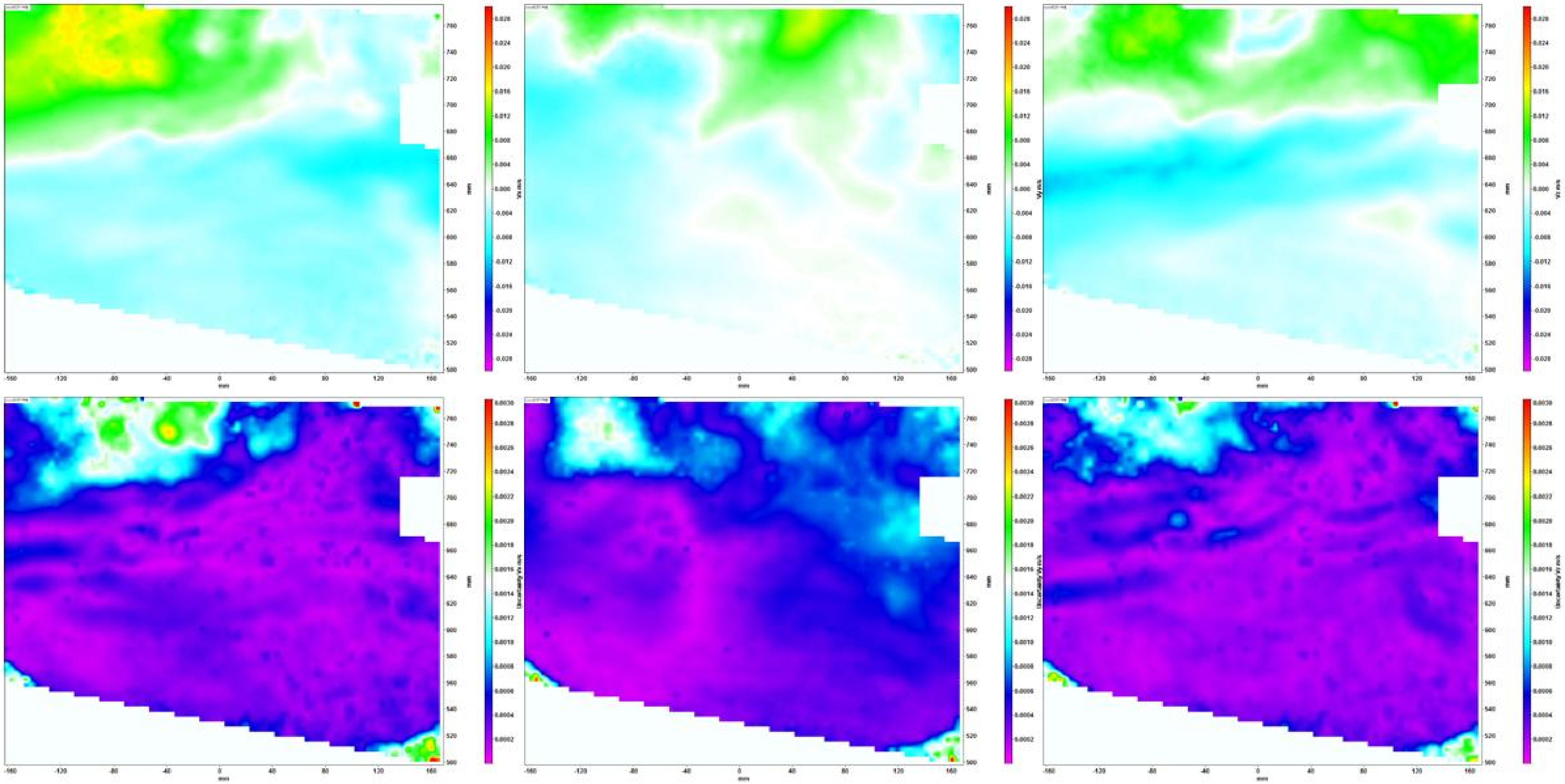

On top components of the averaged vector fields in order of x, y, z from left to right and below the uncertainty fields for respective components from SPA-T8R Test4-4.

SPA-T8R Test4-5 [3156.6 s – 3160.7 s]

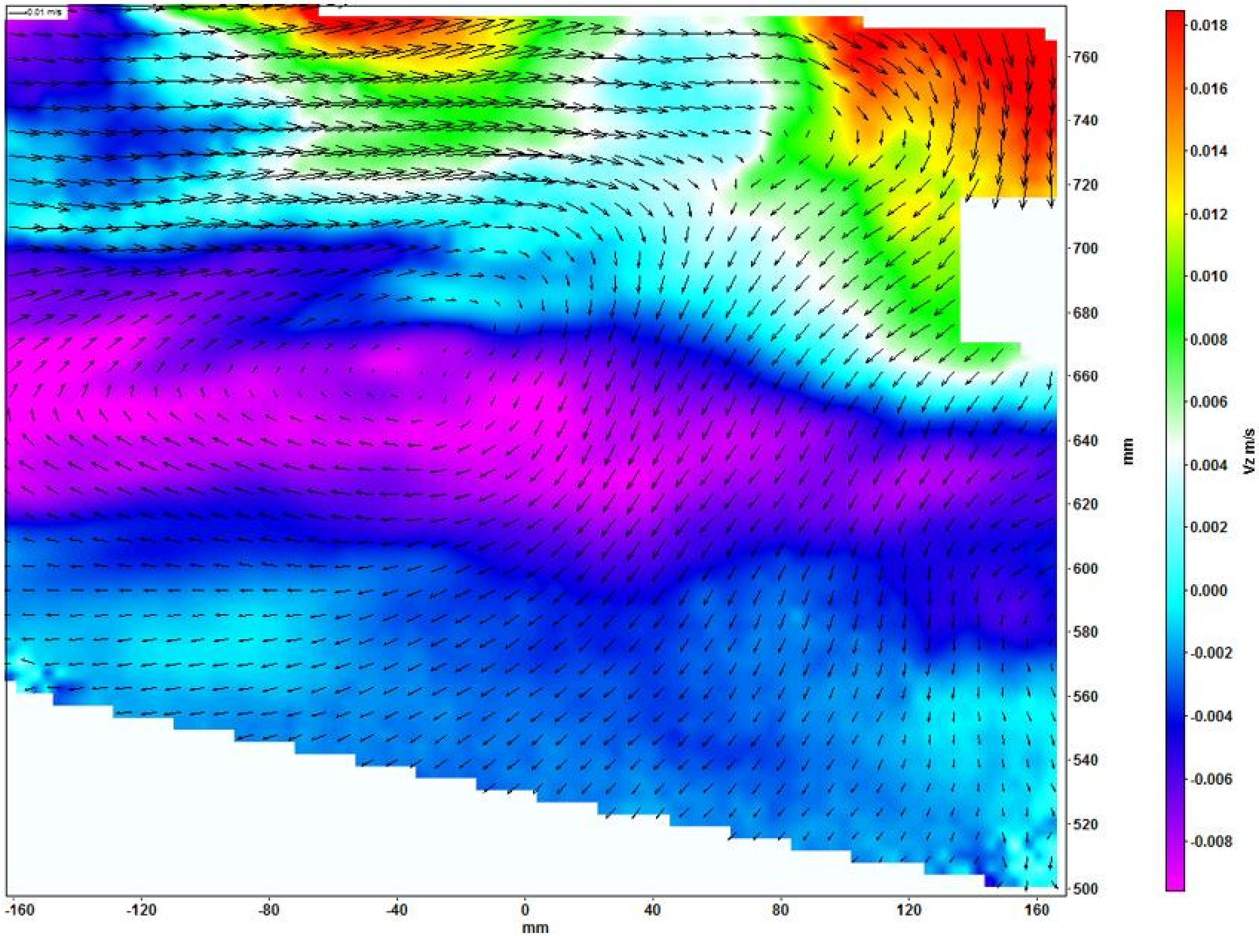

Averaged vector field from SPA-T8R Test4-5.

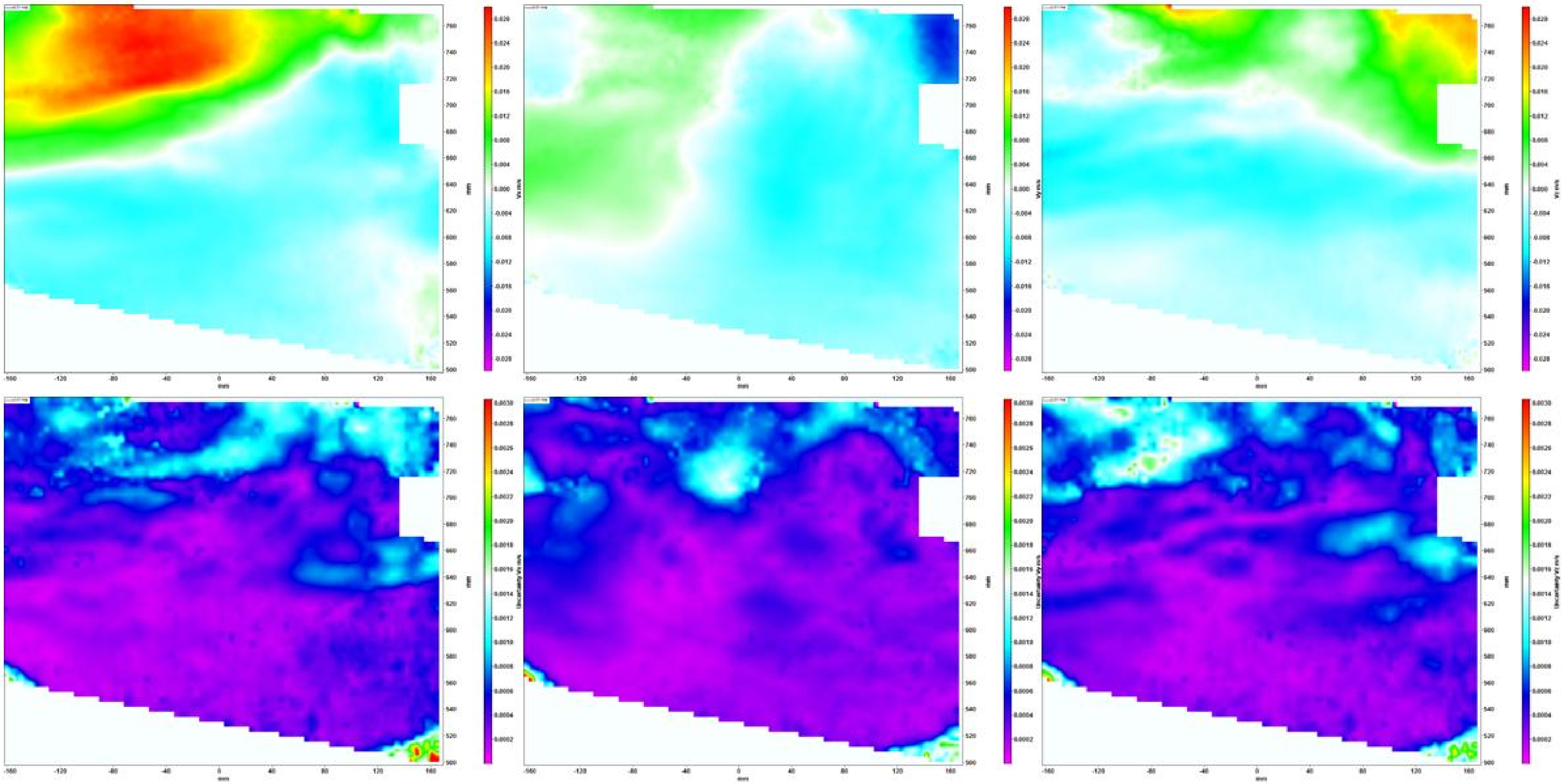

On top components of the averaged vector fields in order of x, y, z from left to right and below the uncertainty fields for respective components from SPA-T8R Test4-5.

SPA-T8R Test4-6 [3162.1 s – 3165.0 s]

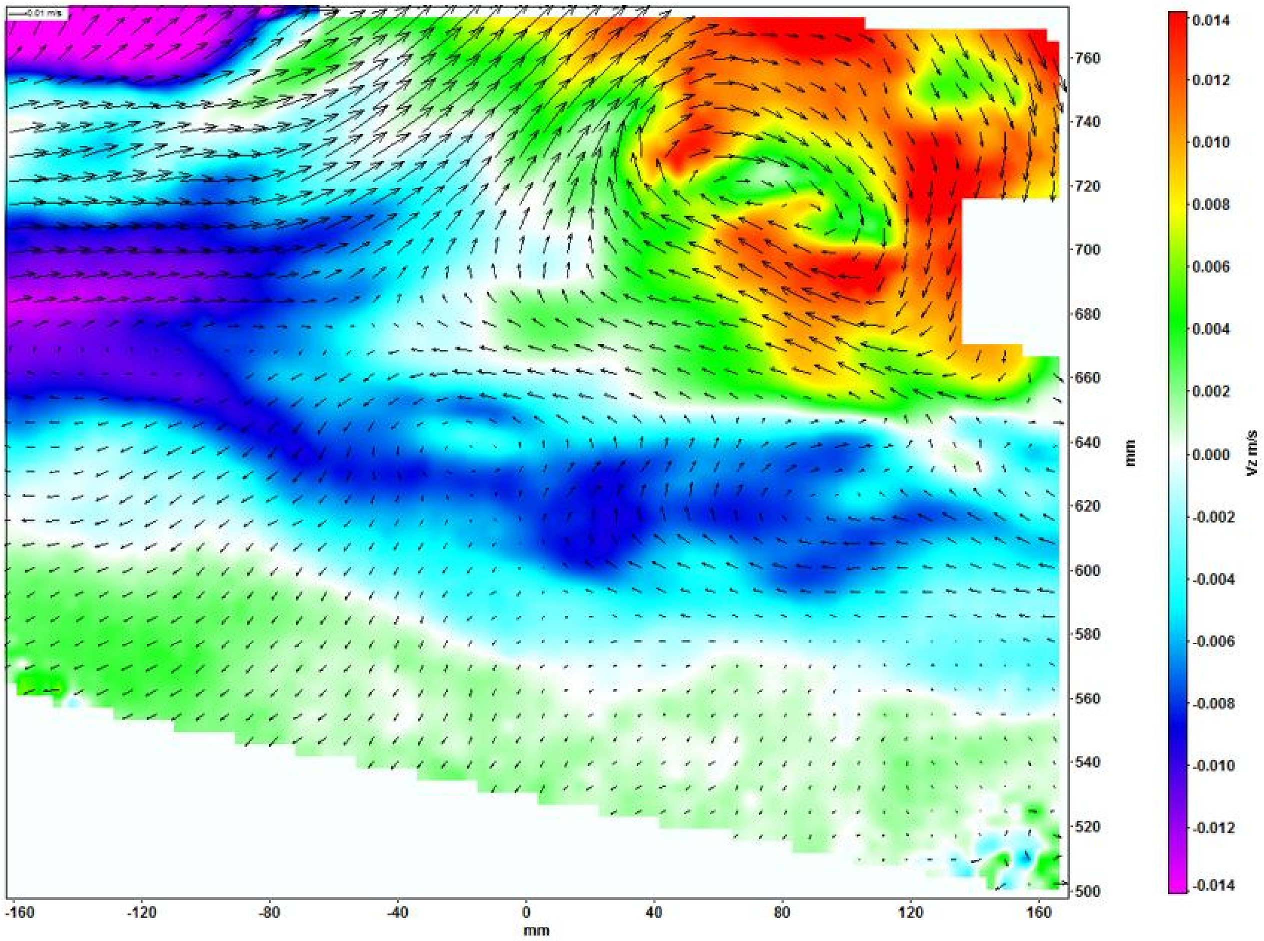

Averaged vector field from SPA-T8R Test4-6.

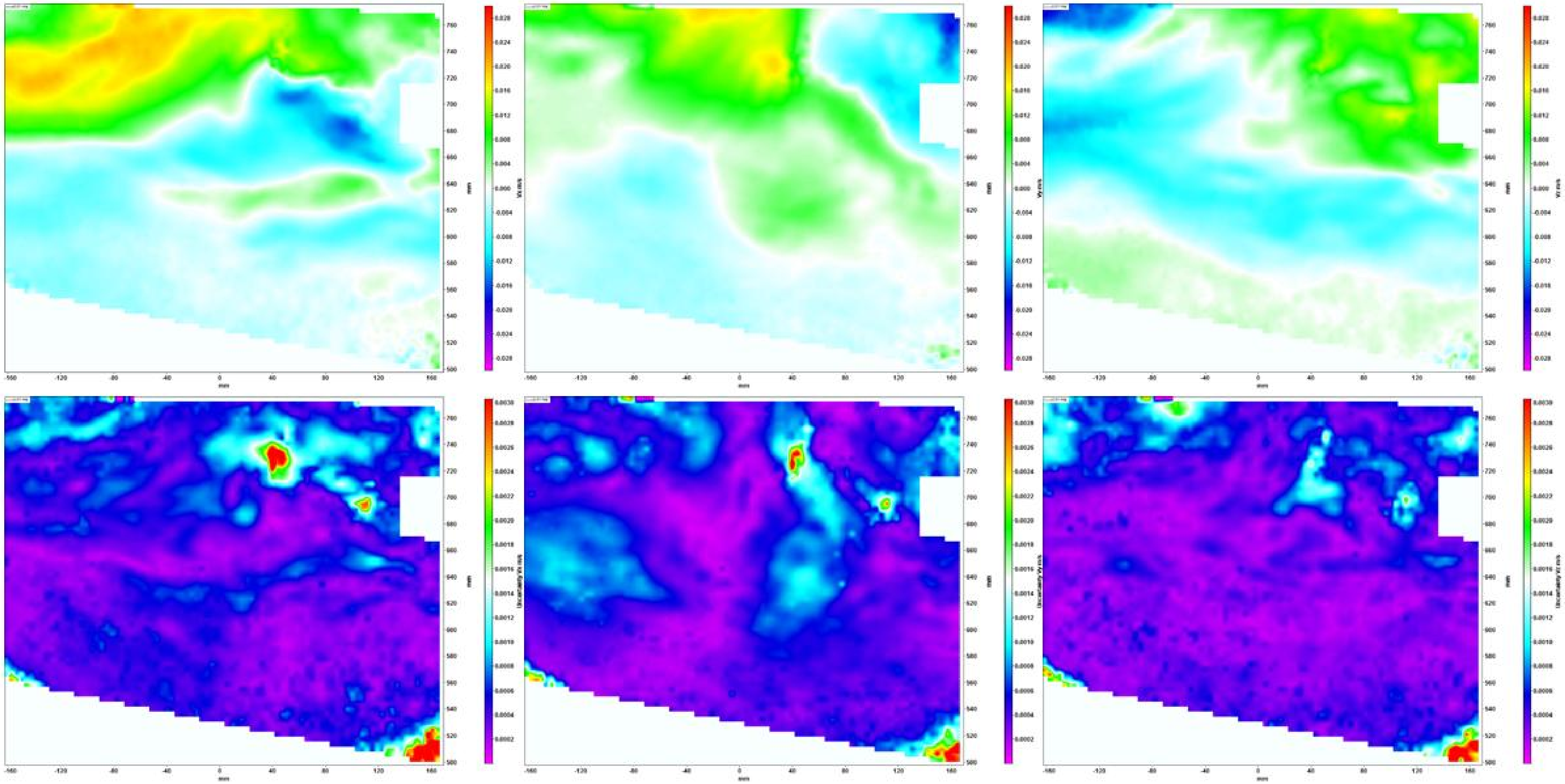

On top components of the averaged vector fields in order of x, y, z from left to right and below the uncertainty fields for respective components from SPA-T8R Test4-6.

Bibliographic Data Sheet **NKS-382**

Title	Sparger Tests in PPOOLEX on the Behaviour of Thermocline
Author(s)	Markku Puustinen, Lauri Pyy, Jani Laine, Antti Räsänen
Affiliation(s)	Lappeenranta University of Technology, School of Energy Systems, Nuclear Engineering
ISBN	978-87-7893-468-0
Date	March 2017
Project	NKS-R / COPSAR
No. of pages	28 p. + app. 46 p.
No. of tables	8
No. of illustrations	16 + 41
No. of references	20

Abstract
max. 2000 characters

This report summarizes the results of the two sparger pipe tests (SPA-T8R and SPA-T9) carried out in the PPOOLEX facility at LUT in 2016. Steam was blown through the vertical DN65 sparger type blowdown pipe to the condensation pool filled with sub-cooled water. Two different flow conditions were tested. Flow was either through all the 32 injection holes at the sparger head or just through eight holes in the bottom row.

The main objective of the tests was to obtain data for the development of the EMS and EHS models to be implemented in GOTHIC code by KTH. KTH plans to extend the models to cover also situations where steam injection into the pool is via a sparger pipe. The test parameters were selected by KTH on the basis of pre-test simulations and analysis of the results of the earlier sparger tests in PPOOLEX. Particularly the behaviour of the thermocline between the cold and warm water volumes was of interest. For this purpose also PIV measurements were tried during the tests.

In SPA-T8R, where flow was via 32 injection holes, the thermocline seemed to be around the elevation of 670 mm at the end of the stratification phase just as predicted by the pre-test simulations. The thermocline moved downwards as the erosion process progressed. The prevailing mixing mechanism during the final mixing phase was also erosion rather than internal circulation.

In SPA-T9, where flow was via eight injection holes, the thermocline was at first at a higher elevation than in SPA-T8R. It then started to shift downwards as the flow rate was increased in small steps. Complete mixing of the pool was achieved with the steam mass flow rate of 85 g/s. Erosion was again the prevailing mechanism in the mixing process.

The few sequences with recognized flow patterns from the PIV measurements indicate that some kind of swirls could exist at the elevation of the thermocline. The flow direction just under the thermocline can also be opposite to that just above the thermocline. The somewhat chaotic nature of the investigated phenomenon creates problems when measuring with a slow-speed PIV system and therefore definitive conclusions on the detailed behaviour of the thermocline can’t be made.

These tests in PPOOLEX verified that mixing of a thermally stratified water pool can happen through an erosion process instead of internal circulation if suitable flow conditions prevail.

Key words condensation pool, sparger, thermocline, mixing

Available on request from the NKS Secretariat, P.O.Box 49, DK-4000 Roskilde, Denmark.
Phone (+45) 4677 4041, e-mail nks@nks.org, www.nks.org